UNIVERSITY OF BIRMINGHAM

ADAPTATIONS OF *CRYPTOCOCCUS* TO THE HOST EXTRACELLULAR NICHE

by

LAMIN SAIDYKHAN

A thesis submitted to University of Birmingham for the degree of

DOCTOR OF PHILOSOPHY

Institute of Microbiology and Infection

School of Biosciences

College of Life and Environmental Sciences

University of Birmingham

August 2022

ABSTRACT

Cryptococcus is an opportunistic human fungal pathogen with the potential to cause life-threatening infections of the central nervous system. Ubiquitous in the environment, *Cryptococcus* switches from a saprotrophic lifestyle in the environment to a pathogenic lifestyle in humans by altering key cellular functions required for adaptation and invasion of the host. Once inhaled, the host extracellular niche (particularly the lung mucosa) serves as a modulator for cryptococcal adaptive phenotypes which are critical for survival and proliferation. However, the cellular changes exhibited by *Cryptococcus* as it responds to the pulmonary environment is poorly understood.

The surface of the lung mucosa is heavily loaded with secretions from host lung cells, such as Type I and II epithelial cells as well as alveolar macrophages. Upon inhalation, *Cryptococcus* comes into close contact with these secretions. The first part of this thesis probed and described the potency of mammalian cells secreted factors (including lung-associated cells) to stimulate phenotypic responses that are associated with *Cryptococcus* adaptive mechanisms. While *C. neoformans* responded to these secreted factors with rapid replication, its sister species *C. gattii* instead demonstrated a high capacity to form enormously enlarged titan-like cells.

Within the lungs, *Cryptococcus* undergoes morphogenesis to form titan cells: exceptionally large cells that are critical for disease establishment. In the second part of this thesis, a new *in vitro* titan-induction approach is introduced. Using this *in vitro* approach, I revealed a remarkably high capacity for titanisation within *C. gattii,* especially in strains associated with the Pacific Northwest Outbreak, and characterised strain-specific differences within the clade. In addition, this approach demonstrates for the first time that the cell-cycle-regulated phenotypes: cell size changes, DNA replication and budding, are not always synchronous during titanisation.

Titan cell formation is triggered by host-specific environmental conditions [such as physiological temperature (37°C) and CO_2 level (5%) coupled with hypoxia, and nutrient limitation] and modulated by genetic regulators including those associated with cell cycle progression. The last part of this thesis established a strong correlation between progression of the cell cycle phenotypes (cell size, DNA replication and budding) and expression of cell cycle genes and identifies the role of cryptococcal quorum sensing peptide Qsp1 peptide and exogenous p-Aminobenzoic acid as a key inducer of titanisation in *C. gattii.*

ACKNOWLEDGEMENTS

All praises be to Allah by whose grace I accomplish this challenging work. Thereafter, I express my deepest gratitude and appreciation to my able and kind supervisor, Professor Robin May, for his awesome supervision. His unique guidance, support and understanding immensely pushed me to overcome both PhD-related and non-academic hurdles during my PhD journey. With all my personal shortcomings, you trusted me, created the opportunity for me to explore my potentials and guided me to realize my hidden strengths. I wish to acknowledge my co-supervisor, Dr Elizabeth Ballou for her invaluable advice and relentless contribution all the way through my PhD research. She had been actively involved in all projects with a great sense of expertise ranging from conceptualization, data curation and analysis, to writing for publication. I cannot forget Dr Leanne Taylor-Smith for training me to start my PhD work and her technical support which laid the foundation for the most outstanding achievement of my PhD research-the discovery of titan-induction model.

My sincere gratitude and gratefulness to the Islamic Development Bank Merit Scholarship for fully funding my studies at the University of Birmingham, UK. It is a privilege and honour to be a scholar of this prestigious and competitive scholarship. Also, I wholeheartedly thank the University of The Gambia for granting a study leave to further my education abroad.

The contribution of my lab (HAPI Lab) members to the success of my PhD program cannot be overemphasized. By way of appreciation, I feel obliged to mention the names of these wonderful lab colleagues whose kindness and support will ever be remembered: Jude Williams, Joao, Herbert, Ebrima, Pizga, Hanna, Sophia, Harlene, Farhana, Xin Zhou (Phoebe), Diana, Guillaume, Chinaemerem Onyishi (Uju) and many more. You have indeed made my PhD journey lot enjoyable and easy. Outside the HAPI Lab, I wish to acknowledge the technical and experimental support of Dr. Patrick Moynihan (School of Bioscience) and Dr. Rebecca

Drummond (College of Medical and Dental Sciences) for extraction and titan *in vivo* work respectively.

I owe a lot of thanks to my family and friends whose moral support and prayers are pivotal to the success of my PhD career. The perpetual nurture and moral support rendered by my brave father, Musa Saidykhan and caring mother, Fatoumata Saidykhan are inevitable to this accomplishment and my entire academic career. It is said behind the success of every man is a woman. This woman for me is my beloved wife, Fatou Drammeh (AKA Baby). Words cannot describe how much your persistent patience, sacrifice, care, love and exhortations trailed me through the journey of life and PhD. My loving and cheerful daughters, Mariam, Zahra, and Hajara have indeed made my PhD journey enjoyable and less stressful. A huge thanks to my siblings: Baboucarr Saidykhan (brother), Fatima Saidykhan (sister) and Amina Saidykhan (sister) for their sincere concerns, prayers and moral support. I cannot possibly enlist all my relatives here, but I thank them all especially my grandmother, Njonya Fofana and my in-laws for all the well-wishing prayers and support.

No doubt, all my close friends have positively contributed (directly or indirectly) to my life and PhD journey but the moral support I obtained from Modou Alieu Jallow, Dr. Muhammed Lamin Sanyang, Abubacarr Sanneh, Abubkr Bah, Joseph Ndenn, Sheikh Sulayman Gaye, Sheikh Sainey Darboe, Dr. Mustapha Jorbateh and Dr. Ali Musa are exceptionally amazing. Some of you are not just friends but inspirational mentors in my academic and non-academic life.

THESIS OVERVIEW

Members of *Cryptococcus neoformans/gattii* species complex, the two pathogenic species of *Cryptococcus*, are the etiological agents of the human fungal infection-cryptococcosis. *C. neoformans* predominantly infects immunocompromised patient and is the leading agent of fungal co-infection of HIV-positive patients, responsible for over 220,000 cases and over 180,000 deaths per year worldwide. In contrast *C. gattii,* although responsible for far fewer infections overall, can act as a primary pathogen causing the largest fungal outbreak (Pacific Northwest Outbreak) in an otherwise healthy population. Central to *Cryptococcus* ability to cause infection is its adaptability to a hostile host environment and immune defence mechanisms. Adaptation to a stressful host environment is accompanied by dynamic cellular changes with underlying genetic regulators. Therefore, it is necessary to decipher the connection between host-relevant cues and *Cryptococcus* responses in order to deeply understand what makes this yeast a pathogen. The core aim of this thesis is to identify those host-specific cues and discover how *Cryptococcus* responds to the host environment as an adaptation mechanism.

This thesis comprises seven chapters. **Chapter 1** (introduction) is a brief introduction of *Cryptococcus* as a unicellular organism and fungal pathogen with a brief description of how a naïve pulmonary niche can potentially shape *Cryptococcus* adaptive features. **Chapter 2** (Literature review) is based on a review paper which highlights some of the major phenotypic differences between *C. neoformans* and *C. gattii* and provides evidences that *C. gattii* is a unique pathogenic yeast with an understudied virulence mechanism, whilst **Chapter 3** covers the methods used in this work.

Chapter 4 reports my work characterising the enhanced cryptococcal replicative growth that is triggered by secreted factors from different mammalian cells lines. The strain-specificity of this form of cryptococcal response and some of the physicochemical properties of the secreted factors were investigated.

Chapter 5 describes the serendipitous discovery of dramatic morphological changes (the formation of enormously enlarged titan-like cells, particularly by *C. gattii*), as a response to the secretome of lung-associated mammalian cell lines. It characterizes the process of titan cell formation in *C. gattii* in detail and reports the first attempts to find the active host-derived factors responsible for the phenotype.

Chapter 6 reports on the discovery of a simple *in vitro* model for inducing *bone fide* titan cells and then uses this model to reveal novel features of titan cells in *C. gattii*. The chapter also highlights how titanization was more prevalent with *C. gattii* (particularly among outbreak strains) and being a polygenetic trait.

Chapter 7 investigated the growth conditions and key (exogenous and endogenous) regulators of the *in vitro* generated *C. gattii* titan cells. This chapter studied the correlation between cell cycle progression and the expression of cell cycle genes in order to understand the mechanism underlying titanisation.

In **chapter 8**, I conclude the findings of the study and propose recommendations for future research.

TABLE OF CONTENTS

LIST OF FIGURES

LIST OF TABLES

ABBREVIATIONS

A549	Human lung epithelial cell line
ALF	Alveolar lining fluid
AM	Alveolar macrophages
cAMP	Cyclic AMP
CDMEM	Conditioned DMEM
CFW	Calcofluor white
CsfDMEM	Conditioned serum-free DMEM
CsfRPMI	Conditioned sfRPMI
DC	Dendritic cells
DMEM	*Dulbecco's Modified Eagle Medium*
DNA	Deoxyribonucleic acid
ELF	Epithelial lining fluid
FBS	Fetal bovine serum
GXM	Glucuronoxylomannan
GXMGal	Galactoxylomannan
HI-CsfDMEM	Heat-inactivated CsfDMEM
IL-	Interleukin
J774	Murine macrophage-like cells J774

MHS	Major histocompatibility complex
pABA	P-aminobenzoic acid
PAMPs	Pathogen associated molecular patterns
PBS	Phosphate-buffer saline
PKA	Protein kinase A
QS	Quorum sensing
Qsp1	Quorum sensing peptide 1
RNA	Ribonucleic acid
RPMI	Roswell Park Memorial Institute Medium
sfDMEM	Serum-free DMEM
sfRPMI	Serum free-RPMI
TCR	T cell receptor
Th1	T helper response type 1
Th17	T helper response type 17
Th2	T helper response type 2
TLR	Toll-like receptor
TNF	Tumour necrosis factor
TNFa	Tumour necrosis factor alpha
YPD	Yeast Peptone Dextrose

CHAPTER 1

INTRODUCTION

1.0 Background

1.1 *Cryptococcus*

Cryptococcus is a basidiomycete fungus that causes infections, incurring high morbidity and mortality in immunocompromised patients [1-3]. With the advent of the AIDS epidemic, this human opportunistic pathogen emerged as a top killer in immunocompromised patients [4]. In addition, a distinct species, *C. gattii,* has been identified to cause fatal diseases in immunocompetent patients [5, 6]. In spite of a considerable reduction in AIDS patients as a result of antiviral therapy, the global incidence of *Cryptococcus* is still very high (>220,000 cases), with an estimate of over >180,000 deaths per annum [3, 7].

In nature, *Cryptococcus* exhibits a sapronoses life, being harboured in avian (especially pigeon) excreta, trees, soil, amoebae and nematodes [1, 8]. While *C. neoformans* has a worldwide distribution, *C. gattii* is more limited, with a predilection to arboreal habitats [1, 9, 10].

Morphologically, *Cryptococcus*is characterized as a spherical, budding, encapsulated yeast cell with a typical size diameter of 5 to 10 μm [11, 12] . However, these traits can vary with life cycle or environmental growth conditions [1, 13-16].

1.2 Evolution and genetic diversity

C. neoformans was discovered in 1894 when it was isolated from peach juice and later from the tibia bone of a 31-year-old woman in the same year [1, 9]. From that time on, several nomenclatures such as *Saccharomyces neoformans*, *Blastomyces neoformans, Cryptococcus hominis*, and *Torula histolytica* were suggested, but the name *Cryptococcus neoformans* was finally adopted to denote the yeast as a single fungal species [11, 17] with two recognized varieties: *C. neoformans* and *C. gattii* [18]. Before the discovery of their teleomorph (sexual

states), *C. neoformans* and *C. gattii* were named as two different anamorph species, *C. neoformans* and *C. bacillispora* respectively [18]. However, teleomorphism was later found in both and subsequently their teleomorph-typified names *Filobasidiella neoformans* and *F. bacillispora* were respectively adopted. Consequently, both species were classified under the genus Filobasidiella, the family Filobasidieceae and the order Filobasidiales which is a member of the Basidiomycota [17, 19]. In 2013, the use of Filobasidiella was abandoned and only the term *Cryptococcus* was endorsed in accordance to the new fungal nomenclature rule of one name for one fungus [20, 21].

C. neoformans and *C. gattii* exist as individual heterothallic haploid yeast species which have diverged approximately 30-40 million years ago [9, 22]. Sexual reproduction is accomplished by exchange of genetic material between the two mating types. However, unisexual reproduction has been confirmed in α mating type (MATα) strains [23, 24]**.** This nonclassical (MATα-MATα mating) sexual reproduction has been implicated in the distribution of *C. gattii* to new geographical niches [23]. Species diversity within *Cryptococcus* is growing as new lineages with different ecological, biochemical and genetic characteristics are discovered [25]. Based on molecular analysis with reference to the *URA5* gene nucleotide sequencing and DNA fingerprinting, three varieties of *Cryptococcus* were recognized: *C. neoformans* var. *grubbii, C. neoformans* var. *neoformans* and *C. neoformans* var. *gattii* [26]. In 2002, *C. neoformans* var. *gattii* was elevated to a distinct species while *C. neoformans* var. *neoformans* and *C. neoformans* var. *grubii* were classified under a single species-*C. neoformans* [16]. Recently, a more advanced molecular sequencing [multilocus sequence typing (MLST)] has identified *C. neoformans* and *C. gattii* as two species complexes comprising of different molecular types: VNI, VNII, and VNIB for *C. neoformans* var. *grubii*; VNIV for *C. neoformans* var. *neoformans*; and VGI, VGII, VGIII and VGIV for *C. neoformans* var. *gattii* (Table 1) [25, 27,

28]. Further, an inter-varietal hybrid between var. *grubii* and var. *neoformans*, VNIII has been discovered [29].

Table 1: Classification of pathogenic *Cryptococcus* species with different molecular types. Adapted from [28] and slightly modified.

Species and Varieties	Molecular Types
C. neoformans var. grubii	VN I, VNII, VNIB
C. gattii	VG I, VG II, VG III, VG IV
C. neoformans var. neoformans	VN IV
C. neoformans	VN III

Recently, the molecular genotypes have been recognized and elevated to distinct species with specific names: *C. neoformans* (VNI and VNII), *C. deneoformans* (VNIV), *C. gattii* (VGI), *C. deuterogattii* (VGII), *C. bacillisporus* (VGIII), *C. tetragattii* (VGIV) and *C. decagattii* (VGV) [30, 31].

1.3 Life cycle

The life cycle of *Cryptococcus* comprises both asexual and sexual phases. Asexual reproduction occurs by mitosis in which small globose, ovoid or apiculate encapsulated cells are produced by budding [11, 32]**.** The degree of encapsulation varies with strains and environmental factors. In responding to unfavourable growth conditions, *Cryptococcus* undergoes cell cycle arrest by entering into a stationary phase from either the G1 or G2 period of the cell cycle [33]. As a result, large unbudded cells with either G2 or G1 DNA content are

formed while small cells possess G1 DNA. Cell cycle arrest occurring at G2 rather than G1 is a strategy to ensure that extra copies of genomic information are made available for repair [33].

Cryptococcus exists in the environment as a haploid budding yeast with two mating types: MAT**a** and MATα [32]. Each of the mating types can undergo vegetative growth by producing fruiting bodies or filamentation (depicting a dimorphism transition) . Sexual reproduction is initiated by conjugation of yeast cells of the same or opposite mating types (Figure 1.1) [11, 17]. Upon conjugation, the two mating cells produce dikaryotic hyphae with clamp connections and haustorial branches. The dikaryotic hyphae swells up to undergo meiosis, which is followed by several mitotic divisions. The repeated mitosis leads to the formation of septate uninucleate basidiospores buds that are positioned terminally or laterally from the hyphae. In contrast to the traditional (MAT**a**-MATα) mating, the nonclassical same-sex (MATα-MATα) mating produces monokaryotic fruiting (Figure 1.1) which are responsible for producing infectious spores [34].

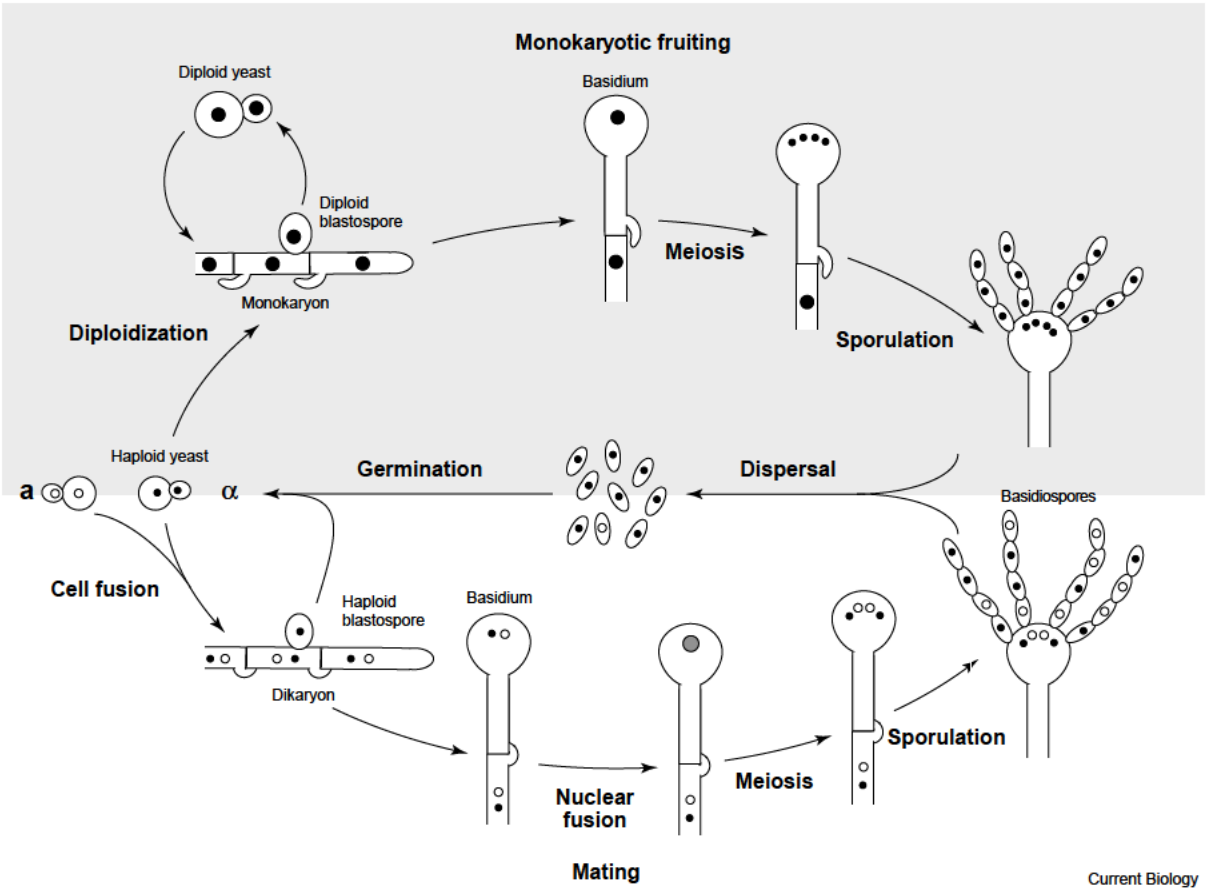

Figure 1.1 Sexual cycles of Cryptococcus neoformans. The lower panel depicts the traditional sexual cycle involving partners of opposite mating type, whereas the upper panel depicts the modified form of sexual reproduction that occurs between partners of the same mating-type during monokaryotic fruiting. *Adapted from* [34].

1.4 Pathogenicity

Cryptococcal infection is initiated by inhalation of desiccated yeast cells from the environment into the lungs. The fungus can reach pulmonary alveoli and cause pneumonia or disseminate to other body parts, to potentially cause other forms of cryptococcosis [20, 28, 35]. Inside the lungs, the infectious propagule can either be efficiently cleared (by the immune system of an immunocompetent host), remain latent within alveolar macrophages, proliferate to cause

severe lung infections (especially in immunocompromised individuals), or preferentially disseminate to the central nervous system (CNS) [1, 28, 36, 37]. Invasion of the CNS causes the fatal condition of cryptococcal meningoencephalitis which is the most common clinical manifestation of cryptococcosis [28, 38]. There are two main routes of dissemination of *C. neoformans* to the CNS: intracellular (making use of migrating-macrophage cells), which is accomplished by a well-known mechanism called "Trojan horse mechanism" and extracellular [39, 40]. The extracellular route of dissemination occurs by direct penetration of respiratory epithelial cells via the process of *transcytosis* (a transcellular route) or by passing between the epithelial cells known as the *paracellular* route.

Pulmonary infection triggers both innate and adaptive host immune response. Two sets of professional phagocytic immune cells that are permanently resident within the lung, alveolar macrophages (AM) and resident dendritic cells (DC), are crucial immunomodulators of the early host defence against pulmonary infection, since they are the first immune cells to encounter cryptococcal cells after deposition into the alveoli [40, 41]. AM and DC perceive *Cryptococcus* via detection of pathogen-associated molecular patterns on the cryptococcal polysaccharide capsule (such as antigens within the capsular polysaccharides GXM and GXMGal) and consequently internalize the fungal cells (phagocytosis) for killing [41]. However, *Cryptococcus* has developed different strategies to evade this killing including total avoidance of phagocytosis [42], inhibition of phagosome maturation [43], and inciting a non-lytic expulsion (vomocytosis) of internalized cells while both phagocyte and fungal cells remain unharmed [44].

During the innate immune response, AM and DC recruit other immune cells via secretion of a plethora of pro-inflammatory cytokines and chemokines that serves as signals to both immune and non-immune cells [41, 45]. However, *Cryptococcus* interferes with host inflammatory

response by downregulating pro-inflammatory cytokines [tumour necrosis factor (TNF)], blocking dendritic cell maturation, inhibiting the production of the pro-inflammatory cytokines interleukin-12 (IL-12) and IL-23, and creating an environment of anti-inflammatory markers (such as IL-4 and IL-33) [1].

During cryptococcal infection, DCs function as the primary antigen-presenting cells to stimulate T cells. Subsequently, T cells differentiate into T helper (Th) cells which are polarized to elicit differential adaptive immune response. Th1 is associated with cryptococcal clearance, Th2 plays a protective role against disease enhancement, whereas Th17 displays both protective and non-protective activities [1, 46]**.** Within the last decade, a novel morphogenetic transition of *Cryptococcus* from a normal yeast cell size (5-7μm) to gigantic titan cells (>10 reaching up to 100μm) has been described *in vitro* and *in vivo* [47-50]. In addition to their massive size, titan cells contribute to *Cryptococcus* pathogenicity by exhibition of key virulence factors including thicker cell wall and tightly compacted capsule [1, 12, 51]. Although the mechanism driving this transition is unclear, titanisation in *Cryptococcus* is apparently a host stress response with a protective role against host innate and adaptive immune system [12, 47, 51, 52].

1.5 Virulence

Cryptococcus is equipped with different virulence factors including: a polysaccharide capsule, melanin deposition in the cell wall, the capacity to grow at 37°C (host temperature), and production of extracellular enzymes such as laccases and urease [53]. *Cryptococcus* successful invasion and survival in the host relies heavily on its capsule, which is considered the most important virulence factor [54-56]. The presence of a thick polysaccharide capsule protects the yeast from desiccation and facilitates escape from macrophages by strongly resisting

phagocytosis [1, 57]. Additionally, the largest component of cryptococcal capsule (GXM) is shed from the yeast and accummulates both inside macrophages, where it confers resistance to macrophage-secreted ROS (reactive oxygen species), and extracellularly, where it attenuates inflammation [57, 59].

Melanization is the second most important cryptococcal virulence factor. Produced by laccase enzyme, melanisation offers protection against stresses including extremes of temperature, osmotic pressure, endogenous ROS of macrophages, UV-light radiation and survival against host immune response [55, 60].

1.6 How does the naïve pulmonary niche influences *Cryptococcus* biological behaviour?

Transition from a saprophytic lifestyle in the environment to living as a human pathogen requires *Cryptococcus* to adapt to new host factors [1, 61]. The interface between fungal exposure to host stress conditions and the ability to circumvent those stresses is fundamental to survival and successful invasion of the host [61, 62]. Fungal cells adapt to dynamic local parameters by detecting environmental signals and transducing the signals to mediate specific cellular processes that result in adaptive responses [8, 36, 37, 51, 61]. Upon inhalation into the lungs, *Cryptococcus* is exposed to the stressful pulmonary conditions of elevated temperature, nutrient (carbon, nitrogen, iron, zinc etc.) limitation, higher physiological CO_2 and hypoxia [61, 63]. *Cryptococcus* responds to these host stresses by developing phenotypic (such as capsule elaboration, cell wall thickening, formation of titan cells) [12, 16, 64] and metabolic traits (such as production of laccase, urease and acetyl-CoA, involved in carbon metabolism) [37, 65, 66] that are regulated by well-coordinated stress signalling pathways and genes [67, 68].

Cryptococcus pathogenicity is predominantly studied with much focus on *Cryptococcus*-host immune interactions (during active immune response) [15, 63, 69-73] rather than how the naïve pulmonary environment influences it phenotypically. The studies dwelling on the adaptations of *Cryptococcus* to the host, presents the pulmonary niche as the first host environment *Cryptococcus* encounters [15, 37].

1.6.1 Effect of pulmonary physiological conditions on the biological traits of *Cryptococcus*

1.6.1.1 Temperature

Temperature is one of the key environmental factors that influences the morphological and physiological traits of not only *Cryptococcus* but other fungal species. Typical dimorphic fungi like *Blastomyces dermatitidis*, *Coccidioides immitis*, *Histoplasma capsulatum*, *Paracoccidioides brasiliensis*, *Sporothrix schenckii* and *Talaromyces marneffei*, transform morphologically from a mould to a yeast state as they switch from ambient temperature in the environment to elevated temperature of their mammalian host. In contrast, *Candida albicans* transform from yeast to hyphal form during host invasion [62]. *Cryptococcus* responds to human physiological temperature (37ºC) by exhibiting a variety of morphological changes including capsule elaboration, cell body enlargement and cell shape alteration [16, 51, 74]. Fungal pathogenicity is strongly correlated with their ability to thrive above ambient temperature [62]. In fact, the ability to grow at mammalian body temperature is a key virulence factor for *Cryptococcus* [75].

Genetic mechanisms underlying *Cryptococcus'*s ability to endure high temperature have been investigated and associated to genes including *NMT1* [73], *RAS1*, *ROM2*, and *CNA1* [76] which encodes proteins that dictates pathways relevant to temperature-sensitivity functions [73, 77, 78]. *Cryptococcus NMT* encodes n-myristyl transferase, which catalyses the transfer of myristate from myristoyl-CoA to the amino-terminal glycine, a process that is essential to *Cryptococcus* viability at 37°C [73]. *Cryptococcus RAS1* gene encodes the RAS homologue which regulates filamentation, mating and growth at high temperature [79]. RAS1 has been shown to act in conjunction with other (downstream) Rho-type GTPases (the Cdc42 paralogs -Cdc42, Cdc20 and Cdc24, and Rac) to control morphogenesis and pathogenesis [80, 81]. Double mutation of *ras1* and any of these proteins results in polarized growth, cytokinesis, and cell cycle progression defects which are accompanied with formation of multiple incomplete buds or large unbudded cells [79]**.**

As a virulence factor, *ROM2* gene is involved in actin and microtubule organization at elevated temperature and hence *Cryptococcus rom2* mutants are hypersensitive and succumb to high temperature conditions with cellular defects in cell morphology and division [78]. Temperature-sensitivity and thermotolerance are regulated by different genes and signal transduction pathways that are also associated with *Cryptococcus* morphogenetic traits (e.g. shape, size, cell cycle progression and ploidy) and/or proliferation traits (e.g. mating, replication and viability) [73, 74, 80-85].

1.6.1.2 Carbon dioxide

Transition from natural ecological niches (trees or soil) to a mammalian host environment requires *Cryptococcus* to adapt and survive higher CO_2 levels (5%) of the mammalian host. The most dramatic biological response of *Cryptococcus* to CO_2 is enchanced capsule

biosynthesis (a key virulence factor) [86, 87]. Ren *et al*. has demonstrated that prolonged incubation in high CO_2 can effectively stimulate the formation of monokaryotic hyphae (filamentation) and spore development in *C. gattii* [88].

*Cryptococcus'*s ability to utilize CO_2 is associated with conversion of CO_2 into bicarbonate ions (HCO_3^-) via a hydration process which is catalysed by carbonic anhydrases (CA) [86, 87]. In *C. neoformans*, the class of CA involved in this conversion is b-CA (beta-carbonic anhydrase). b-CA is encoded by *CAN2* gene which is a growth factor in low CO_2 levels [86, 87] but dispensable for *in vivo* proliferation and virulence of *C. gattii* [88]. Mutation in *CAN2* gene results in a growth defect when *C. neoformans* is exposed to ambient environment but this defect is rescued within the host environment (with a higher *in vivo* concentration of CO_2).

In a CO_2-deprived condition, HCO_3^- (generated from CO_2 conversion) stimulates the activity of an enzyme-adenylyl cyclase (Cac1) which in turn activates the cAMP-signaling pathway [74]. This pathway controls major virulence determinants such as capsule biosynthesis. Although CA and Cac1 have been identified as the main CO_2-sensing enzymes in *C. neoformans*, their role in a high CO_2 environment is dispensable. Rather, HCO_3^- is abundant and spontaneously generated in the CO_2-high host environment and drives the expression of capsule induction signals [87, 89]. It worth mentioning that CO_2-HCO_3^- inter-conversion, especially in the pulmonary niche, contributes to the pulmonary pH, which is another salient factor influencing the adaptive behavior and cellular processes of an infectious *Cryptococcus* [89, 90].

1.6.1.3 pH

Being a facultative intracellular pathogen, *Cryptococcus* can manipulate and survive within the internal acidic niche of macrophages during phagocytosis [53, 91]. Generally, microbial killing

is accomplished via acidification of the macrophage phagosome containing the infectious cells. Interestingly, *C. neoformans* is able to modulate the phagosomal pH through the acid-base property of its capsule [57].

Adaption to the dynamic pH levels of a human host is a universal phenomenon among human fungal pathogens. Fungal pathogens share a common transcription factor (Rim101/PacC) for sensing and coordinating cellular response to the acidic or neutral mucosal surfaces and lightly alkaline blood and tissues [61]. Fluctuations in pH stresses fungal cells and triggers dramatic phenotypic responses. For example, *Candida albicans,* via the CaRim101 pathway, switches from a yeast to hyphal growth when a pH is changed from neutral to alkaline [62, 92]. Although the Rim10/Pac pathway is conserved among fungal-species, its role in *Cryptococcus* is unique. Cryptococcal Rim101 regulates the cell wall structure and controls surface capsule re-modelling during adaptive response to the acidic pH of the pulmonary epithelial lining fluid [62, 90, 92, 93]. Exposure of highly immunogenic epitopes of their cell wall causes *rim101* mutants to paradoxically provoke hyper-inflammatory responses in animals [90].

1.6.1.4 Effect of pulmonary epithelial lining fluid on *Cryptococcus*

The pulmonary epithelial lining fluid (ELF) is a thin superficial layer of the lung mucosa, the physical barrier that first encounters inhaled microorganisms [93-95]. ELF spans the entire respiratory tract, but its chemistry and physiology vary between the conducting airways and the alveoli where it is primarily comprised of pulmonary surfactants [93, 95, 96]. The pulmonary surfactant is composed of lipids and proteins. The surfactant proteins comprise four specific proteins labelled as SP-A, -B, -C, and -D; serum proteins and a wide variety of hydrolases which are derived from alveolar cells: macrophages, monocytes, lymphocytes, neutrophils, and type I and II epithelial cells [96, 97]. The ELF accommodates these innate

immune cells and, through their secretions, provides key immunomodulatory compounds involved in fighting against inhaled microbial particles [98, 99].

As an innate immune factor, human ELF has been implicated in modifying the cell surface of *Mycobacterium tuberculosis* (a bacterial intracellular pathogen) in a way which favours bacterial infection [100, 101]. Similarly, being a component of ELF, surfactant protein D has been implicated in enhancing proliferation and consequent survival of *Cryptococcus* in the host lungs [69]. To date, however, the role of other surfactant proteins remains unexplored.

1.7 Aims and objectives

My PhD research aimed to investigate the influence of the host extracellular niche on the biological functions of *Cryptococcus*. To date, relatively few studies have been undertaken to characterize the initial response of *Cryptococcus* after inhalation, prior to the onset of inflammation. Our lab made the serendipitous discovery, during a co-incubation of *Cryptococcus* and macrophages, that *Cryptococcus* extracellular cells proliferate better than those in media alone. This finding suggested that secreted compounds from these mammalian cell lines may impact on cryptococcal growth. Consequently, I set out to investigate how *Cryptococci* respond to the mammalian (pulmonary epithelial and pulmonary phagocytic) cells secretome. Using both lung epithelial and immune cells, I aimed to characterize how *Cryptococci* respond to secreted factors from both immune and non-immune host cells and predict the cryptococcal adaptive features in the lungs. By using *in vitro* conditions tailored to mimic host-specific environment, I aimed to induce the phenotypic traits (such as growth rate, cell body size and shape, cell capsule size, and cell wall thickness) that *Cryptococcus* exhibits

in response to the host environment and study the underlying metabolic and genetic mechanisms.

CHAPTER 2

LITERATURE REVIEW

CRYPTOCOCCUS GATTII: A UNIQUE PATHOGENIC YEAST WITH AN UNDERSTUDIED VILURENCE MECHANISMS

This chapter has been published:

L. Saidykhan, C. U. Onyishi and R. C. May. 2022. The *Cryptococcus gattii* species complex*:* unique pathogenic yeasts with understudied virulence mechanisms. PLOS Neglected Tropical Diseases (Proof of publication: appendix I).

2.1 Introduction

Cryptococcus gattii was first recognized and described as a distinct cryptococcal strain from *C. neoformans* in 1970 [102]. *C. gattii* and *C. neoformans* are the main causative agents of the life-threatening disease cryptococcosis in humans [103]. *C. neoformans,* which accounts for more than 99% of cases worldwide [104-106] typically presents as fungal meningitis in immunocompromised patients. In contrast, *C. gattii* occurs more commonly in otherwise healthy individuals and can often present as fungal pneumonia. During the 20th century, most research considered *C. gattii* and *C. neoformans* to be interchangeable in their biology. However, the emergence of *C. gattii* as the cause of the most devastating and unprecedented fungal outbreak in healthy population [107, 108] refocused attention on this species and, as a result, recent researches have highlighted key differences between *C. gattii* and *C. neoformans*. In particular, the apparently low propensity for *C. gattii* to disseminate from the lung to the central nervous system, and its ability to act as a primary pathogen in healthy individuals, remain key unanswered questions [5, 71, 72].

2.2 Phylogeny and speciation

Since *C. gattii* divergence from *C. neoformans* [109, 110], *C. gattii* has maintained diversity by continuous recombination and evolved into novel lineages with significant genetic diversity that warranted their classification into monophyletic genotypes [110-112]. Within the *C. gattii* species complex [30], *C. deuterogatti*/VGII has been identified as the basal lineage [109, 110, 112]. *C. gattii*/VGI, *C. tetragattii*/VGIV and *C. bacillisporus*/VGIII diverged from VGII approximately 12.4 million years ago [110, 113]**.** Thereafter**,** *C. tetragattii*/VGIV diverged from *C. bacillisporus*/VGIII and *C. gattii*/VGI sister clades 11.7 million years ago and *C. bacillisporus*/VGIII from *C. gattii*/VGI 8.5 million years ago.

To date, the majority of *C. gattii* studies have focused on VGII/*C. deuterogattii*, because of its exceedingly high pathogenicity [107, 114] and its role as the predominant etiological agent of the devastating Pacific Northwest Outbreak (PNW) [107, 108, 115, 116]**.** VGII is not only the origin of the outbreak [23, 117] but also possesses a high recombination frequency (via sexual macroevolution and asexual microevolution) [118] producing the highly clonal lineages VGIIa, VGIIIb, VGIIc (novel) and VGIIx (novel) which were responsible for the dissemination of the outbreak [1, 107, 118, 119]. The high clonality of the VGII subtypes has been found to emanate from VGII exhibition of the non-classical same-sex mating where sexual reproduction occurs between two alpha mating-types (MATα- MATα) parents [23] which has only been previously described in *C. neoformans* [120]. Hence, the PNW outbreak owes its origin and dissemination to this VGII-specific reproductive phenotype.

2.3. Morphological differences between *C. gattii* and *C. neoformans*

Most of the virulence-related phenotypic differences between *C. gattii* and *C. neoformans* are morphological. Within the *Cryptococcus* species complex, variation in morphological traits such as cell body/capsule size, shape, budding, surface morphology, and cell wall structure and composition are key factors employed not only for the identification of the different cryptococcal lineages [13, 20, 121-123], but also provide justification for their elevation to distinct species [30]**.** In an *in vitro* study of 70 cryptococcal clinical isolates (53 *C. neoformans* and 16 *C. gattii*), Fernandes *et al.* documented that cellular and capsular enlargement in response to a host-relevant environment is more common in *C. gattii* while capsule shedding and production of micro cells were primarily *C. neoformans* traits (Table 2) [124]. In the same study "giant cells" (also known as titan cells [50]) measuring >15 μm were predominantly found in *C. gattii* rather than *C. neoformans* (50.0% vs 10.75%, respectively); an observation that was recapitulated in a *Drosophila* model of infection [125].

Table 2. Comparison of morphological attributes between 70 *C. gattii* and *C. neoformans* clinical isolates from HIV/AIDS patients in Botswana-Africa (Adapted from [124] and summarized)

Species/genotype (No. of isolates)	Mean Cell diameter (µm)	Mean Capsule thickness (µm)	Giant cells (%)	Micro cells (%)	Shed capsule (%)
C. neoformans/ VNI (17)	7.0	5.5	12	82	94
/ VNII (2)	6.9	3.9	0	0	50
/VNBI (25)	8.3	7.3	20	52	80
/VNBII (9)	7.1	5.3	11	44	67
All *C. neoformans* (53)	**7.32**	**5.5**	**10.75**	**44.5**	**72.75**
C. gattii /VGI (1)	10.2	15.7	50		0
C. tetragattii /VGIV (16)	9.9	9.3	50	0	0
All *C. gattii* (17)	**10.05**	**12.0**	**50**	**0**	**0**

Using an *in vitro* titan-induction system dsecribed in chapter 6, we showed that the capacity to produce titan cells is more abundant in *C. gattii* than *C. neoformans* [126]**.** Interestingly, this correlates with a 'staggered' cell cycle in *C. gattii*, in which cell size increase precedes DNA replication – something that is not seen in *C. neoformans* [126]**.** Whereas *C. neoformans* titan cells undergo cell division to produce daughter cells [49, 71, 126, 127]**,** *C. gattii* titan cells exhibit a growth arrest to form large unbudded cells [126] (Figure 2.1)**.** It is possible that this

difference may partially explain *C. gattii's* lower ability to disseminate outside the lungs, since *C. neoformans* titan cells likely rely on their small-sized daughter cells for dissemination [22, 23].

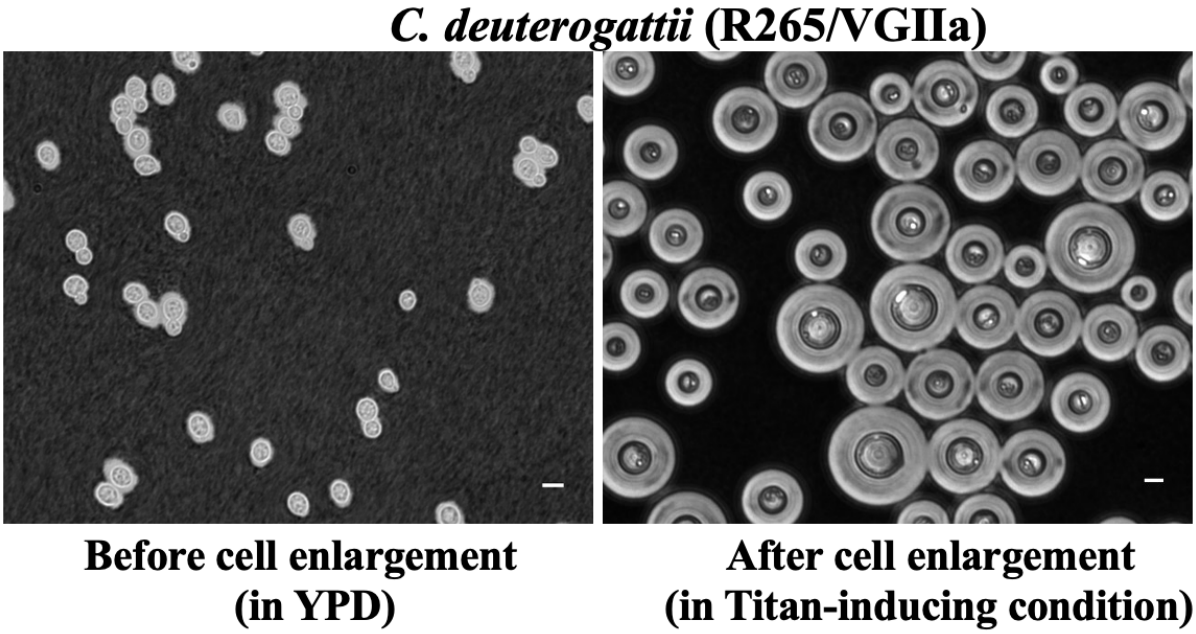

Figure 2.1 Micrograph showing the budding nature of *C. gattii* yeast (left panel) vs Titan (right panel) cells [126]**.** Titan induction was performed by first growing cells in YPD overnight, followed by growth in RPMI at low density for 72 hours at 37 °C in an atmosphere of 5% CO_2. Scale bar=5µm .

These morphological differences also lead to differences in the host response. For example, the presence of enlarged *C. gattii* cells was associated with high $CD4^+$ T cell count [124], whilst the formation of small phenotype 'micro' cells by *C. neoformans* correlates with meningeal irritation and an aggressive inflammatory response.

Compositional differences in capsule are also likely to play a major role in varying virulence profiles. While exploring the interaction of *C. gattii* with the phagocytic amoebae *Acantheamoeba castellanii*, Malliaris *et al.* [128] discovered a significantly lower phagocytosis profile and reduced virulence of an acapsular cryptococcal mutant strain, *cap67*, when the

mutant strain was coated with capsular extract from *C. gattii*, versus extract from *C. neoformans.* Although the underlying mechanism is not known, the result suggests the presence of structural difference(s) in *C. gattii* capsular polysaccharide which have a direct impact on virulence.

After the polysaccharide capsule, the most important virulence determinant of Cryptococci [129, 130] is cell wall melanisation [60, 121, 131-135]**.** Melanin is a negatively charged hydrophobic pigment formed by the oxidative polymerization of phenolic compounds [60] and its synthesis is catalysed by laccase. The production of melanin is not only essential for maintaining cell wall integrity but also protects the fungi from environmental stressors, such as UV light and high temperature, and the host immune system [136]. Interestingly, its pattern of distribution varies between strains; for instance, being homogenous in the VGII/*C. deuterogattii* hypervirulent outbreak strain CDCR265 [121] but heterogeneously distributed in *C. neoformans* H99. Interestingly, in a *Galleria melloella* infection model, melanization profiles (as determined by laccase activity) of the four *C. gattii* molecular types has been directly associated to virulence, such that *C. gattii* strains with higher melanin production showed higher lethality towards *Galleria* larvae [121]**.**

2.4. Immunomodulatory attributes of *C. gatttii*

The morphological and molecular traits of *C. gattii* discussed above influence how the host immune system responds to infection. The *C. gattii* outbreak in the Pacific Northwest (outside its regions of endemicity) that started in 1999 [137] had a mortality rate ranging from 8.7% to 50% even when treated with antifungal drugs [138-143] and highlighting significant differences in the host response to this infection.

2.4.1 Innate Immune Response to *C. gattii*

Cryptococcal infection begins with the inhalation of the fungi into the lungs. Lung resident macrophages are among the first host immune cells that inhaled fungi interact with; however, there are relatively few studies that investigate the precise mechanisms by which phagocytes respond to the presence of *C. gattii* in the host. It has been shown that the *C. gattii* capsule, which is composed of a majority glucuronoxylomannan (GXM) and a minority galactoxylomannan (GXMGal) polysaccharide, functions as a fungal virulence factor and has antiphagocytic properties [6]. The phagocytosis of foreign particles is initiated by the recognition of pathogen associated molecular patterns (PAMPs) by host pattern recognition receptors (PRRs), such as members of the Toll-like Receptor (TLR) family and the C-type Lectin Receptor (CLR) family [144]. GXM from *C. gattii* serotype B (VGII/*C. deuterogattii*) was found to be recognised by Dectin-3, a CLR, ultimately leading to NF-κB and ERK-dependent inflammatory responses (Figure 2.2A) [145]. In the same study, wildtype and *Dectin3*$^{-/-}$ mice were infected with *C. gattii* serotype B (VGII/*C. deuterogattii*) intratracheally, and it was observed that *Dectin3*$^{-/-}$ mice had decreased survival, greater lung and brain fungal burden, and decreased TNF-α and IL-6 production (Figure 2.2B). Thus, engagement of Dectin-3 with *C. gattii* GXM may activate a broader anti-cryptococcal immune response. In another study, HEK293A cells transfected with TLR2/1 and TLR2/6 were able to induce NF-κB activation after stimulation with GXM isolated from five different cryptococcus strains among which were *C. gattii* (VGII/*C. deuterogattii*) and VGIII/*C. bacillusporus* and *C. neoformans* (VNI) *and C. deneoformans* (VNIV) [146]. Interestingly, GXM from the VGII/*C. deuterogattii* (*C. gattii*) strain resulted in the greatest activation of NF-κB, suggesting the existence of structural and immunomodulatory differences between the strains [146] in a way that is reminiscent of the study by Malliaris *et al.* [128] discussed above. The five GXM samples were also used to stimulate nitric oxide (NO) production by RAW264.7 macrophages,

and it was found that GXM samples from both *C. gattii* strains were able to induce NO production, whilst those from three *C. neoformans* strains did not [146].

In a study that sought to define the cytokine profile produced by cryptococcal infection, human peripheral blood mononuclear cells (PBMCs) from healthy individuals were infected with heat-killed *C. gatti* and *C. neoformans* strains. It was found that *C. gattii* induced a greater expression of IL-1β, TNF-α, IL-6, IL-17 and IL-22, compared to *C. neoformans* [147]. Meanwhile, there was no difference in IL1Ra levels between the strains. Lastly, it was observed that the modulation of *C. gattii*-induced cytokine production required TLR4 and TLR9, but not TLR2.

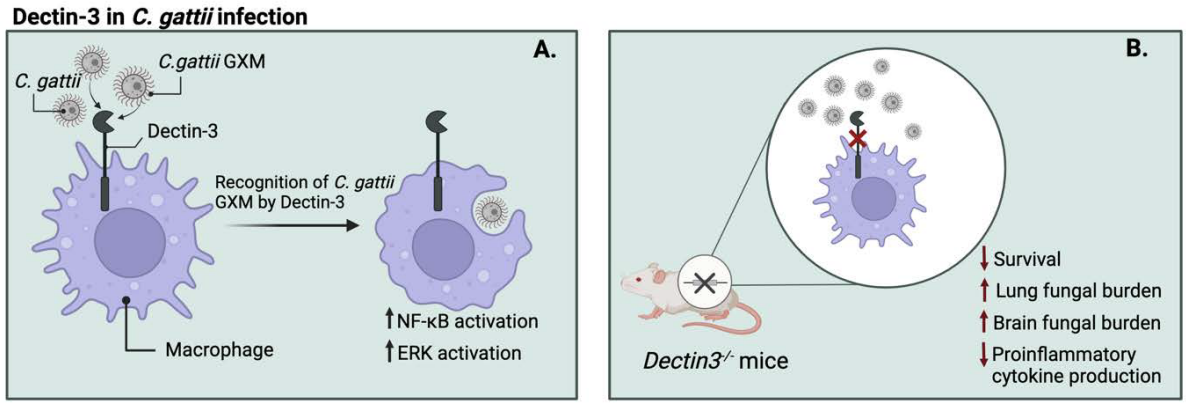

Figure 2.2: The role of Dectin-3 in host response to *C. gattii* infection *in vitro* and *in vivo*. (A) The C-type lectin receptor, Dectin-3, recognises *C. gattii* capsular glucuronoxylomannan (GXM) [145]. The recognition of GXM leads to the activation of NF-κB and ERK signalling pathways to drive proinflammatory cytokine production. (B) Dectin-3 deficient mice showed increased susceptibility to *C. gattii* infection [145]. Figure created with BioRender.com

2.4.2 Adaptive Immune Response to *C. gattii*

The uptake of fungi into phagosomes and subsequent phagosome maturation results in the degradation of the fungus and the presentation of fungal peptides on major histocompatibility complex (MHC) molecules [148]. These peptides are then recognised by $CD4^+$ T cells, thereby activating the adaptive immune response [149]. Additionally, the cytokine profile produced by the activation of PRRs results in the differentiation of naïve T cells into Th1, Th2 or Th17 cells [150]. The Th1 and Th17 responses are known to be protective against *C. neoformans, Candida albicans and Aspergillus fumigatus* [151-153]. Meanwhile, the Th2 response is anti-inflammatory and promotes fungal survival and dissemination in *Cryptococcus* [148, 154]. It has been shown that mice infected with *C. gattii* R265 (VGII/*C. deuterogattii*) strain had a significantly lower number of Th1 and Th17 cells in their lungs compared to those infected with *C. neoformans* [59]. This suggests that *C. gattii* is able to successfully infect immunocompetent hosts by dampening the activation of the protective Th1/Th17 response and enhancing the non-protective Th2 response [59]. Also, the diminished Th1/Th17 response was likely driven by a decrease in the expression of MHC-II on the surface of dendritic cells from *C. gattii* infected mice. Huston *et al.* 2013 [155], have also shown that dendritic cells infected with *C. gattii* fail to exhibit increased expression of MHC-II molecules, CD86, CD83, CD80, and CCR7 which are needed for T cell activation. Therefore, *C. gattii* is able to subvert dendritic cell mediated activation of the adaptive immune response.

However, all these studies point to the existence of significant variation in immune response to *C. gattii* and *C. neoformans* infection. As more is understood about host interaction with *C. gattii*, novel therapeutic agents can be developed to decrease the case-fatality rate of infection with cryptococci.

2.5 What are the drivers of the *C. deuterogattii* Pacific Northwest outbreak?

In 1999 an outbreak of *C. gattii* (now recognised as *C. deuterogattii*) was identified in British Columbia which went on to become the largest life-threatening primary fungal outbreak in a healthy population. This unprecedented outbreak has driven an intense research effort to discover the underlying determining factors [114, 115, 156, 157]**.** Over the last decade, studies focused on outbreak strains revealed a hypervirulent *C. gattii* molecular type-VGII/*C. deuterogattii,* to be the primary agent driving the pathogenesis [107, 158, 159] and spread [23, 160] of the outbreak.

VGII/*C. deuterogattii* outbreak isolates harbour several unique cellular and genetic attributes that contribute to their hypervirulence and pathogenicity. Compared to other *C. gattii* lineages VGII outbreak strains display higher resistance to host immune defence mechanism [158, 159] and an overall increased survival profile within the host [159, 161]. Upon phagocytosis by macrophages, *C. gattii*/VGII responds to the host oxidative burst by triggering a rapid intracellular proliferation [158]. Studies revealed that there is in fact a 'division of labour' mechanism where a subpopulation of the VGII outbreak isolates undergo growth arrest (driven by mitochondria fusion) , thereby facilitating the rapid proliferation of neighbouring fungal cells [159], in a process that is mediated through the exchange of extracellular vehicles (EVs) [161]. Interestingly, the pattern of titan cell formation also differs in this outbreak lineage (discussed above) and it will be interesting to explore and potentially establish the correlation between this unique VGII-titan feature, division of labour responses and their combined influence on virulence.

In additional to cellular phenotypes, novel genomic traits found in PNW outbreak VGII isolates are thought to contribute to their hypervirulence [113, 119]. Genomic analysis among the four VG lineages reveals that, unlike other VG lineages, VGII outbreak isolates have acquired genes

encoding proteins involved with membrane trafficking [Friend of Prmt1 (Fop)] and heat tolerance [heat shock protein 70 (HSP70)]- that are known to be required for virulence in *C. neoformans* [162]. Perhaps the most striking genomic trait of VGII is the lack of RNA interference (RNAi) machinery due to the absence of genes encoding the Argonaute proteins Ago1 and Ago2 [113], PAZ, Piwi, and DUF1785 genes which are key regulator of the RNAi machinery in *C. neoformans* [119, 163]**.** In fact, analysis from whole genome studies discovered a total of 146 genes (including the RNAi-associated ones) missing in VGII outbreak isolates which is three times more than those lost in VGI-III-IV combined [119]. Although the true significance of the absence of these genes/pathways as a whole is not yet elucidated, it is likely that they contribute to the unique host-pathogen interaction seen in this lineage [23, 164].

2.6 Understudied virulence-associated phenotypes of *C. gattii*

Studies elucidating the virulence of *C. gattii* phenotypes and their impact on pathogenesis and disease outcomes are somewhat overshadowed by that of *C. neoformans* [156]. Often, the biology, virulence factors and pathogenicity of *Cryptococcus* are highlighted using *C. neoformans* as a model or the primary theme of study [130, 134, 165, 166]. Below are some examples of understudied *C. gattii* virulence phenotypes.

2.6.1 Capsule

The cryptococcal polysaccharide capsule is essential for both cellular function and pathogenesis of *Cryptococcus*, protecting the fungus against desiccation in the environment and playing the synergistic role of a shield and virulence mechanism in animal host [129, 130]. Evidence has shown that capsular size and its impact on host immune response in *C. gattii* differs from that of *C. neoformans* [124, 164]. Despite these differences in capsule properties,

the biosynthesis properties [167], biophysical properties [130, 168-170] and immunogenic properties [171] of cryptococcal capsule have primarily been characterized in *C. neoformans*. Although the physical impact of capsule on fungal biology is likely to be similar for both species, the impact of varying capsule composition on *C. gattii* virulence remains less well understood [172].

2.6.2 Morphogenesis

The most dramatic host adaption phenotype exhibited by *Cryptococcus* is the formation of titan cells [12, 15, 49], a phenomenon that has thus far been largely studied in *C. neoformans* [12, 173-176]. We and others have recently investigated titan cell formation in *C. gattii*, which has revealed some subtle differences in this species, described in the following chapters. The impact of these differences on the *C. gattii*-host interaction remains largely unknown [177-179]**.** Similarly, whilst several signalling pathways, receptors and genes have been identified as driving titan cell formation in *C. neoformans* [including the cyclic AMP (cAMP)/protein kinase A (PKA) pathway (putatively associated with *C. neoformans* pathogenesis), G protein-coupled receptors (Gpr4 and Gpr5), St3a [50], and the CLN1 genes [176]], such investigations are yet to be performed with *C. gattii.*

2.6.3 Extracellular vesicles

Extracellular vesicles (EVs) are rounded bilayered particles produced by prokaryotic and eukaryotic cells to mediate intercellular communication by transferring information between cells [180]. EVs have significant roles in the cellular and pathogenic lifestyle of cells including stress response, intercellular competition, lateral gene transfer (via RNA or DNA), pathogenicity and detoxification [181]. The first fungal EV was described in *C. neoformans*

and therefore the biology of EVs and its role in *C. neoformans* virulence is well studied and documented [182-185]. Cryptococcal EVs are carriers of several virulence molecules such as capsular GXM, laccase, urease, and a repertoire of immunogenic proteins and thus have been termed as "virulence bags" [184, 185].

The biological and functional features of EVs including biosynthesis, secretory pathways, composition, structure, virulence properties and mechanism, influence in pathogen-host interaction, and immunogenic-related attributes have been well-characterized in *C. neoformans* [182, 184-187]. However, our knowledge and concepts of *C. neoformans*-derived EV cannot be directly applied to *C. gattii,* since evidence has shown distinctive features of EVs in the two species [182]. For instance, the size of *C. deuterogattii* EVs is significantly smaller than *C. neoformans* and *C. deneoformans* [182]. Although homologous EV-protein families, such as the putative glyoxal oxidase (Gox protiens) and Ricin-type beta-trefoil lectin domain-containing protein (Ril), were characterized in all three species, the Sur7/Pal1 family of tetraspanin membrane proteins was exclusive to *C. deuterogattii* [182]. Moreover, two of the ferroxidase Cfo proteins investigated were found to be expressed only by *C. deuterogattii* EVs but not in the two other species [188].

In terms of function, the novel discovery of *C. gattii* EV-based long-distance pathogen-to-pathogen communication (which has not been reported for non-*gattii* strains) [161], its role in exploiting host immune cells and ultimate impact on virulence [159, 161] provide strong evidence that the functional mechanism of EVs in *C. gattii* is distinct from *C. neoformans*. This discovery and other findings on *C. gattii*-specific EV traits highlight the need for probing the already-studied concepts of *C. neoformans*-derived EV and novel EV-associated phenotypes in *C. gattii*. Research focused on *C. gattii* EVs will not only diversify our understanding of cryptococcal EVs but also holds potential for revealing new paradigms around the biological and pathogenic functions of fungal EVs more broadly.

I conclude this section with a list of *C. neoformans* phenotypic virulence traits which are somewhat neglected and could potentially be studied in *C. gattii* (Table 3.0).

Table 3: List of virulence-related phenotypic traits whose underlying molecular, genetic and metabolic mechanism has been studied in *C. neoformans* but not *C. gattii*.

Virulence factor	**Virulence factor regulatory genes/pathways**	**Mode of action/functional mechanism**	**References**
Capsule	*Cap59* gene	Encodes transmembrane proteins and is involved in GXM synthesis	[189] [190, 191]
	Cap64 gene	Complements an acapsular strain and is required for capsule synthesis	[192]
	Cap60 gene	Encodes proteins localized to the nuclear membrane and cytoplasm; required for both capsule formation and virulence	[193]
	Uge1p gene; putative UPD-galactose epimerase	Required for GalXM synthesis and consequent crossing of the blood-brain barrier	[194]
	Putative G1/S cyclin (Cln1)	Regulates the cell cycle during capsule formation; required for virulence at 37ºC	[195]

	Rim101 transcription factor via cAMP/PKA pathways	Required for polysaccharide attachment to the cell wall surface	[196]
Titan cell formation	CLN1 gene	Encodes *C. neoformans* cyclin Cln1; critical for balancing DNA replication and cell division during titan cell formation; negatively regulates *in vivo* titan cell formation	[176]
	Rim101 transcription factor via cAMP/PKA pathways	Required for the generation of titan cells	[48]
	Usv101 transcription factor, GPA1, CAC1, Ric8, and PKA1 genes associated with cAMP/PKA pathway	Negatively regulates titan cell formation *in vivo* and *in vitro*	[197] [71] [48]

Cell wall	G1/S cyclin (Cln1)	Required for cell wall stability and production of melanin; protective against oxidative damage; positively regulates the production of laccase	[198]
Degradative enzymes (proteinase, phospholipases, urease)	Proteinase	Proteolytic activity against host proteins including collagen, elastin, fibrinogen, immunoglobulins, and complement factors	[199]
	Phospholipase enzyme (PLB1 gene)	Regulates phospholipase B (PLB), lysophospholipase hydrolase, and lysophospholipase transacylase activities; Positively regulates virulence *in vivo* and is required for intracellular growth and vomocytosis	[200] [201]
	Urease (Ure1 gene)	Required for virulence in mice, CNS invasion; and vomocytosis	[202] [201]
Ability to grow at physiological temperature	CNA1 gene	Encodes the *C. neoformans* calcineurin A; required for growth at mammalian physiological temperature; required for virulence in immunocompromised animal model	[76]

2.7. Concluding remarks

Despite their similar appearance, it is now clear that many features of *C. gattii* are remarkably different from those in *C. neoformans* (Figure. 2.3). However, studies elucidating the virulence of *C. gattii* phenotypes and their impact on pathogenesis and disease outcomes have been overshadowed by those focusing on *C. neoformans*. While the prevalence of cryptococcosis due to *C. neoformans* makes this a logical choice, several unique features of *C. gattii* warrant further investigation such as its ability to infect otherwise healthy individuals, its role in an unprecedented fungal outbreak and several distinct phenotypic traits that differ from those in *C. neoformans*. Such features are likely to underlie important differences in clinical presentation between the two pathogens, most notably in their varying patterns of dissemination from the lungs to the brain. In the future, it will be important to revisit many paradigms of cryptococcal pathogenesis in *C. gattii*, and indeed other *Cryptococcus* species, and in doing so reveal the full range of diversity within this genus.

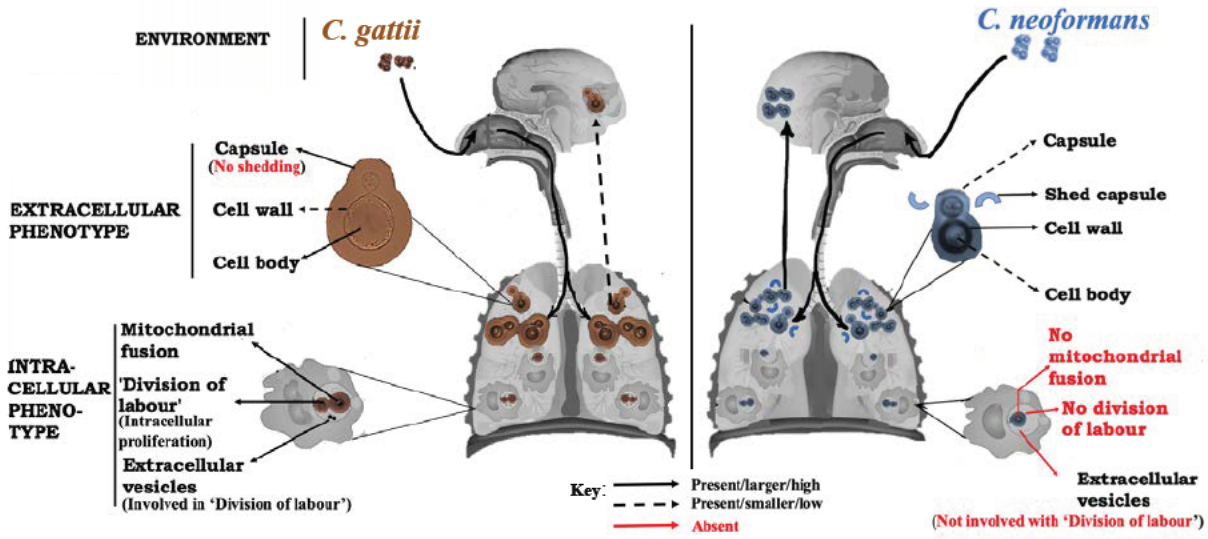

Figure 2.3: Schematic diagram illustrating *C. gattii* distinct phenotypic virulence traits as compared to *C. neoformans*. Upon inhalation from the environment, *C. gattii* yeast cells/spores responds to the lung extracellular niche by exhibiting phenotypic traits including

larger capsule (with less immunogenic properties); larger cell body (with higher degree of homogeneity) and thinner but more compacted cell wall with higher chitosan content than *C. neoformans.* The manner in which *C. gattii* exhibits these host adaptive traits is perhaps responsible for its low affinity to disseminate from the lungs to the brain. Within the host macrophage, the intracellular phenotypes (mitochondrial fusion and 'division of labour' proliferation mechanism mediated by extracellular vesicles) exhibited by *C. gattii* (which drives the fatal *C. gattii* outbreak) are absent in *C. neoformans.*

CHAPTER 3

MATERIAL AND METHODS

Major parts of this chapter have been published:

L. Saidykhan, Correia J, Romanyuk A, Desanti G. E, Taylor-Smith L, Makarova M, E.R Ballou, R. C. May. 2022. An in vitro method for inducing titan cells reveals novel features of yeast-to-titan switching in the human fungal pathogen *Cryptococcus gattii*. **PLOS Pathogens** (Proof of publication: appendix II).

L. Saidykhan, C. U. Onyishi and R. C. May. 2022**.** The *Cryptococcus gattii* species complex*:* unique pathogenic yeasts with understudied virulence mechanisms. PLOS Neglected Tropical Diseases (Proof of publication: appendix I).

3.1 Storage and maintenance of cell cultures

3.1.1 Cryptococcal strains

The cryptococcal wildtype and mutant strains used during this project are listed in Table 4. All the wildtype strains were isolates obtained from the May Lab fungal collection library, School of Bioscience, University of Birmingham, UK. The *C. neoformans ras1Δ* mutant strain was provided by Dr. Elizabeth Ballou (University of Exeter).

Table 4. Cryptococcal species and strains used in this study. Genotype and source are provided where available.

Species and strains	**Genotype**	**Source**
C. gattii WM265	VGI	Clinical isolate, Brazil
C. gattii WM179	VGI	Clinical isolate, Australia
C. gattii CBS8755	VGI	
C. gattii C384	VGI	
C. gattii NIH312	VGI	Clinical
C. gattii B4546	VGI	Clinical
C. gattii EJB11	VGI	
C. gattii MMCO8-897	VGI	
C. gattii CBS1508	VGI	
C. gattii CBS1873	VGI	
C. gattii R265	VGIIa	Clinical isolate, Vancouver, Canada
C. gattii CDCR271	VGIIa	Clinical isolate, immunocompetent patient,

		Kelowna, British Columbia, Canada
C. gattii ENV152	VGIIa	Environmental isolate, Alder tree, Vancouver Island, Canada
C. gattii ICB180	VGII	Environmental isolate, Eucalyptus tree, Brazil
C. gattii CBS10089	VGII	Clinical isolate, Brazil
C. gattii CDCR272	VGII	Clinical isolate, Greece
C. gattii B7735	VGIIb	Clinical isolate, Vancouver, Canada
C. gattii EJB11	VGIIb	
C. gattii EJB52	VGIIc	Clinical isolate, Oregon, USA
C. gattii CBS6955	VGIII	Clinical isolate, Oregon, USA
C. gattii CBS6993	VGIII	Clinical isolate, USA
C. gattii CBS1622	VGIII	
C. gattii WM1243	VGIII	
C. gattii B13C	VGIII	Clinical isolate, Asia
C. gattii CA2350	VGIII	Clinical isolate
C. gattii CA1227	VGIII	Clinical isolate
C. gattii LA584	VGII	Clinical isolate, Colombia

C. gattii B5464	VGIII	Clinical isolate, USA
C. gattii WM779	VGIV	Clinical isolate, USA
C. gattii B5742	VGIV	
C. gattii B5748	VGIV	
C. gattii CBS10101	VGIV	
C. gattii CBS1010	VGIV	Veterinary, South Africa
C. neoformans H99	VNI	Clinical isolate, USA
C. neoformans Kn99α	VNI	Clinical isolate, USA
C. neoformans Zc1	VNI	
C. neoformans Zc8	VNI	Clinical, Zambia
C. neoformans Z12	VNI	Clinical, Zambia
C. neoformans 125.91	VNI	Clinical, Tanzania
C. neoformans Tu369-2	VNI	Environmental isolate, Mopane tree bark, Botswana
C. neoformans HAMDANC C'3-1	VNII	Pigeon droppings, Belo Horizonte, Brazil
C. neoformans B3501	VNIV	Clinical isolate, usa
C. neoformans CBS6995	VNIV	Clinical isolate, USA

C. neoformans CBS8336	VNI	Wood of Cassia tree, Brazil
C. neoformans ras1Δ		

3.1.2 Cryptococcal culture conditions

Cryptococcal strains were grown overnight for 18hrs in 3mL yeast peptone dextrose (YPD) medium (2% glucose,1% peptone and 1% yeast extract) with shaking (240 r.p.m.) at 25 °C. Stock were frozen down in 20% glycerol and stored in -80 °C. Yeast cells from overnight cultures were collected (by centrifugation at 4000 r.p.m for 2 mins), washed three times with phosphate buffered saline (PBS), re-suspended in 3mL PBS and counted on a haemocytometer to determine the cell densities.

3.1.3 Mammalian cell line culture

Mammalian cell lines were defrosted rapidly from liquid nitrogen storage and grown in their respective media. The mammalian cell lines were: murine macrophage-like cells J774 [43], human lung epithelial cell line (A549) [203], and a continuous cell line of murine alveolar macrophages MH-S (ATCC CRL-2019) [204]. J774 cells were maintained in *Dulbecco's Modified Eagle Medium (*DMEM) supplemented with 10% foetal bovine serum, 1% L-glutamine (stock of 2 mM/mL), 1% penicillin/streptomycin (stocks of 100 units/mL penicillin and 100 units/mL streptomycin). The A549 cells were kept in the same media formula as the J774 except for the serum being heat-inactivated. The MH-S cells were maintained in RPMI 1640 media supplemented with 10% fetal bovine serum and 0.05mM of 2-mercaptoethanol. All three cell types were incubated in a humidified environment at 37°C with 5% CO_2 and used

between 3 and 15 passages. During sub-culturing, A549 and MH-S were detached by 0.25% trypsin and 0.53 mM EDTA solution while a cell scraper was used to gentle scrape J774 cells.

3.1.4 Mammalian cell line stocks

Stocks of the mammalian cell lines were made by freezing down the cells in filter sterile freezing media: 50% FBS, 40% DMEM (for J774 and A549) or RPMI (for MH-S) and 10% Dimethyl sulfoxide (DMSO). One millilitre of these cells was transfer to a cryovial and frozen for 24 hr at -20°C and then -80°C respectively. Finally, the cells were quickly transferred and stored in a liquid nitrogen.

3.2 Generation of mammalian cells conditioned media and cryptococcal responses

3.2.1 Production of conditioned media

The cell lines were grown in their respective serum-free or serum supplemented growth media and allowed to reach 80% confluence (Figure 3.1). After 18 hours of incubation, supernatants were collected, aliquoted and stored at -20 °C for subsequent works. The conditioned media were denoted as cDMEM (conditioned DMEM) or cRPMI (conditioned RPMI).

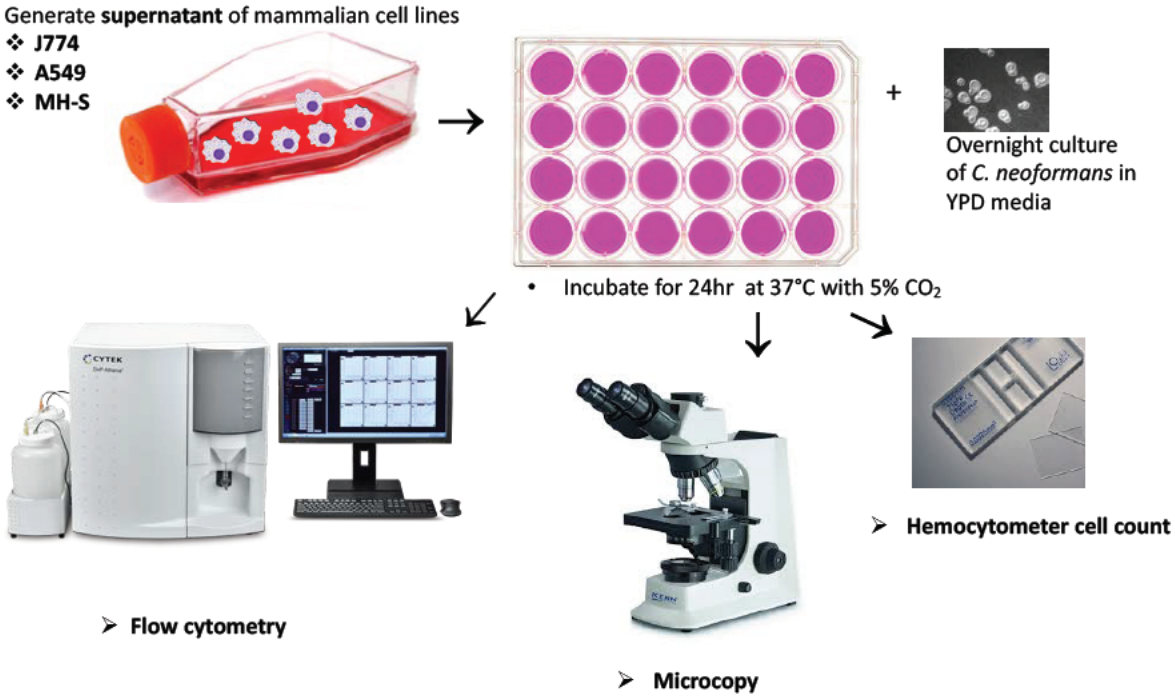

Figure 3.1. Experimental design illustrating the approach and equipment employed for: generation of conditioned media from the mammalian cell lines (J774, A549 and MH-S); determining the proliferation, morphology (capsule and cell body size) and ploidy of *Cryptococcus* before and after exposure to the conditioned media.

3.2.2 *Cryptococcus* proliferation assay

The tested cryptococcal strains were grown in naïve or conditioned media from the mammalian cell lines at $5x10^5$ cells/mL for 24 hours at 37°C in 5% CO_2. After incubation, the samples were mixed via pipetting and sufficiently diluted to enable accurate counting on haemocytometer. The total number of fungal cells were calculated for each sample well. In addition to haemocytometer counting, a colony forming unit (CFU) test was performed to determine the fungal cell viability. The mixed samples were serially diluted tenfold (using a 96 well plate), plated out on YPD agar and incubated for 48 hours at 25°C. After 48 hours, the CFU was determined by counting the fungal cell colonies of each dilution factor for each

sample. Finally, fungal cell viability was confirmed by comparing the CFU results with of the haemocytometer counting (Figure 3.1).

3.2.3 Generation and size measurement of titan-like cells from conditioned media

Cells of cryptococcal strains from YPD overnight culture were inoculated in 24 well plates containing naïve or conditioned media from the mammalian cell lines at $5x10^4$ cells/mL concentration. The plate was incubated for 24 hours at 37°C in 5% CO_2 without shaking. To prepare for microscopy imaging, the cells were collected in 1.5 mL tubes (Eppendorf), washed in PBS, fixed with 4% methanol-free paraformaldehyde for 10 mins and stained with calcofluor white (CFW, 10 µg/ml) for another 10 mins [51]. Finally, the cells were pelleted, counterstained with India Ink (Remel; RMLR21518) to visualize the capsule and images, and imaged on a Nikon Eclipse TE200-U microscope. The total cell and cell body diameters (figure 3.2) were measured using Image J software and the capsule size was calculated by dividing the difference between the cell body diameter and the total cell diameter, by 2.

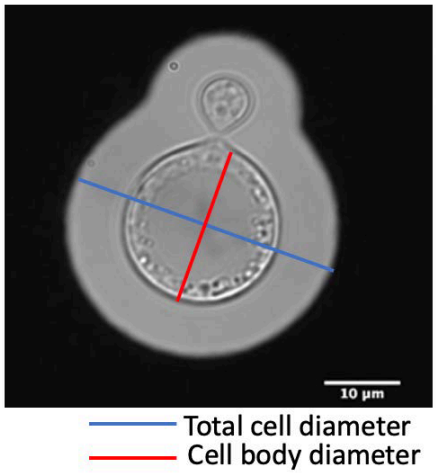

Figure 3.2 Cryptococcus titan-like cells generated by growth in conditioned media from mammalian cells. Total cell body (blue) and cell body diameter (red).

3.2.4 Physicochemical characterization of active compound from conditioned media

3.2.4.1 Heat stability and proteinase digestibility tests

Conditioned media from mammalian cell lines (J774 or MH-S) were heat inactivated by incubation in water bath at 90°C or 56°C for 1 hr. The heat-inactivated media was stored at -20°C and pre-warmed to 37°C when needed. Cryptococcal cells were grown in the heat-inactivated conditioned media at 37°C in 5% CO_2 for 24 hr. Proliferation rate was determined by cell count using haemocytometer while the capacity to generate titan-like cell formation was determined by measuring the cell body diameters.

The Proteinase digestibility tests was performed by mixing proteinase K with conditioned media at 5% final concentration followed by incubation at 37°C for 2 hr. The proteinase K treated samples were frozen at -20°C until required for testing cryptococcal response. Cryptococcal cells were grown in the proteinase K treated conditioned media at 37°C in 5% CO_2 for 24 hr. Proliferation rate was determined by cell count using haemocytometer while the capacity to generate titan-like cell formation was determined by measuring the cell body diameters.

3.2.4.2 Determination of molecular size via size exclusion

The molecular size of the active compound from conditioned media (J774 or MH-S) were determined using ultracentrifuge 50 mL tubes fitted with 30 kDa or 3 kDa size exclusion filters columns (Purchased from Merck, Millipore). Fifteen millilitres of the conditioned media was placed in the tube and centrifuged at 3000 g for 30 mins at room temp. The supernatant and flow through of the column were collected in a 15 mL falcon tubes for cryptococcal proliferation or titan-like cell formation assays.

3.2.4.3 Chloroform: methanol extraction

Conditioned media from J774 were extracted as described by Bligh et al. [205]**.** The J774 conditioned media was added to a mixture of chloroform/methanol (2:1, v/v) in a glass tube. One millilitre of distilled water was added to the mixture and shaken vigorously and centrifuged 4000*g* at 4 °C for 5 min. Thereafter, the aqueous phase was gently pipetted into a new tube. This process was repeated with the remaining chloroform fraction (bottom fraction) at least twice. Finally, the aqueous and chloroform fractions were dried appropriately and the dried samples were reconstituted in naïve media for phenotypic analysis.

3.2.5 Induction and cellular characterization of RPMI-induced Titan cells

3.2.5.1 *In vitro* induction of Titan cells in RPMI

Yeast cells from overnight cultures were collected (by centrifugation at 4000 r.p.m for 2 mins), washed three times with phosphate buffered saline (PBS), re-suspended in 3mL PBS and counted on a haemocytometer to determine cell densities [43, 206]. Except where otherwise noted, titan induction was achieved by inoculating $5x10^3$ yeast cells in 1 mL serum free-RPMI 1640 within a 24 well tissue culture plate for 24 hours to 21 days at 37°C in 5% CO_2 without shaking.

For generation of daughter cells, the 7 day old titan-inducing culture was passed through a >20µm cell strainer and >20µm-sized titan cells were re-cultured in YPD overnight. Then, the daughter cells were isolated by filtering the overnight culture using a 15µm cell strainer and collecting the flow-through.

3.2.5.2 Cell size measurement

Cells recovered from titan induced or YPD grown cultures were washed in PBS and fixed with 50% methanol. After Indian ink staining for capsule visualization, cellular images were obtained using a Nikon Eclipse TE2000-U microscope equipped with phase-contrast 20X optics. Cell body and capsule sizes for individual cells were measured by using ImageJ software in combination with automated measurement based on Circle Hough Transformation algorithm [207].

3.2.5.3 Cell wall and capsule

Cells were fixed with 4% methanol-free paraformaldehyde for 10 mins and stained with calcofluor white (CFW, 10 μg/ml) for another 10 mins [51]. Total chitin was determined by flow cytometry on an Attune NXT instrument, with quantification of CFW staining using FlowJo software. For capsule visualization, cells were counterstained with India Ink (Remel; RMLR21518) and images acquired using a Nikon TE2000 microscope and analysed using ImageJ software.

3.2.5.4 DNA content measurement Ploidy

RPMI and YPD grown cells were recovered, washed 3x in PBS, fixed in 50% methanol and stained with 3 ug/ml DAPI at 10^5 cells/mL. For each sample, about 10000 cells were acquired on an Attune NXT flow cytometer and the result was analysed using FlowJo v. 10.7.1. Cells were sorted for doublet and clump exclusion by using FSC-A vs FSC-H gating strategy and compared to control, YPD grown, yeast cells.

3.2.5.5 Nuclei morphology

Seven-day old titan cells, generated according to the *in vitro* protocol (Section 3.2.5.1) were collected, washed in PBS and fixed with 30% methanol for 10 mins. The fixed cells were DAPI stained for 1 hr in the dark and their nuclei were visualized with Zeiss Axio Observer at 63X magnification using bright-filed and DAPI channels.

3.2.6 Exogenous and endogenous regulators of titan cells formation

3.2.6.1 Quorum sensing effect

The quorum sensing Qsp1 (NFGAPGGAYPWG) and scrambled Qsp1 [(AWAGYFPGPNG), control] peptides were synthesized at the University of Birmingham and then dissolved in sterile distilled water at 1mM and frozen at -20℃ for future use. The peptides were then added to RPMI media at concentration of 20µM and R265 yeast cells from overnight culture were grown in the mixture at 37℃ in 5% CO_2 for 72 hr. Finally, the cell body size of R265 cells in the test media were analysed.

3.2.6.2 Identification of RPMI-titan inducing compound(s)/factors

RPMI-specific compounds (which are absent in DMEM) were supplemented to DMEM media and tested for capacity to induce titan cells in R265 (*C. gattii*). Accordingly, DMEM media was first supplemented with 'RPMI-specific' amino acids at their original concentration in RPMI: L-Glutamic acid (20 mg/L), L-Aspartic acid (20 mg/L), L-Arginine (200 mg/L), L-Glutathione (1 mg/L), L-Asparagine (50 mg/L) and L-Proline (20 mg/L). All the amino acids were purchase in powder form from Sigma-Aldrich and stock solutions were made by dissolving them according to manufacturer's instruction.

To investigate if the glucose concentration difference between RPMI (high concentration) and DMEM (low concentration) was responsible for titan cell formation, DMEM was supplemented with D glucose (Purchase from Sigma-Aldrich) at a final concentration of 2000 mg/L (RPMI concentration). D glucose was purchased in powder form and stock solution was prepare according to manufacturer's instructions.

Finally, DMEM media was first supplemented with other 'RPMI-specific' compounds at their original concentration in RPMI: Vitamin B12 (0.005 mg/L), Biotin (0.2 mg/L), and para-aminobenzoic acid [(pABA) 1.0 mg/L]. All these compounds were purchased from Sigma-Alrich in powder form and stock solutions were prepared according to manufacturer's instructions.

3.2.6.3 RT-qPCR and gene expression analysis

The extracted RNAs (section 3.2.7.1) from YPD grown and titan-induced cells were reversed transcribed (RT) to cDNA by using FastSCRIPT^{TM} cDNA Synthesis protocol (Catalogue Number: 31-5300-0025R]. In brief, 15µL of RNA samples were mixed with 1µL of RTase and 4µL of FastSCRIPT^{TM} cDNA Synthesis Mix (5X) before 30 min incubation at 42ºC and subsequent 10 min incubation at 85ºC. Quantitative PCR for the selected putative cell cycle genes was determined for each RT samples by mixing 2µL of the RT samples with 38µL master mixed of KAPA enzyme (KABA SYBR FAST qPCR Kits) and designed primers (table 5) and run in a real-time PCR detection system (CFX96 Touch Real-Time PCR Detection System; Ref. no. :1845096).

Table 5. List of cell cycle phenotypes of titan induced and associated genes

Induction time points	**Phenotype/Cell cycle phase**	**Cyclin gene in C. neoformans (*S. cerevisiae*)**	**Orthologous gene in R265 (function)**	**Primers**
24 hr	Bud formation/G1 & M	CNAG_02196 (CDC11)	CNBG_5339 (Septin)	GTCATTCCCGTCATTGGCAA ATCTTCCTCGGCGTCATAGG
3 days	Mitosis exist/ G1/S	CNAG_06092 (CLN1)	CNBG_4803 (Cyclin 1)	AGCTCCCAACGGTAGTATCG ATGTGGGAAGTGATGTCGGT
5 days	DNA REPLICATION/**S**	CNAG_03962 (MCM6)	CNBG_5506 (minichromosom-e maintenance protein 6)	CGAGCAAACTGTCAACACGA TCAGTTGTGGGTCCTCATCC
7 days	G2 arrest	CNAG_05406	CNBG_4446 (mitotic check point protein bub2)	ACCAGCCACCCATCTACTTC CTGCGTATCCTTTTGAGGCC
Gene control GAPDH			CNBG_1866 glyceraldehyde-3-phosphate dehydrogenase	GAAGGTCGTCATTTCCGCTC GCTTGTAGGCATCGAGGTTG

Gene expression level was obtained and normalized according to change difference with the housekeeping gene, *GAPDH*. Finally, the relative expression profile was expressed as a function of comparative threshold cycle (C_T) by using the follow formula (III):

I. Delta $C_T = C_{T\,gene} - C_{T\,GAPDH}$

II. Delta delta $C_T = C_{Tgene}$-average Delta C_T

III. Relative gene expression= $2^{-\text{delta deltaCt}}$

3.2.7 Molecular techniques

3.2.7.1 RNA extraction and purification

Total RNA extraction was performed on uninduced (YPD grown) and titan-induced R265 cells by employing the protocol of QIAGEN (RNeasy Micro Kit [50]); Cat. No./ID74004) with slight modification. Samples of overnight YPD grown, R265 cultures and titan-induced cells of the different time-points (24 hr, 72 hr, 5 days and 7 days) were harvested, washed three times in PBS, adjusted to ~10^6 cells/mL and pelleted in 1.5mL Eppendorf tubes. The cell pellets were flash-frozen in liquid nitrogen and stored at -80°C overnight. The cells were lysed by mixing in 400µL of RLT buffer, transferring to a 2 mL lysing tubes (MP Biomedicals™ 116960100) and beating with a bead beater (MP Biomedicals 116004500 FastPrep 24 Instrument Homogenizer) for thorough cell disruption. The homogenized sample was centrifuged for 3 min at 10,000xg at room temperature. The aqueous portion was separated, mixed with 70% ethanol at 1:1 ratio and transferred to an RNeasy Mini Spin Column. Finally, RNA extraction and purification were carried out as described in manufacturer's protocol, including purification through a gDNA eliminator column to remove DNA contamination.

3.2.7.2 Metabolic activity of titan cells

The metabolic state of R265 titan cells was confirmed by using FUN-1 reporter dye. The freshly obtained RPMI-induced 7 day old titan and YPD overnight (control) cells cultures were collected and aliquoted into two. Cells from an aliquot from the two conditions were heat-killed for 1 hr in a heating block (Stuart Heating Block). Both heat-inactivated and fresh cell samples were stained with Fun-l at 5µM for 30 mins. Microscopy images were taken with Zeiss Axio Observer at 63X magnification with fluorescent emission wavelength set at 590 nm [208].

3.2.8 Statistical analysis

All data analyses were performed with GraphPad Prism 6. The Shapiro-Wilk test was used to check normality of the data. Non-parametric (Kruskal-Wallis) test was applied for all the size distribution data where significant difference between the median cell (body or capsule) size was confirmed by $p<0.05$ and the number asterisks depict level of significance: *=$p<0.01$, **$p<0.001$, ***=$p<0.0001$ and ****=$p<0.0001$. In particular, the cell body size difference between 5 and 7 days titan-induced cells (Fig. 6.3A) was confirmed by Mann-Whitney test as size distribution for both time points were non-parametric (Shapiro-Wilk test). Normally distributed data was analysed by one-way ANOVA, where comparison between conditions was considered significantly different when $p<0.05$ and the number asterisks depict level of significance: *=$p<0.01$, **$p<0.001$, ***=$p<0.0001$ and ****=$p<0.00001$.

CHAPTER 4

ENHANCED CRYPTOCOCCAL GROWTH IN RESPONSE TO MAMMALIAN CELL SECRETED COMPOUNDS

During infection, *Cryptococcus* interacts with host immune cells such as macrophages and this interaction is classically characterized by binding (primarily via antigen-antibody mediated recognition) and internalisation of the fungus. Phagocytosed cryptococci can be destroyed through the activities of degradative enzymes deposited in the phagosome containing the fungal cells. However, not only has *Cryptococcus* developed mechanisms for complete avoidance of phagocytosis but it has also evolved various sophisticated tactics to resist and circumvent the enzymatic insult of the phagosome thereby enhancing intracellular survival. In addition to growth within cells, Cryptococci are also capable of extracellular growth, in particular within the granuloma [140].

Before an effective immune response is mounted, cryptococcal cells first encounter a host extracellular niches [209]. However, how this environment (in the lung, bloodstream, and central nervous system) influences cryptococcal adaptive behavior is poorly understood [63]. We made the chance discovery that *C. neoformans* exhibits an increased extracellular proliferation when co-incubated with J774 macrophages *in vitro*. Therefore, this chapter is dedicated to characterizing the enhanced cryptococcal growth in response to the secretome of mammalian cell lines and taking the first steps to identify the trophic factors underlying the enhanced proliferation.

4.1 Proliferative growth effect of J774 secretome on *Cryptococcus*

In our lab, we previously observed an enhanced growth of extracellular fungal cells when *Cryptococcus* was co-cultured with the mammalian cell line J774. To confirm if this enhanced growth was triggered by the supernatant of J774 and independent of the *Cryptococcus*-J774 physical contact, I generated conditioned media from J774 (‘conditioned’ DMEM, hereafter

referred to as CDMEM) and tested its effect on cryptococcal proliferation *in vitro*. Two *C. neoformans* (H99 and Kn99α) and one *C. gattii* (R265) strains were explored by measuring their growth rates after 24 hrs and 48 hrs incubation in CDMEM at 37°C in 5% CO_2 (initial inoculum= $5x10^5$ cells/mL). the naïve DMEM were in two forms: with and without serum (DMEM and sfDMEM) and their corresponding conditioned media were designated as CDMEM (conditioned-DMEM) and CsfDMEM (conditioned serum-free DMEM). Interestingly, the two *C. neoformans* strains, H99 and Kn99α, showed significantly increased replication in the conditioned media (both CDMEM and CsfDMEM), but growth of the *C. gattii* strain R265 was unaffected (Figure 4.1). This is suggestive either of a trophic factor contained in the J774 secretome which is absent in the naive media (sfDMEM) or, equally, that J774 may remove some molecule which is inhibitory to growth of *C. neoformans* strains, but not *C. gattii*.

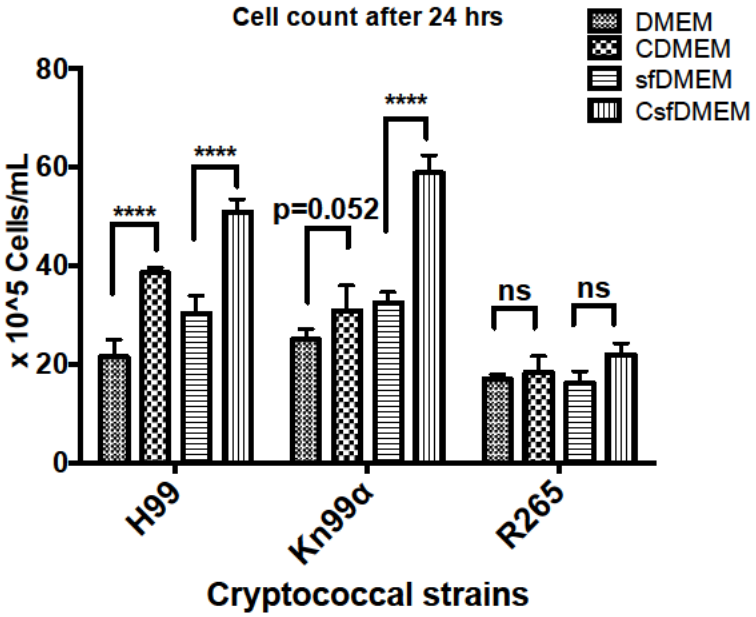

Figure 4.1 Proliferative effect of J774 conditioned media on of *C. neoformans* (H99 and Kn99α) and *C. gattii* (R265) strains. Yeast cells of the tested strains were grown in naive (DMEM or sfDMEM) and J774 conditioned media (CDMEM or CsfDMEM) at 10^5 cells/mL

for 24 hrs at 37°C in 5 % CO_2 and cell number was verified before and after incubation based on haemocytometer counting. The graph represents three biological repeats and statistical significance was verified by two-way ANOVA analysis where ****=$p<0.0001$ and ns=$p>0.05$.

I noted that the cell counts for H99 and Kn99α in sfDMEM were higher than that of DMEM. This implies an inhibitory effect due to the presence of serum [fetal bovine serum (FBS)]. This is in line with the fact that concentrations of serum above 10% inhibit growth [210]. On account of this finding I decide to use serum-free media for subsequent assays.

4.3 Heat stability and dose-dependence of the proliferative effect

The proliferative growth effect of J774 conditioned media on *Cryptococcus* was further characterized to find whether the impact of conditioned media is dose-dependent. The *Cryptococcus* strains H99 and R265, were grown in diluted conditioned media (1:1 v/v with sfDMEM) and the resulting proliferation was analysed. The proliferative effect of CsfDMEM was attenuated due to dilution and H99 proliferation was reduced although it did not reach statistical significance (Figure 4.2). This further suggests that the trophic factor enhances H99 proliferation in dose-dependent fashion.

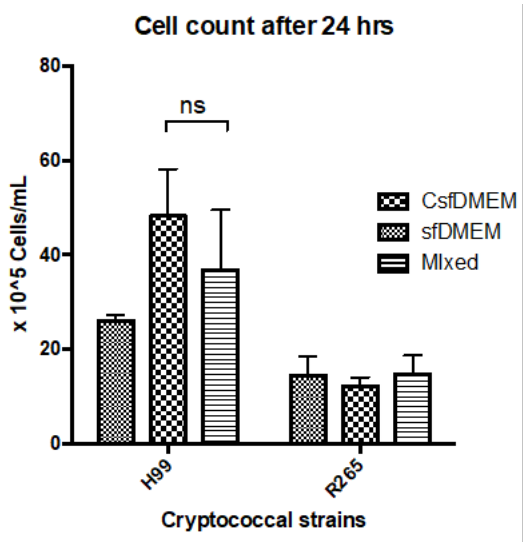

Figure 4.2 Dose dependency. Proliferation of *Cryptococcus* in crude vs diluted CsfDMEM (J774) to show dose dependency. (Error bars represent SEM of 3 biological replicates).

4.4 Strain specificity

The observed proliferative effect of conditioned media from J774 was further tested across other cryptococcal species and strains to study the species- or strain-specificity of this effect. Initially, I screened at least one representative strain of the four cryptococcal serotypes A-D belonging to the genotypes: VNI, VNII, VNIV, VGI, VGIII and VGIV. None of the other genotypes showed the same proliferative response as H99, although notably a VGIV strain, WM779 (a *C. gattii*), showed slightly enhanced growth in CsfDMEM that did not reach the level of statistical significance (p=0.0618) (Figure 4.3).

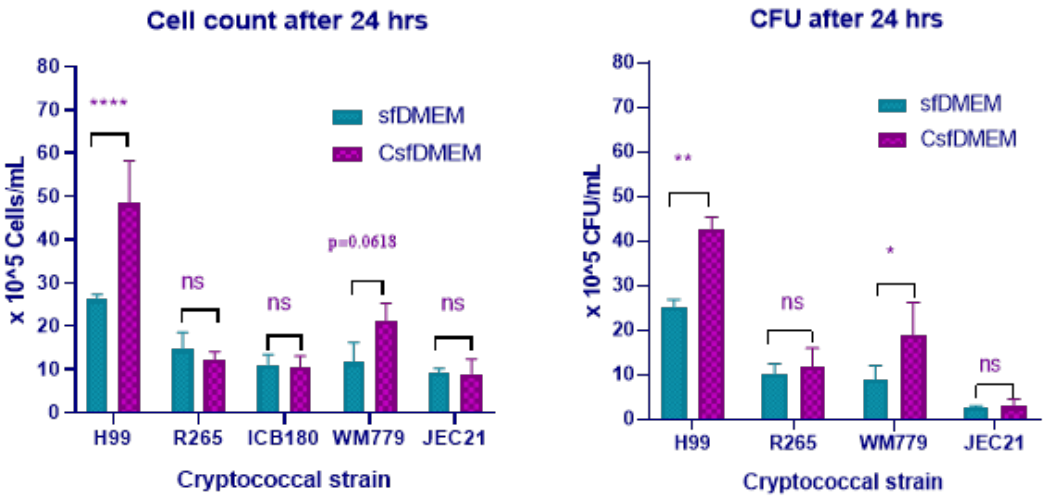

a **b**

Figure 4.3 Strain specificity of *Cryptococcus* proliferation in CsfDMEM. The cryptococcal strains were grown in naive (DMEM) and J774 conditioned media (CsfDMEM) at 37°C in 5% CO_2 and growth: cell count (a) and CFU (b) were determined after 24 hr. (**=p=0.0015, *p=0.0396, ns=*p>0.05*; error bars depict SEM from 3 biological repeats).

I then investigated more closely within strains more closely related to H99 using isolates: H99/VNI (clinical), 125.91/VN1 (clinical), CBS8336/VNI (environmental), HAMDANC C3-1/VNII (environmental), CBS1931 (environmental), ZcI/VNI (clinical) and Zc8/VNI (clinical). The proliferative response exhibited by H99/VNI (Figure 4.4) was absent in the other VNI strains except Zc1/VNI and Zc8/VNI which expressed significant growth enhancement in CsfDMEM. Interestingly, although the VNI clinical isolate, 125.91, expressed a similar proliferation rate in the naïve media as H99, its growth was not enhanced in CsfDMEM. Thus, the proliferative impact of conditioned media seems to be restricted to some, but not all, strains within VNI.

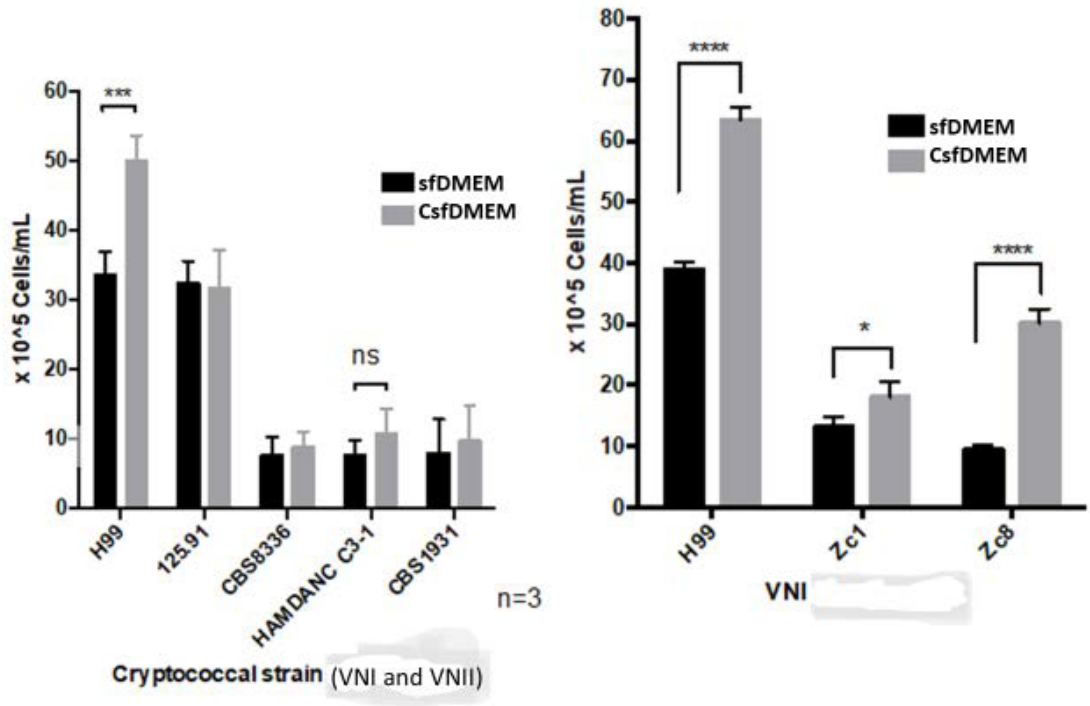

(a) (b)

Figure 4.4 Proliferation of different genotype (VNI and VNII) and clinically relevant (environmental vs clinical) strains. (a) Proliferation rate of *C. neoformans* strains belonging to either VNI (H99, 125.91, CBS8336) or VNII (HAMDANC C3-1, CBS1931) genotypes in response to conditioned media (CsfDMEM) from J774. (b) Proliferative rate of *C. neoformans* clinical strains belonging to only VNI genotype in response to conditioned media (CsfDMEM) from J774. (****=p<0.00001, ***=p<0.0001, *=p<0.01 and ns=*p>0.05*; error bars depict SEM from 3 biological repeats)

4.5 Proliferation of *Cryptococcus* in response to lung epithelial cell secretion

To ask whether this effect was specific to macrophages, the cryptococcal response to conditioned media from A549 cells (a lung epithelial type II cell line) was investigated. As with J774 media, H99 proliferation was enhanced by exposure to CsfDMEM from A549 cells

(Figure 4.5). As shown previously for macrophages, this phenomenon occurred only in H99 and the two Zc strains (Figure 4.5).

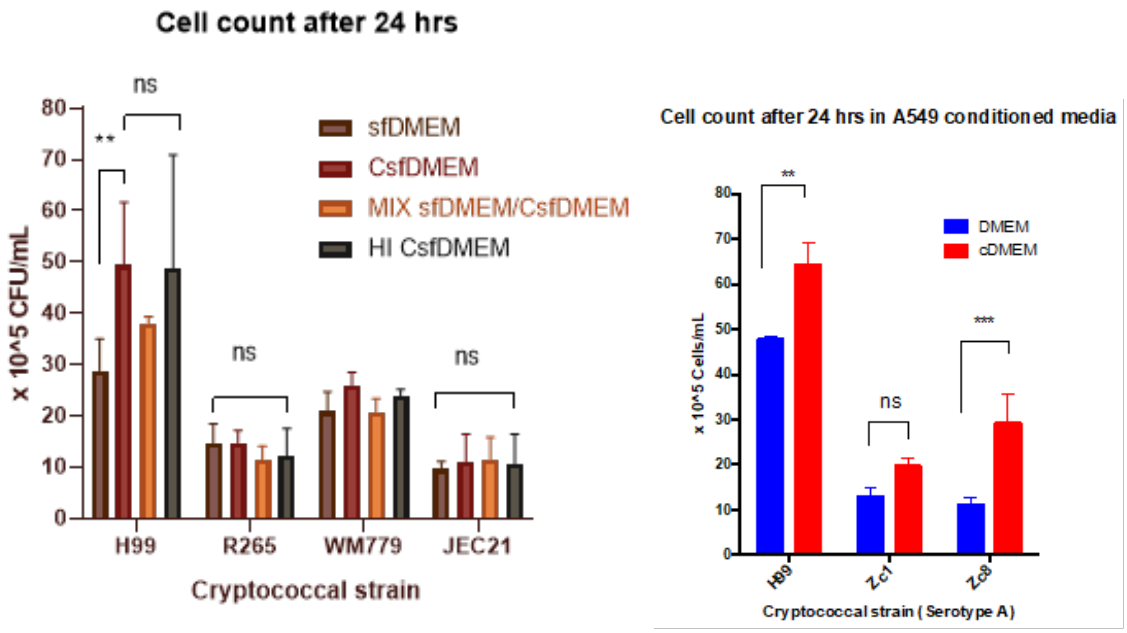

a b

Figure 4.5 Proliferation of *Cryptococcus* in A549 conditioned media. A549 secretome (CsfDMEM) possess proliferative effect but specific to H99 and Zc8. In addition, the trophic factor is not heat labile. (**= p=0.0082, ns=p>0.05; error bars represent SEM of three biological repeats).

The result from A549 conditioned media is almost identical to the one from murine macrophage J774 cells, including the fact that the trophic factor (H99/VNI) is dose dependent (Figure 4.5a). Consequently, it appears that this growth-enhancing effect is not specific to mammalian macrophages, but rather may be a product of multiple different mammalian cell types. However, the proliferative response triggered by conditioned media from J774 seems to be stronger than A549.

During the experiments outlined above, it was observed that JEC21 is less temperature-tolerant than other cryptococcal strains. Not all *Cryptococcus* strains are tolerant to elevated temperature [211]. Therefore, I performed a temperature sensitivity test assay on JEC21 to verify the suitability of this strain (as a *C. deneoformans* representative strain) for the experiment. The temperature sensitivity test was performed according to Odom *et al*. [76]. As anticipated, JEC21 displayed a growth defect (similar to that of the Ras 1-negative control strain) on YPD agar plate at 37°C while H99 (positive control) exhibited normal growth (Figure 4.6a). Consequently, another VNI [(B3501) serotype D] strain was tested using the same temperature-sensitivity assay protocol. B3501 turns out to be tolerant to elevated temperature (37°C) (Figure 4.6b) and was therefore used to replace JEC21 in subsequent experiments.

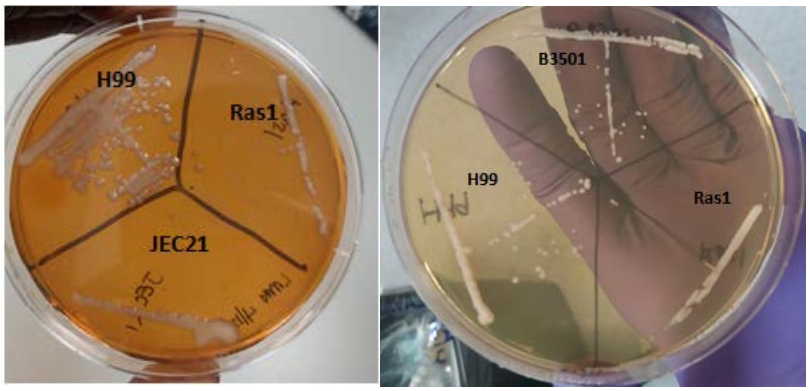

a b

Figure 4.6 Temperature sensitivity assay. The tested cryptococcal strains were grown on YPD agar and incubated at 37°C for two days. a) JEC21 expressed retarded growth due to elevated temperature-37°C and b) B3501 temperature tolerance similar to H99 (a positive control).

In spite of expressing tolerance to elevated temperature (Figure 4.6b), B3501 did not demonstrate any significant proliferation towards the conditioned media of J774 or A549

(Figure 4.7b). This result confirms that the secretome from the mammalian cell lines-J774 and A549, do not enhance fungal cell proliferation in *C. denoeformans* (VNI) strains.

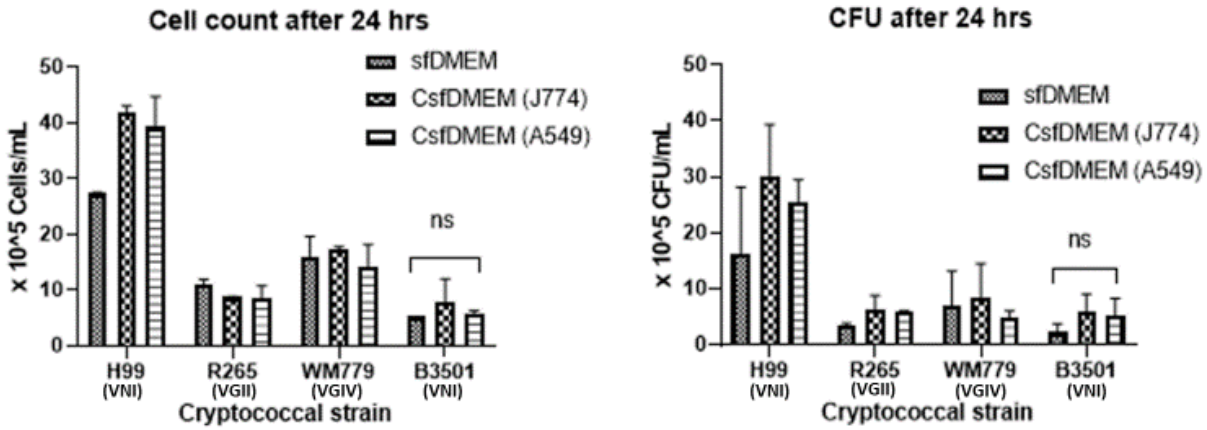

a **b**

Figure 4.7 Proliferation of B3501 to evaluate the effect of temperature. B3501 proliferation results as indicated by a) cell count b) CFU after 24 hrs incubation in J774 or A549 conditioned media (CsfDMEM). The result is a representation of 3 biological replicates and statistical significance was confirmed with a two-way ANOVA where ns=p>0.05.

4.6 Proliferation of *Cryptococcus* in response to the alveolar macrophage secretome

Further to showing the cryptococcal enhance growth in conditioned media from A549 (epithelial cell line) I tested the proliferation of *Cryptococcus* in conditioned media from MH-S alveolar macrophages. Unlike the other two tested conditioned media (from J774 and A549), the conditioned media from MH-S (CsfRPMI) did not stimulate cryptococcal growth (Figure 4.8). In fact, CsfRPMI had an inhibitory impact on fungal growth and this was somewhat recovered by dilution of CsfRPMI with sfRPMI. It should be pointed out that MH-S cells grow in RPMI media, rather than DMEM, and therefore further work would be needed to establish whether it is the difference in cell type or media composition that underlies this difference. It

is also worth mentioning that R265 demonstrated relatively bigger cell sizes in MH-S conditioned media (CsfRPMI) which are predictor of titan cell formation [212]. This will be expounded on in the next chapter (Chapter 5).

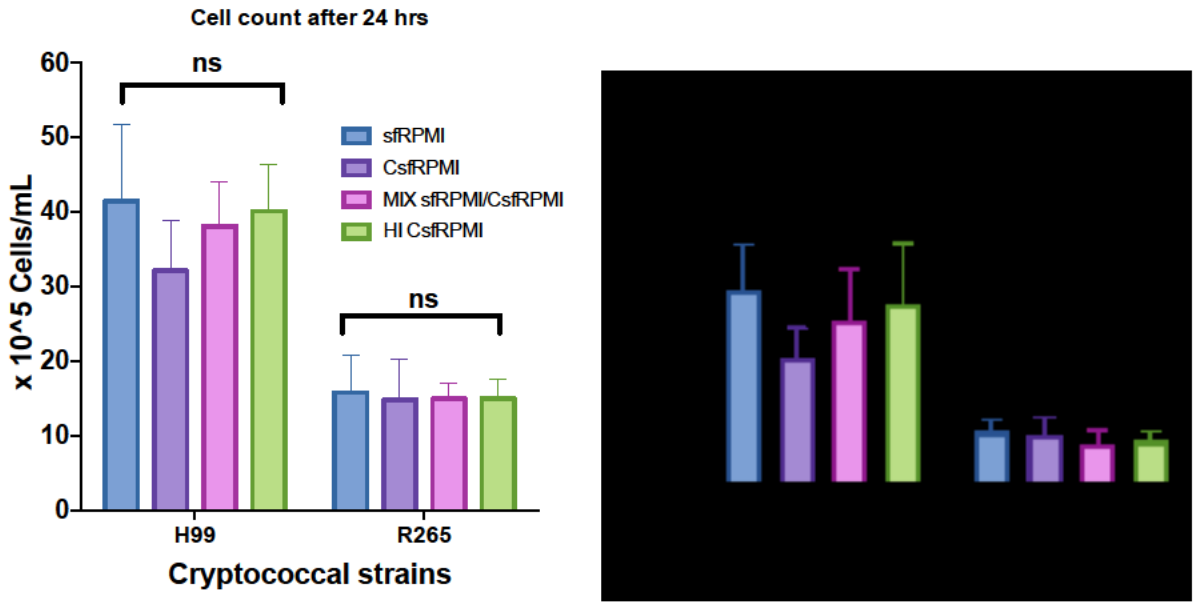

Figure 4.8 Proliferation of *Cryptococcus* in MH-S conditioned media. a) Cell count and b) CFU of cryptococcal strains after 24 hrs incubation in naive (sfRPMI), conditioned (CsfRPMI), mixed (sfRPMI/CsfRPMI) and heat inactivated RPMI media. (ns=p>0.05, error bars represent SEM from 3 biological repeats).

4.7 Effect of experimental conditions: temperature and CO_2

To test the impact of 37°C incubation, *Cryptococcus* (H99) growth difference in conditioned media from J774 (CsfDMEM) was determined between 30°C vs 37°C. The environmental temperature for *Cryptococcus* is ~30°C whereas an elevated temperature of ~37°C is found in the mammalian host environment [75]. Surprisingly, H99 exhibited a significantly higher proliferation at 37°C than 30°C (Figure 4.9a). I deduce from these results that the elevated

physiological temperature of 37°C, is an essential experimental parameter for the enhancement of cryptococcal growth in CsfDMEM.

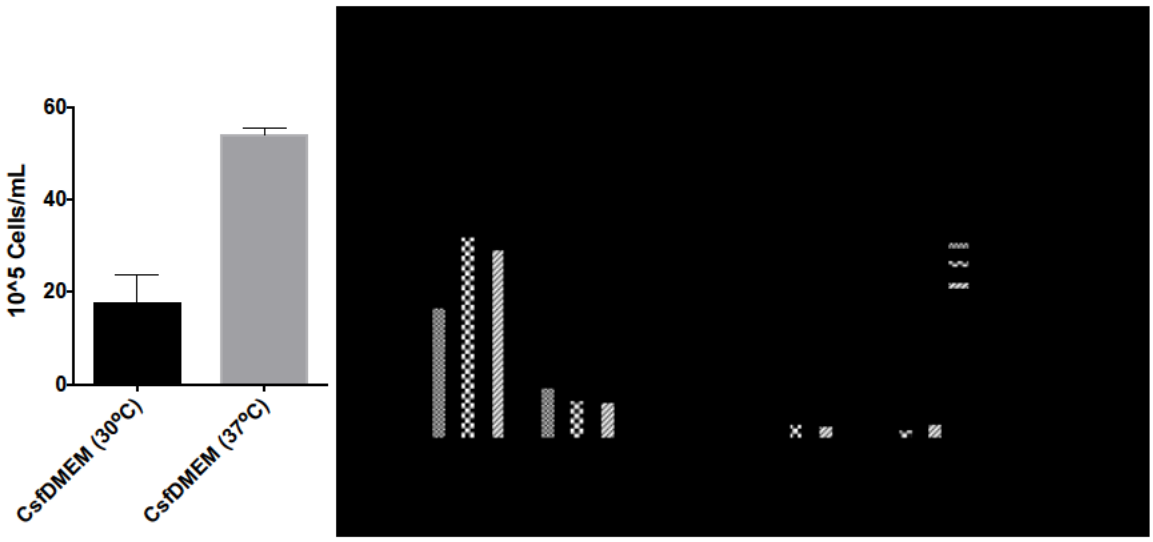

Figure 4.9 Effect of experimental conditions: a) Effect of temperature (30°C vs 37°C) on H99 proliferation in J774 conditioned media (CsfDMEM). b) The proliferation of *Cryptococcus* in conditioned media from J774 and A549 in the presence and absence of CO_2. (****=p<0.0001, *=p=0.0458; error bars represent SEM of three biological repeats).

The effect of CO_2 as an experimental condition was also investigated. Notably, CO_2–free incubation significantly reduced the proliferation of H99 and R265 in J774 and A549 conditioned media (Figure 4.9b), suggesting that CO_2 is essential for the normal growth of the cryptococcal strains, H99 and R265.

4.8 Physicochemical characterization of J774 conditioned media

The physicochemical properties of CsfDMEM (J774) were characterized in order to try and identify the active compound(s) that is/are responsible for the observed cryptococcal proliferation. Heat stability was tested by growing cryptococcal cells in heat-inactivated CsfDMEM (HI-CsfDMEM) and measuring the proliferation. I found out that the trophic

compound/factor was heat labile as the proliferation of H99 in the HI-CsfDMEM was significantly less than the fresh CsfDMEM (Figure 4.10a). I further investigated the effect of proteinase K digestion on CsfDMEM and its resultant effect of H99 proliferation. At 5% proteinase K digestion, the proliferation of H99 was significantly reduced which implies that the active compound is a protein/peptide (Figure 4.10b).

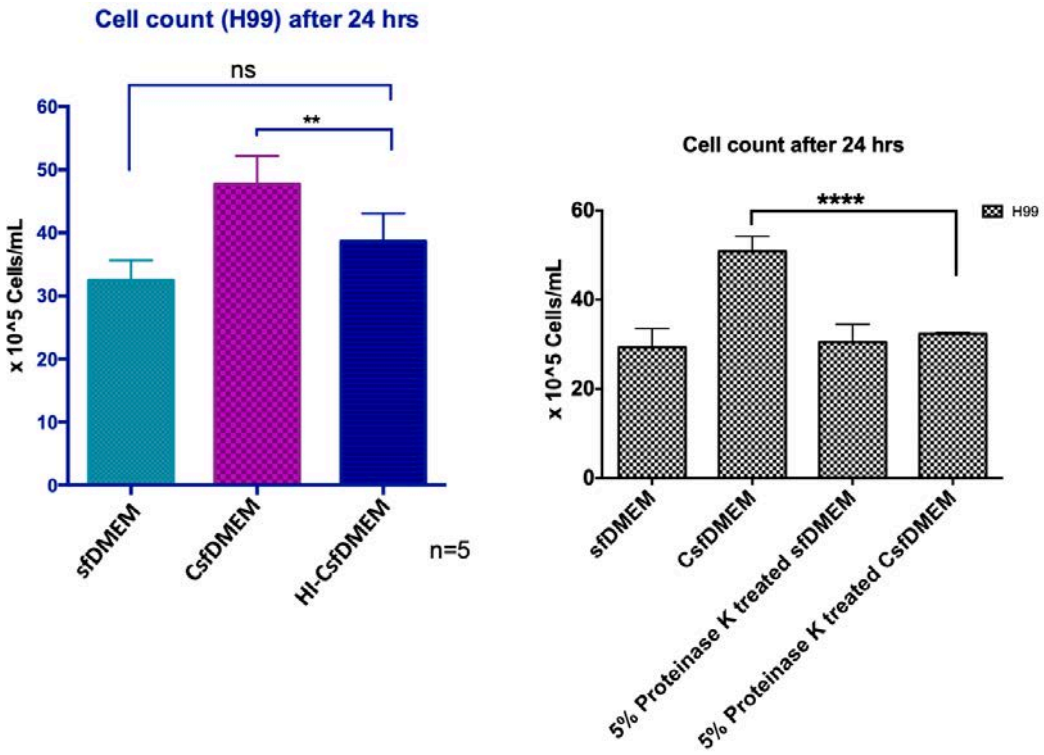

a b

Figure 4.10 Effect of heat inactivation (a) and proteinase K digestion (b) on proliferative effect of CsfDMEM. Cryptococcal cells (H99) were grown in heat inactivated and proteinase K treated CsfDMEM, growth was confirmed by haemocytometer counting after 24 hr incubation at 37°C in 5 % CO_2. Statistical significance was confirmed by one way ANOVA analysis where ****=p< 0.00001, **=p<0.001 and ns=p>0.05.

The molecular size of the active compound was determined via a size exclusion experiment. CsfDMEM was ultra-centrifuged in tubes fitted with 30 kDa and 3 kDa column filters

respectively and both the flow through and the supernatant (remaining in the top of the column) were tested for H99 proliferation. Interestingly, the flow-through from both filters maintained the ability to enhance the growth of H99, similar to unfiltered CsfDMEM, while their corresponding supernatants failed to enhance proliferation (Figure 4.11). Taken together, this suggests that the growth-enhancing molecule is a small peptide.

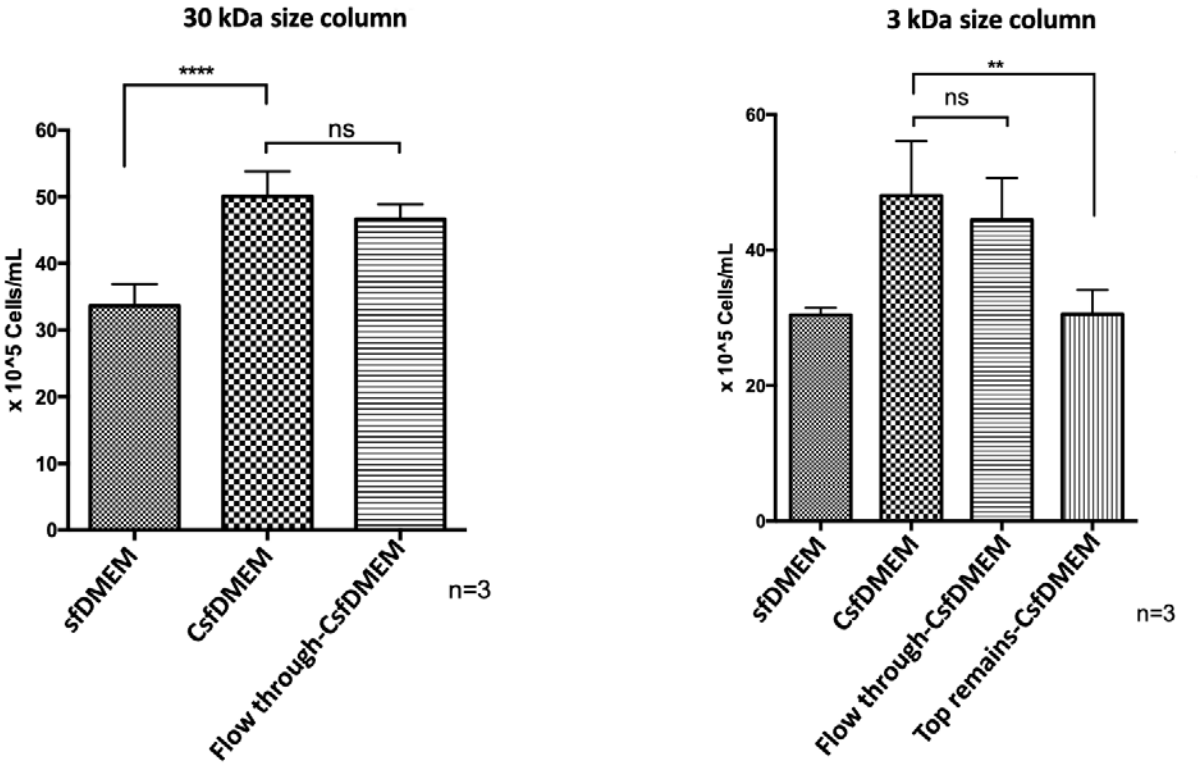

a b

Figure 4.11 Molecular size of the trophic factor. Conditioned media from J774 (cDMEM) was filtered through columns for (a) 30 kDa and (b) 3 kDa fractionation and the column (Top remains) and filtered (Flow through) portions were tested for cryptococcal (H99) proliferation. Three biological repeats were performed, and the error bars represent S.E.M where, **=p< 0.001, ****=p<0.00001 and ns =p>0.05.

To determine the polarity of the proliferative compound, I conducted a chloroform extraction of J774 conditioned media. This approach traps the compound in question within the aqueous or chloroform phase based on hydrophilic or hydrophobic nature of the compound. After growing H99 in the extracted CsfDMEM, the chloroform fraction was found to significantly enhance growth while a significant growth reduction was observed with the aqueous portion (Figure 4.12). This further characterized the active compound to be hydrophobic as it was dissolvable in the chloroform.

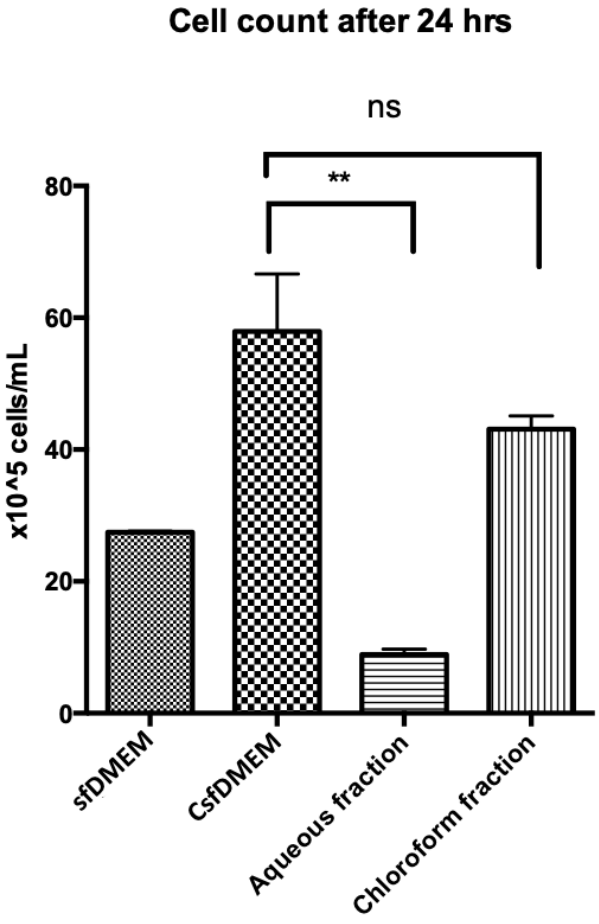

Figure 4.12 Activity of extracted CsfDMEM on proliferation of *Cryptococcus* (H99). The extracted fractions (aqueous and chloroform) were tested for cryptococcal proliferation by growing H99 yeasts cells in them for 24 hr at 37°C in 5% CO_2. The statistical significance was

confirmed by one-way ANOVA and the error bars are representative of 3 biological experimental repeats where **=$p<0.001$ and ns=$p>0.05$.

4.8 Discussion

Transition from a saprophytic lifestyle in the environment to living as a human pathogen requires *Cryptococcus* to adapt to different host niches [1, 61]. Notably, included in these niches are extracellular sites in the lung, bloodstream, and the central nervous system [2] where among other host factors, *Cryptococcus* interacts with the extracellular micro-environment of host immune cells. The intracellular fate of *Cryptococcus* during *Cryptococcus*-macrophage interaction has been well-characterized [42, 158, 159, 213]. Although a major determinant of *Cryptococcus* adaptive features, little is known about the role of the host immune cell micro-environment in driving cryptococcal adaptive mechanisms [2, 63]. Here, I investigated and characterized the proliferation of cryptococcal strains/genotypes as a phenotypic response to exudates of host-derived cells. Interestingly, conditioned media from J774 (a murine macrophage-like cell line) and A549 (a human lung epithelial cell line) enhanced *Cryptococcus* proliferation in a dose-dependent manner. In addition, the enhanced growth effect was strain specific, with the stimulating proliferative response seen only in certain *C. neoformans* strains (H99, Kn99α, Zc1 and Zc8). H99 and Kn99α are congenic at chromosome and high-resolution genomic levels [214] and thus share many characteristics. Both strains exhibit similar key *Cryptococcus* virulence factors and their response to nutrients sources and chemicals further suggest high similarity at the phenotypic level [160, 161]. Zc1 and Zc8 may have expressed similar growth response with H99 because of being clinical isolates [71].

It is evident from the results that both elevated temperature and high level of CO_2 are essential for the proliferative phenotype exhibited by *C. neoformans*. These conditions mimic the human pulmonary physiological environment, suggesting the proliferative response to be a host-relevant phenotype. In attempt to decipher the underlying trophic factors, I characterized the physiochemical properties of CsfDMEM (J774). Knowing the physicochemical nature of the active compound is important for studying their activities and mechanisms driving the phenotype. It is intriguing to find that the growth stimulation compound was smaller than 3 kDa, heat-labile, digestible by proteinase K and hydrophobic, suggesting it is most likely a small, hydrophobic peptide. Further proteomic characterization will be necessary to reveal the full identity of this growth stimulating molecule.

Lung epithelial cells constitute the membranous layer (mucosa) that lines the surfaces of the bronchus and alveolus and are therefore considered the first host cells that *Cryptococcus* encounters [32, 89, 91]. A549, a human lung epithelial type II cell line, has been extensively studied in association with *Cryptococcus* [91, 95, 98, 140, 169]. However, the central interest of those studies focuses on interactions and outcomes of *Cryptococcus* infection when immune responses have already been established. Since a substantial portion of the biomolecules/compounds contained in the epithelial lining fluid (ELF) are produced by the type II alveolar epithelial cells [93], findings from the interaction between *Cryptococcus* and A549 secretome could reveal some of the adaptations and virulence mechanisms of *Cryptococcus* upon inhalation. Recent studies have shown that alveolar lining fluid (AFL) has a growth stimulating effect on *Mycobacterium tuberculosis* (MtB) such that high ALF-exposure elevates MtB's replication [100]. Although evolutionarily unrelated, both Mtb and *Cryptococcus* are opportunistic intracellular pathogens associated with the respiratory tract and exhibit similar virulence factors such as an ability to inhibit phagosome maturation of

phagocytes. I suggest that studying the interaction between *Cryptococcus* and the secretome of lung epithelial cells in more detail will reveal more of the adaptive behaviour virulence mechanisms *Cryptococcus* exhibits during infection.

Interestingly, the alveolar macrophage cell line-MH-S was not associated with the enhanced proliferation of *C. neoformans.* Rather than increased replication, *Cryptococcus* responded to conditioned media from MH-S (CsfRPMI) by cell size increase which was only observable in *C. gattii.* Alveolar macrophages are the first immune cells to interact with *Cryptococcus* and evidence of enhanced intracellular proliferation has been reported [99, 158]. The result is predictive that MH-S cells could play an important role in the formation of titan cells-atypical cellular morphotype exhibited as a major cryptococcal virulence mechanisms in response to the lung environmental cues [12, 71].

Overall, the findings in this chapter reveal an often-overlooked phenomena: the impact of an otherwise healthy host pulmonary niche on the adaptive biological traits of *Cryptococcus.* The observed phenotypic responses (proliferation and formation of large cells) coupled with other forms of interactions can potentially define the outcome of disease especially when they are weighed on the scale of pathogenicity and virulence factors.

CHAPTER 5

THE SECRETOME OF DIFFERENT LUNG-ASSOCIATED MAMMALIAN CELLS INDUCES FORMATION OF TITAN-LIKE CELLS IN *CRYPTOCOCCUS GATTII*

As with other inhaled microbes, the first surface that *Cryptococcus* encounters after deposition in the lung is the pulmonary mucosa [99]. This environment is heavily loaded by secretions from host cells within the lung, such as Type I and II epithelial cells as well as alveolar macrophages. The pulmonary mucosa environment is stressful to most microbes and consequently stimulates cryptococcal adaptive mechanisms. The most dramatic adaptive response to the lung environment in *Cryptococcus* is the formation of titan cells [50]. To date, there has been little work undertaken on the response of *C. gattii* to lung-associated mammalian cell secreted factors. In this chapter, I begin to probe this response by using a range of mammalian lung-associated cell types.

5.1 *C. gattii* exhibits enormous cell size increase in response to MH-S conditioned media

In the previous chapter (Chapter 4), the enhanced fungal growth of cryptococcus due to the proliferative effect of supernatant derived from the mammalian cell line J774 was clearly demonstrated. In follow on work, while testing this phenomenon for two lung-associated cell lines (A549 lung epithelial type II and MH-S alveolar macrophages), a subset of enormously enlarged and distinct cryptococcal cells was microscopically detectable. I exposed fungal cells to conditioned media (cDMEM or cRPMI), obtained by growing the respective cell lines in that media for 24 hrs and then evaluated cryptococcal cell size (cell body and capsule) relative to that of the cells in corresponding naive media (DMEM or RPMI) and YPD (Figure 5.1). Interestingly, conditioning the media enhanced the cell enlargement of *C. gattii* strain R265 (VGII/*C. deuterogattii*) when grown at $5x10^5$ cells/mL initial inoculum concentration for both MH-S (cRPMI: conditioned-RPMI) and A549 (cDMEM) cells. However, given the previously shown (Chapter 4) impact of cRPMI on titan cell formation, this effect was far more pronounced for cRPMI (Figure 1). Consequently, I focused most subsequent works on MH-S cells conditioned media (cRPMI).

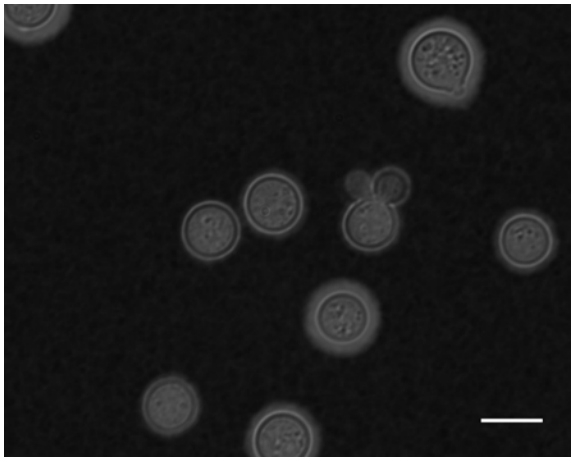

YPD

(A)

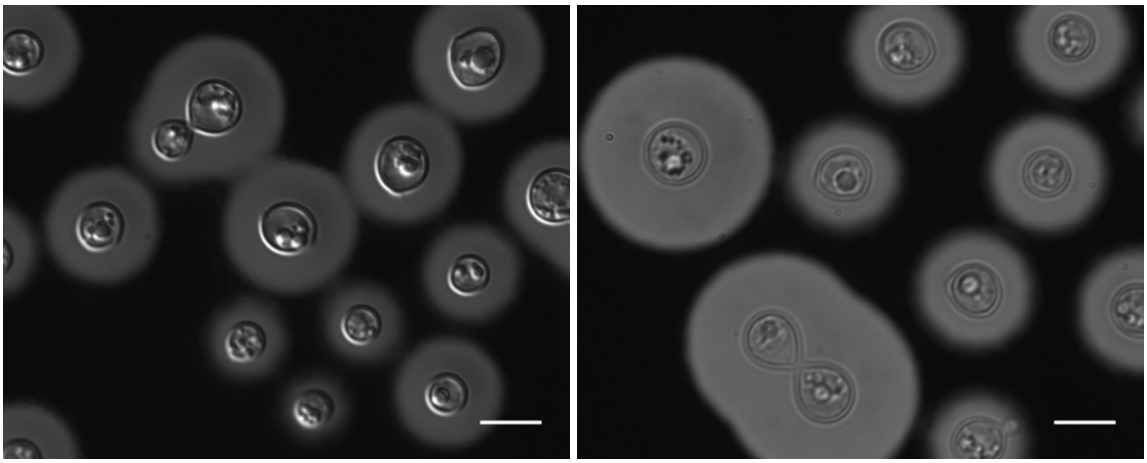

DMEM cDMEM (J774)

(B)

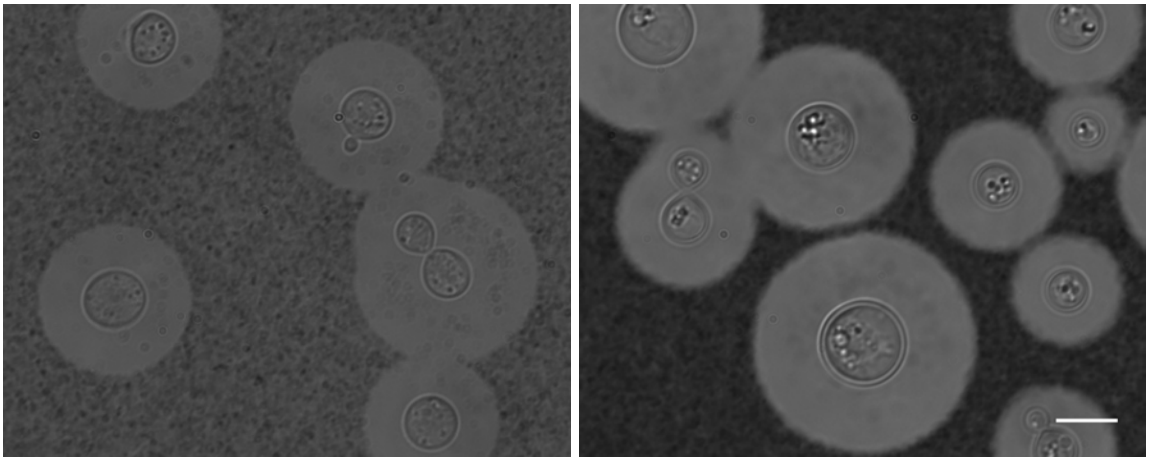

DMEM cDMEM (A549)

(C)

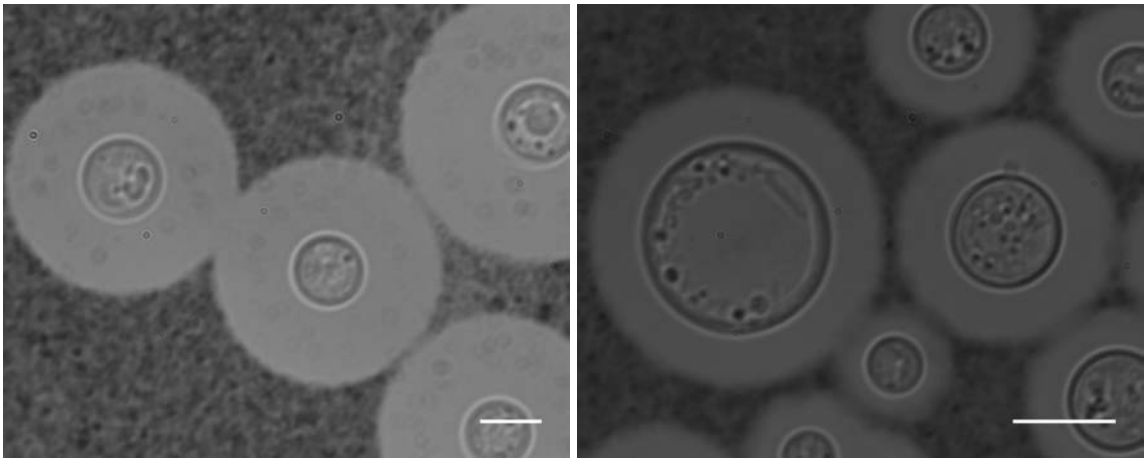

RPMI cRPMI (MH-S)

(D)

Figure 5.1 Morphological changes of R265 yeast cells (5x10^5 cells/mL) after 24 hrs incubation at 37°C with 5% CO_2 in (a) YPD, (b) DMEM vs cDMEM (J774), (c) DMEM vs cDMEM (A549) and (d) RPMI vs cRPMI (MH-S). The cells were stained in Indian ink and microscopy imaging was done at 100X magnification. Scale bar =10µm.

Microscopically, these enlarged cells resemble titan cells. Titan cells are defined with cell body diameter of >10µm [12]. To account for the proportional occurrence of the R265 enlarged cells,

I measured the cell body diameter and percentage of cells >10µm. Relative to RPMI, the median cell body diameter of R265 cells in cRPMI was significantly higher [median size: 9.6 µm (5.3-20.6) vs 8.6 (4.6-13.7)] (Figure 5.2). Similarly, the proportion of R265 titan-like cells generated by cRPMI was significantly higher (40.2%) than RPMI (11.3%). This suggests that R265 yeast cells undergo a morphological switch (small to large size) in response to MH-S factors.

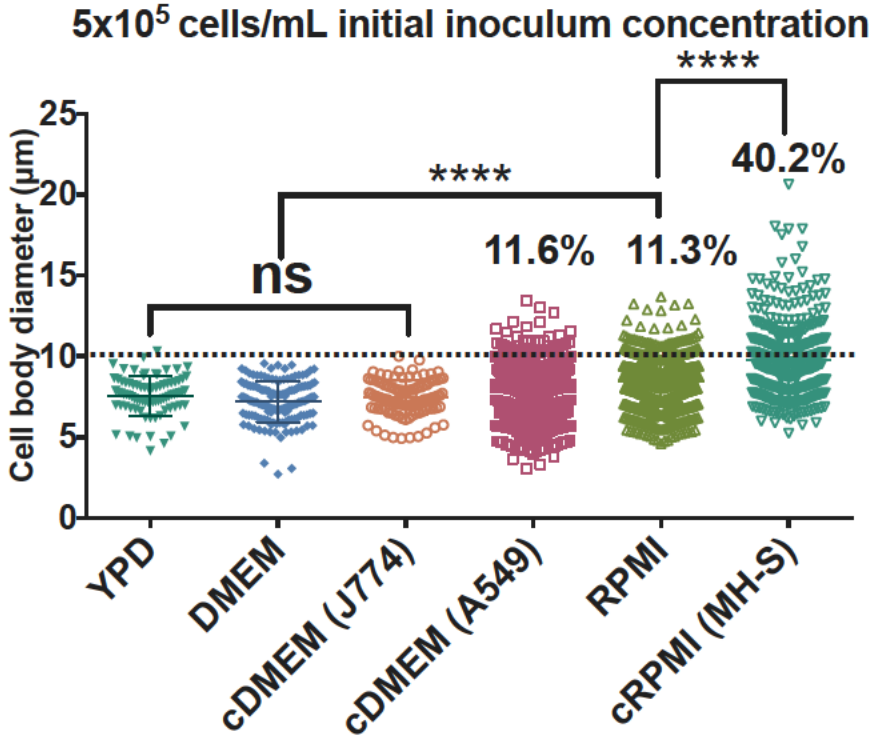

Figure 5.2 Cell body measurement of R265 yeast cells (5x10^5 cells/mL) after 24 hrs incubation at 37 degree with 5% CO_2 in YPD, DMEM vs cDMEM (J774 or A549) and RPMI vs cRPMI (MH-S). At least, 100 cells were analysed for each test media and statistical significance was confirmed by one-way ANOVA where ****=p<0.00001.

Interestingly, I noted that, in addition to the formation of titan cells, conditioned media also appeared to enhance capsule formation. I measured the capsule size of R265 in YPD (control), naïve and conditioned media from the three mammalian cell lines. Compared to their corresponding naïve media, cDMEM (from J774) and cRPMI significantly increased the median capsule sizes of R265 from 15.06µm [6.69-22.00] to 19.05µm [10.19-29.72] respectively and from 8.36µm [1.34-12.01] to 11.03µm [1.98-30.20] respectively, while cDMEM from A549 cells didin't demomstrate any increasement in capsule size (Fig. 5.3). In contrast, cDMEM from A549 cells did not demonstrate capsule size increase relative to naive DMEM. DMEM [124] and RPMI [215] have been previously employed for optimal capsule induction in *C. neoformans* [216] but the fact that capsule formation is further enhanced in conditioned media from both macrophage lines, but not epithelial cells, suggests that one or more macrophage-specific factors may stimulate capsule formation in *Cryptococci*.

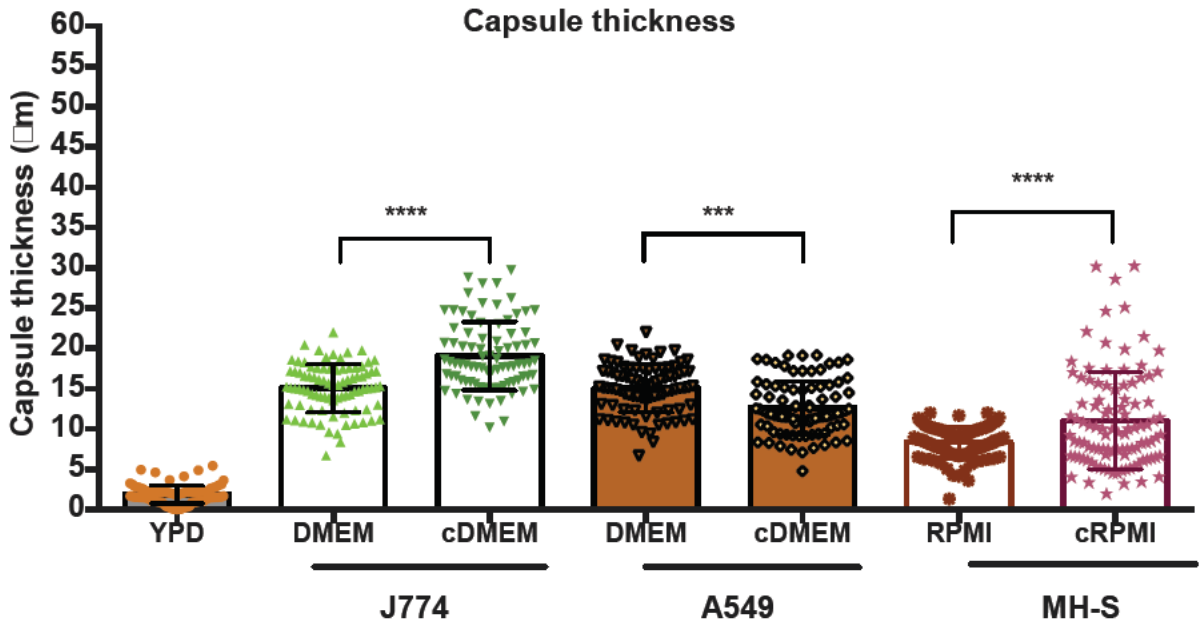

Figure 5.3 Capsule size measurement of R265 yeast cells after 24 hrs incubation at 37 degree with 5% CO_2 in (a) YPD, (b) DMEM vs cDMEM (J774), (c) DMEM vs cDMEM (A549) and (d) RPMI vs cRPMI (MH-S). At least 200 cells were analysed for the test samples and statistical significance was established using one-way ANOVA where ****=p< 0.0001.

5.2 The proportion and size of *C. gattii* titan-like cells are inversely correlated with cell density

During experimental work, enlarged cryptococcal cells were predominantly observed at periphery of the culture wells where the cell density is relatively lower. This signals a density-dependent phenomenon. The effect of cell density on titan cell formation has been highlighted by both *in vitro* and *in vivo* studies where optimum proportion of titan cells are obtained at lower inoculum concentration [48, 49, 217]. To determine the optimum initial inoculum concentration producing the largest and highest proportion of titan-like cells, I slightly modified the method from Trevijano-Contador *et al*. [217]**.** R265 yeast cells from overnight YPD cultures were inoculated in naïve RPMI and MH-S conditioned cRPMI at five decreasing inoculum concentrations (10^6, $5x10^5$, $5x10^5$, 10^4 and $5x10^3$ cells/mL) and cell body size analysed after 72 hr incubation at 37°C in 5% CO_2. Based on the cut-off cell size >10µm, the highest percentage of titan-like cells was obtained at $5x10^3$ cells/mL (91.0%) (Figure 5.4), whereas the titan-like cells seen at the higher cell density (10^6 cells/mL) was negligible (0.2%). Therefore, $5x10^3$ was taken as the optimal initial inoculum concentration and used for subsequent titan-induction in cRPMI. Taken together, the results depict a cell density-dependent mechanism of R265 titan-like cells formation, in line with earlier *in vivo* observations by Zaragoza *et al.* [49].

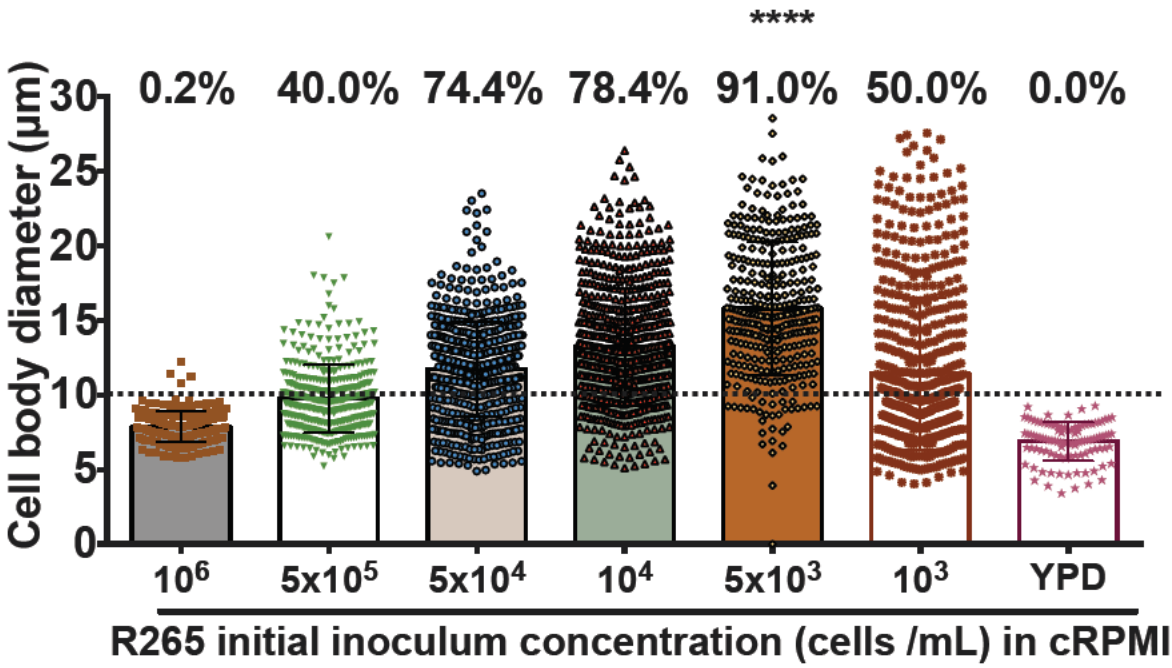

Figure 5.4 Effect of cell density on R265 titan-like cell production in cRPMI. R265 yeast cells were grown in cRPMI at the six decreasing initial inoculum concentrations (10^6 to 10^3 cells/mL) for 72 hours at 37°C in 5% CO_2 and harvested for cell body size analysis. At least 200 cells were analyzed for the test samples and statistical significance was establish with one-way ANOVA where ****=$p<0.00001$.

5.3 The capacity to form R265 titan-like cells correlates with incubation time

With the aim of characterizing other growth dynamics influencing the production of R265 titan-like cells, I investigated the effect of incubation time on the percentage of titan-like cells formed in cRPMI. Thus, I extended the incubation time up to 7 days and determined the impact on titan-like cell formation. The proportion of titan-like cells steadily increased with incubation time from 24 hr (69.0%), reaching a peak at 4 days (96.0%) through 7 days (97.1%) when almost all the cells were of titan size. The observed pattern of titan-like cells production is consistent with other titan-induction results. In their *in vivo* studies, Zaragoza *et al*. recovered

maximum titan cells after 1day post-infection and this was maintained throughout the course of infection [49]. Similarly, from their *in vitro* approach, Hommel *et al*. produced titan cells with the highest proportion achieved at 24 hrs which was maintained at further time points [48].

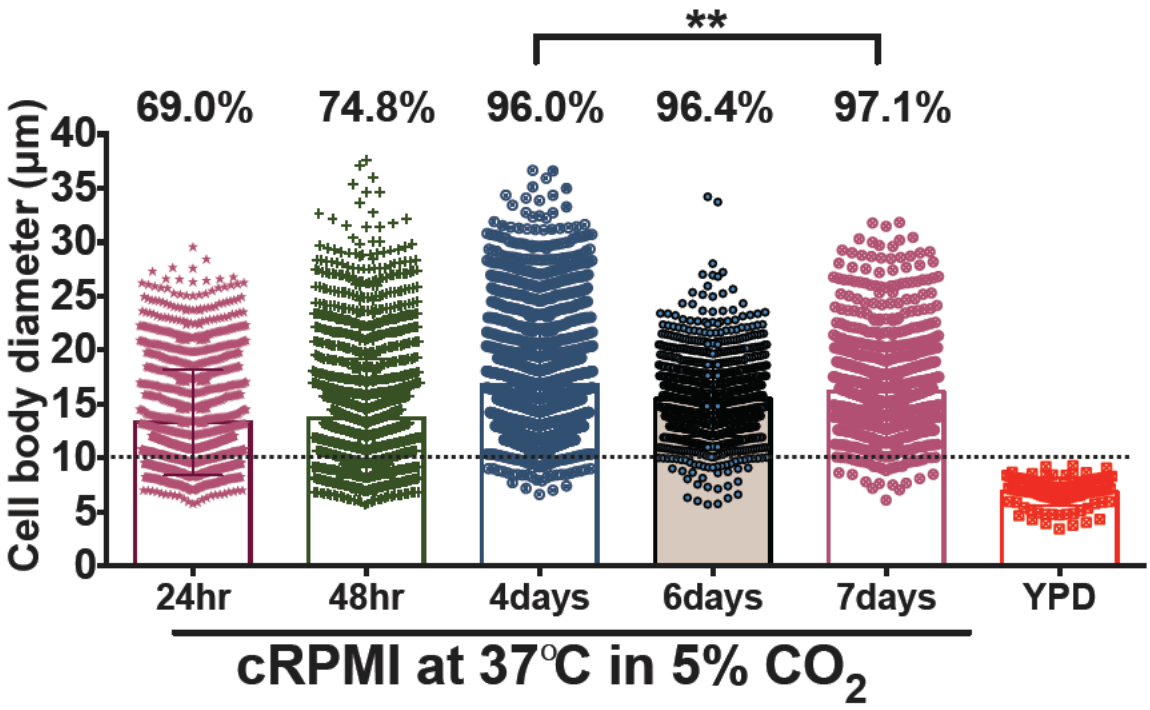

Figure 5.5 Effect of incubation time on the proportion of R265 titan-like cells. R265 yeast cells were grown in cRPMI at 37°C in 5% CO_2 for 24hr to 7days and samples were collected ay each incubation time point and analyzed for cell body size and the proportion of titan-like cells (>10µm). At least 1000 cells were analyzed for each test sample and statistical significance was determined using one-way ANOVA where **=P<0.001.

5.4 The formation of titan-like in response to cRPMI is bais to *C. gattii*

Phenotypic variation delineating species within *C. neoformans/gattii* species complex strongly correlates with the phylogenic divergences that defines their distinct molecular genotypes [22, 218, 219]. To potentially reveal the strain specificity of titan-like cell formation (in cRPMI) within the *C. neofromans/gattii* species complex, 28 representative cryptococcal isolates of

different molecular genotypes: 16 *C. gattii* (VGI-VGIV); 10 *C. neoformans* (VNI and VNII); and 2 *C. deneoformans* (VNII), were tested (Fig. 5.6). Overall, the capacity to form titan-like cells was remarkably higher in *C. gattii* than C. *neoformans* and *C. deneoformans* combined (41.6% vs 8.2% for C. *neoformans/ deneoformans*). Within the *C. gattii* species (Fig. 5.6A, Fig. 5.6B, and Fig. 5.6C) isolates of the VGII molecular genotype demonstrated the highest potential to form titan-like cells (52.2% vs 26.1% for the other *C. gattii* molecular genotypes combined). In fact, the highest percentage (72.5%) and median cell size (14.0µm) were scored by the two VGII strains: CBS10089 and CDCR272 respectively. Five (CDCR271, ENV152, R265, CBS10089, CDCR272) out of eight VGII isolates scored significantly higher median cell body size in cRPMI than RPMI (based on median size), supporting the suggestion that cRPMI contains MH-S secretions that enhance the formation of titan-like cells. Within the non-*C. gattii* strains (*C. neoformans/deneoformans*), the highest number of titan-like cells was 31.3% with some showing no titan-like cells at all (Fig. 5.6 D and Fig. 5.6E). Taken together, the result confirms that *C. gattii* responds more strongly to cRPMI in the formation of titan-like cells than other lineages.

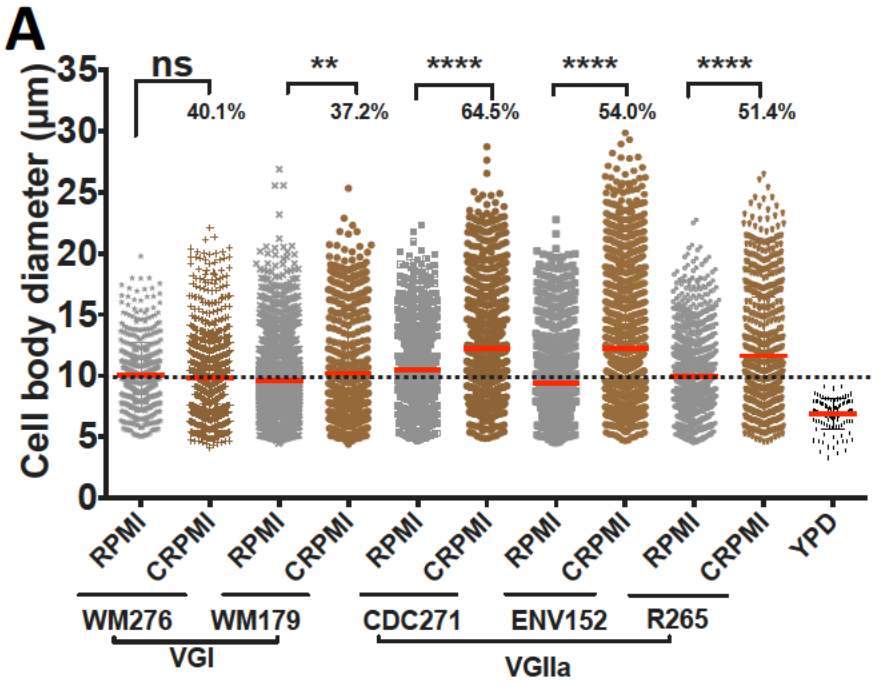
A
Cell body diameter (μm)
ns
**
****
****
****
40.1%
37.2%
64.5%
54.0%
51.4%
RPMI
CRPMI
YPD
WM276
WM179
CDC271
ENV152
R265
VGI
VGIIa

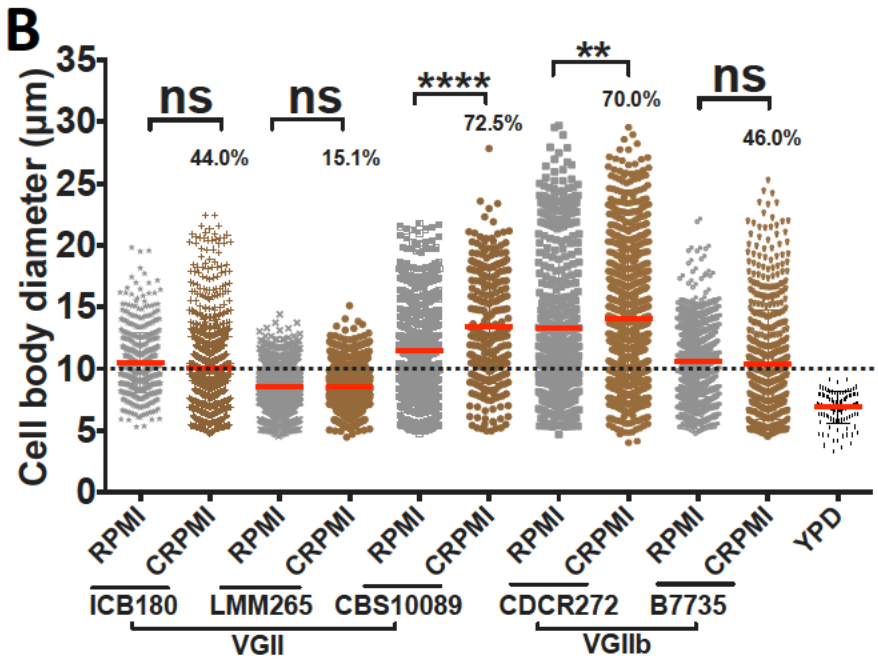
B
Cell body diameter (μm)
ns
ns
****
**
ns
44.0%
15.1%
72.5%
70.0%
46.0%
RPMI
CRPMI
YPD
ICB180
LMM265
CBS10089
CDCR272
B7735
VGII
VGIIb

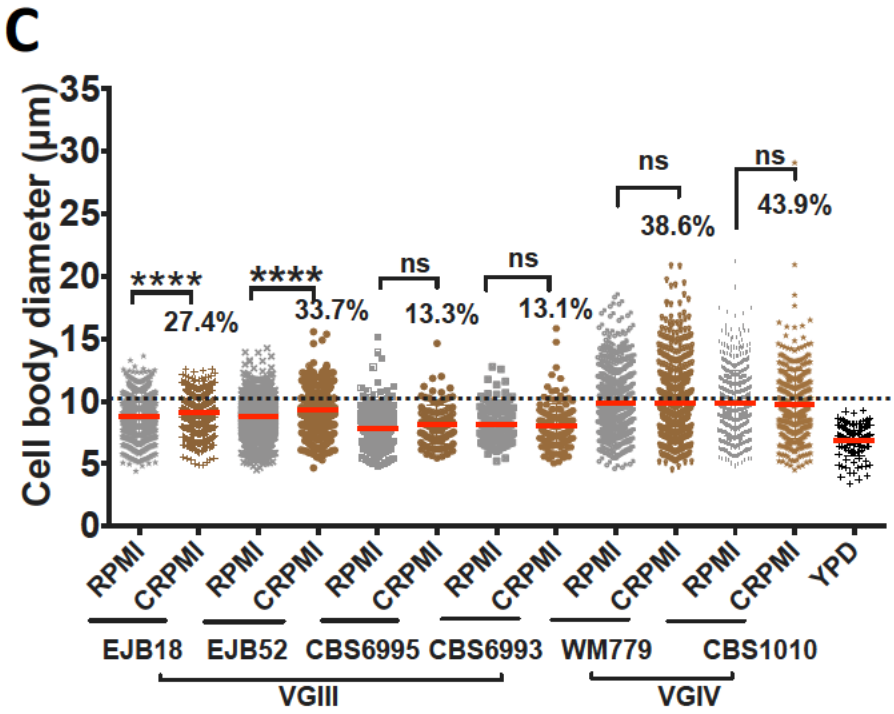
C
Cell body diameter (μm)
0
5
10
15
20
25
30
35
****
27.4%
****
33.7%
ns
13.3%
ns
13.1%
ns
38.6%
ns
43.9%
RPMI
CRPMI
YPD
EJB18
EJB52
CBS6995
CBS6993
WM779
CBS1010
VGIII
VGIV

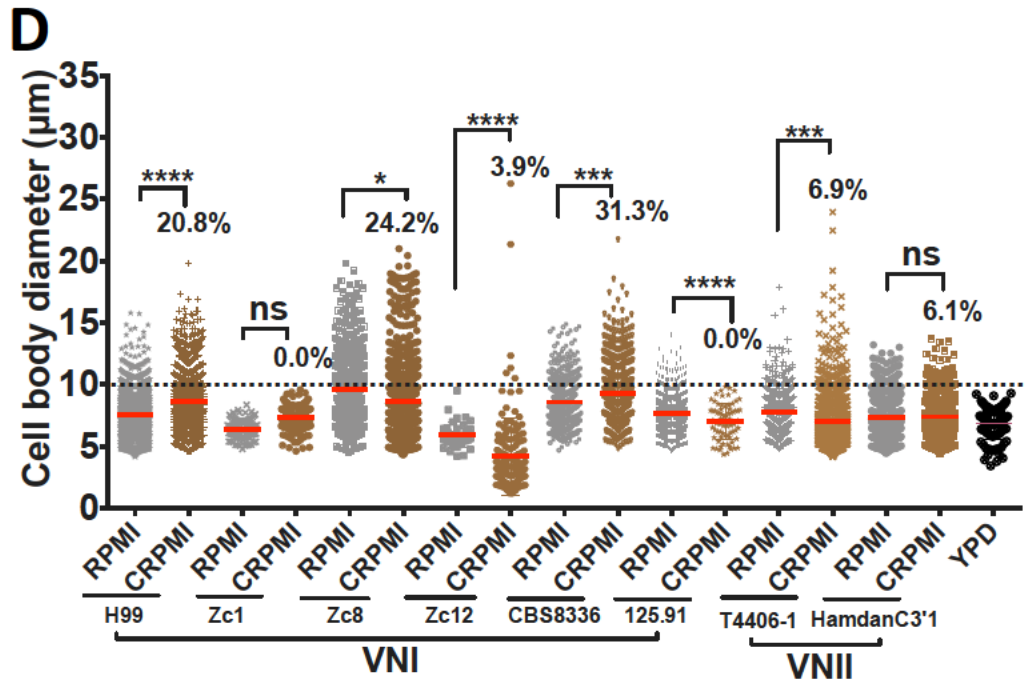
D
Cell body diameter (μm)
0
5
10
15
20
25
30
35
****
20.8%
ns
0.0%
*
24.2%
****
3.9%
***
31.3%
****
0.0%
***
6.9%
ns
6.1%
RPMI
CRPMI
YPD
H99
Zc1
Zc8
Zc12
CBS8336
125.91
T4406-1
HamdanC3'1
VNI
VNII

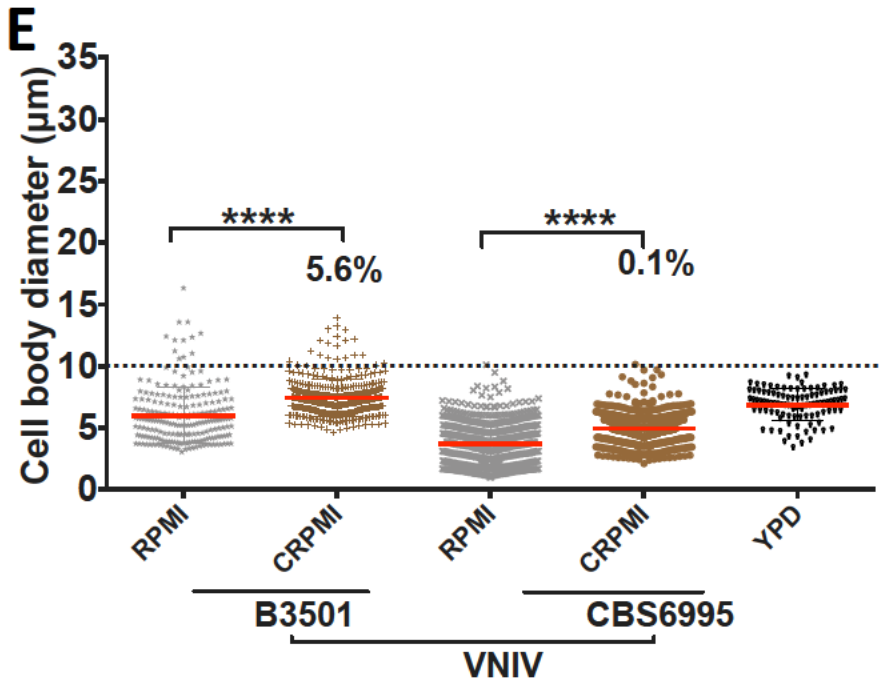

Figure 5.6 Differential titan-like production response of strains within the *C. neoformans/gatii* species to cRPMI. A), B), C) Capacity of *C. gattii* isolates representing the four *C. gattii* molecular genotypes (VGI-VGIV) to form titan-like cells in response to cRPMI. D), E) Capacity of *C. neoformans* (VNI and VNII)/*deneoformans* (VNIV) isolates to form titan-like cells in response to cRPMI. The respective isolates were grown in the test media (RPMI vs cRPMI) for 24 hr at 37°C in 5% CO_2 and then harvested for cell body size measurement.

5.5 Physicochemical characterization of factors in titan-like cell inducing media (cRPMI)

The titan-like cell inducing effect of conditioned media from MH-S (cRPMI: conditioned RPMI) suggests that these mammalian cells secrete compound(s) that influence the formation of titan-like cells in *C. gattii* (R265). To try and further characterize the active compound(s) in cRPMI, I investigated the physicochemical properties of these compounds starting with the molecular size. The molecular size of the active compound(s) was estimated by filtering the

(raw) cRPMI through a 3kDa filter column and testing the two column fractions (flow through and supernatant) for their capacity to induce titan-like cells (Figure 5.7 A). Whilst the supernatant fraction showed a slightly stronger effect than unfiltered cRPMI (57.8% vs 56.8%; p=0.202), the flow through was significantly less effective at inducing titan cells (54.9% vs 56.8%; S.E.M: 11.21 vs 12.23µm, $p<0.05$). This implies that the active compound(s) is/are larger than 3kDa. Interestingly, the flow-through fraction exhibited a stronger effect than the naive RPMI media (negative control), ($p<0.0001$). This suggests that not all the active compounds were retained in the supernatant.

I then characterized the heat stability and proteinase K degradation profile of the cRPMI active compound(s). Notably, both heat inactivation and proteinase K treatment reduced the titan cell profile back to that of naïve RPMI, strongly suggesting that the titan-inducing compounds are heat-labile proteins larger than 3kDa.

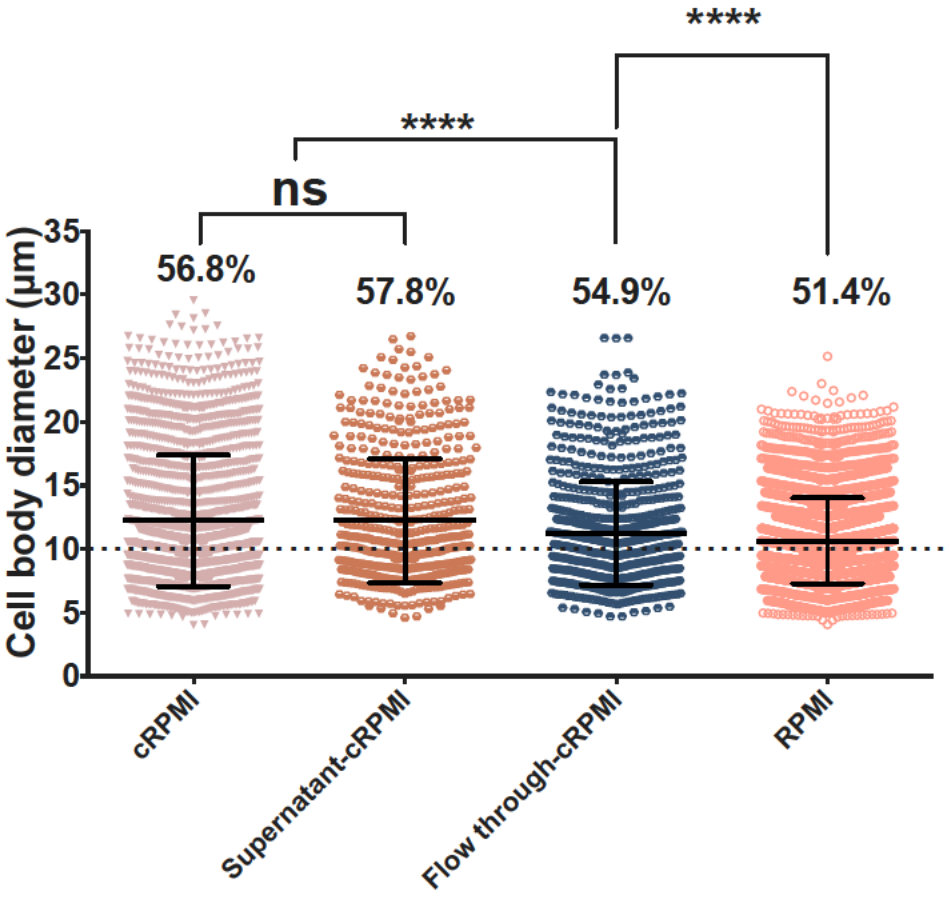

(A)

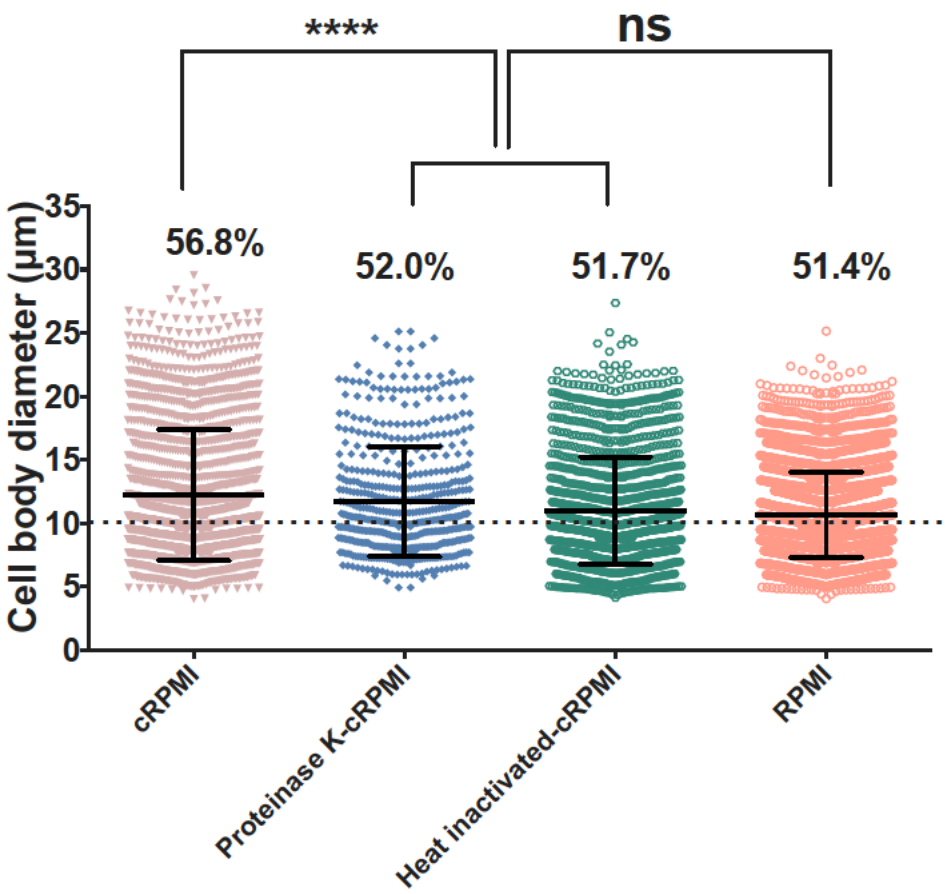

(B)

Figure 5.7 Physicochemical properties of cRPMI active compound(s). The molecular size of the active compound(s) in cRPMI was determined by ultracentrifugation of cRPMI through a 3kDa filter column and evaluating the capacity of the two fractions (flow through and supernatant) of the column to induce titan cell formation. B) The effect of proteinase K digestion (5% proteinase K for 2 hr) and heat inactivation (at 56°C for 1 hr) on cRPMI's capacity to induce titan formation. At least 150 cells were counted for each samples and statistical significance was determined by using one-way ANOVA where ****=$p<0.0001$based on S.E.M shown by the error bars.

5.6 Discussion

In the previous chapter (chapter 4), the enhanced growth of cryptococcal cells in response to conditioned media from J774 macrophages was elucidated. By extension, I investigated the impact of conditioned media from pulmonary-associated mammalian cell lines: A549 epithelial type II cell and MH-S alveolar macrophages, on *Cryptococcus*. Upon inhalation, *Cryptococcus* first encounters pulmonary secretions of the lung mucosa [39, 99] which are heavily loaded with secreted hydrolases from the two cell types. Interestingly, previous work has shown that one of these, surfactant protein D, can enhance the survival and proliferation of *Cryptococcus in vivo* [69]. Here, I report an *in vitro* morphological transformation of *Cryptococcus* (*C. gattii* in particular) from a yeast to dramatically enlarged titan-like cells in response to conditioned media from MH-S alveolar macrophages. These cells are termed "titan-like" in the current chapter as the key defining features of the titan phenotype (besides size) such as polyploidization, cell wall alteration etc. have not yet been tested. Titan-like cells were also inducible in A549 conditioned media (albeit to a lesser extent) while conditioned media from the murine macrophage line J774 lacks the capacity to induce these cells. The fact that both the pulmonary-derived cells lines are associated with titan-like cell formation is remarkable, since titan cells are a lung-associated phenotype [12, 49, 71]. Previous work has demonstrated that extracts from Bronchial Alveolar Lavage (BAL) can induce titan cell formation in *C. neoformans* [71]**,** with the active factor thought to be derived from the bacterial cell wall (from lung-resident microbiome). This is unlikely to be the case in the assays I present here, since they were conducted in sterile conditions, suggesting that secretions from host cells can directly augment titan cell formation.

Titan cells formation is a cell density-dependent phenotype [12, 48] regulated by quorum sensing (QS) molecules [48, 217]. Although, the role of cryptococcal QS molecules was not tested here, the inverse correlation between cell density (initial inoculum concentration) and

the capacity of R265 (*C. gattii*) to form titan-like cells in cRPMI, strongly suggests that the phenotype is density dependent. It will be worthwhile to investigate if the putative cryptococcal QS molecule (Qsp1) which in addition to titanisation [48, 217] regulates other key virulence mechanisms in *Cryptococcus* [220], also regulates the cRPMI-induced titan-like cells. By employing an *in vitro* titan inducing protocol, Qsp1 peptide has been proven (section 7.2 of this thesis) to negatively regulate the formation of *C. gattii* titan cells. The use of conditioned media from MH-S for induction of R265 titan-like cells partially mimics the *in vivo* scenario during which *Cryptococcus* responds to the pulmonary environment before inflammation commences. Zaragoza *et al.* have previously demonstrated that titan cells are maximal in the absence of inflammation [49]. Since titan cells form as a combined influence of multiple host-related signals [48, 217] including cell density and pulmonary-derived cues, I predict that R265 titan-like cells are produced by the combinational influence of QS (a cell density-related phenomenon) and the alveolar macrophage secretome.

To preliminarily explore the strain specificity of cRPMI-induced titan-like cells, I screened 28 (16 *C. gattii,* 10 *C. neoformans* and 2 *C. deneoformans*) cryptococcal isolates of different genotypes. Based on the genotypic diversity recognized within the *Cryptococcus gattii/Cryptococcus neoformans* species complex, Hagen *et al*. re-classified the cryptococcal species complex elevating *C. gattii* to four distinct new species (according to their respective molecular genotypes: VGI, VGII, VGIII and VGIV) and *C. neoformans* into two separated species [*C. neoformans* (VNI and VNII) and *C. deneoformans* (VNIV)]. Since this re-classification, many studies have been conducted to understand underlying phenotypic and clinical variations that define the diversity of these species [28, 216, 221-223]**.** In my study, a genotypic-dependent was displayed such that the titan-like cells were exceedingly inducible within *C. gattii* strains as compared to non-gattii (*C. neoformans/deneoformans*) isolates.

It is notable, however, that within the *C. gattii* species, significant variation exists, with CBS10089/VGII attaining the highest proportion of titan-like cells (72.5%), whereas the VGIII isolates scored as low as 13.1% (CBS6993).

The cell size difference between *C. gattii* and *C. neoformans* is a factor that may contribute to their etiological differences, as *C. gattii* predominately affect immunocompetent individuals while *C. neoformans* is more prevalent in immunosuppressed patients [20, 58, 224]. To back this assumption, it will be interesting to conduct an *in vivo* correlation between their titan-like cell formation and host immunomodulatory responses.

My findings suggest a potential role for pulmonary cell factors in the adaptive behavior of *Cryptococcus*. Intriguingly, the titan-like cells were also inducible in naive RPMI media (Fig. 5.2 and Fig. 5.6) which implies that the naive media contains specific titan inducing factors. Since RPMI alone triggers titan cell formation and the phenotype is further enhanced by mammalian cell 'conditioning', the most likely scenario is that multiple chemical and proteinaceous signals synergise to drive maximal cell enlargement. In the future, studying the chemistry of RPMI-specific and cRPMI-specific compounds will hopefully help discover the underlying mechanism of titan cell formation in this organism.

CHAPTER 6

AN *IN VITRO* METHOD FOR INDUCING TITAN CELLS REVEALS NOVEL FEATURES OF YEAST-TO-TITAN SWITCH IN *CRYPTOCOCCUS GATTII*

This chapter is part of an article that has been published:

L. Saidykhan, Correia J, Romanyuk A, Desanti G. E, Taylor-Smith L, Makarova M, E.R Ballou, R. C. May. 2022. An in vitro method for inducing titan cells reveals novel features of yeast-to-titan switching in the human fungal pathogen *Cryptococcus gattii*. **PLOS Pathogens** (Proof of publication: appendix II)

Upon inhalation into the lungs, *Cryptococcus* is exposed to a repertoire of host factors (e.g., elevated temperature, nutrient deprivation, higher physiological CO_2 and hypoxia), [61, 63] which trigger adaptive phenotypes such as the formation of titan cells. This atypical morphotype is characterized by many attributes such as enlarged cell size, thicker cell wall, and altered capsule composition, which confer resistance to host immune defence and enhance survival in the host [15, 47, 166]. The recently-discovered *in vitro* titan production models, rely on experimental conditions that mimic the host factors to induce titan cells formation. The discovery of *in vitro* induction protocols is considered a major breakthrough, as efforts employed towards understanding the biology and mechanism underlying titanisation were impeded by the ethical and technical challenges associated with using animal models. Although titanisation is also thought to be a major virulence factor of *C. gattii* [13, 124, 225], the defining attributes and underlying mechanism of titanisation have thus far been mainly characterized in *C. neoformans* [127, 173, 226]. This chapter describes a facile *in vitro* induction approach that reveals a novel strategy for titanisation in *C. gattii*.

6.1 Titan cells are induced by growth in RPMI medium

In the previous chapter (Chapter 5), the ability of naive growth media of alveolar macrophage cell line (MH-S), RPMI, to produce titan cells in *Cryptococcus* was highlighted. By working at a lower cell density, exposure of R265 (a *C. gattii* strain) cells, obtained from YPD overnight culture, to sterile RPMI media at 37°C in an atmosphere of 5% CO_2 induced dramatic cell size increase within 24 hrs (Fig. 6.1A and B). The ability of serum-free RPMI to produce these enlarged cells provided the opportunity to characterize in detail the features of titanisation in this species using a simple, chemically-defined medium. Extending the incubation period to seven days enabled these cells to achieve cell bodies of up to 30μm in diameter, resulting in a

population with a median size significantly higher than yeast cells grown in YPD at 37°C in an atmosphere of 5% CO_2 for 7 days [median size: 13.7µm (5.1-29.8) vs 10.17µm (3.00-19.11) ($p<0.0001$)] (Fig. 6.1C and E [α=cell body diameter]).

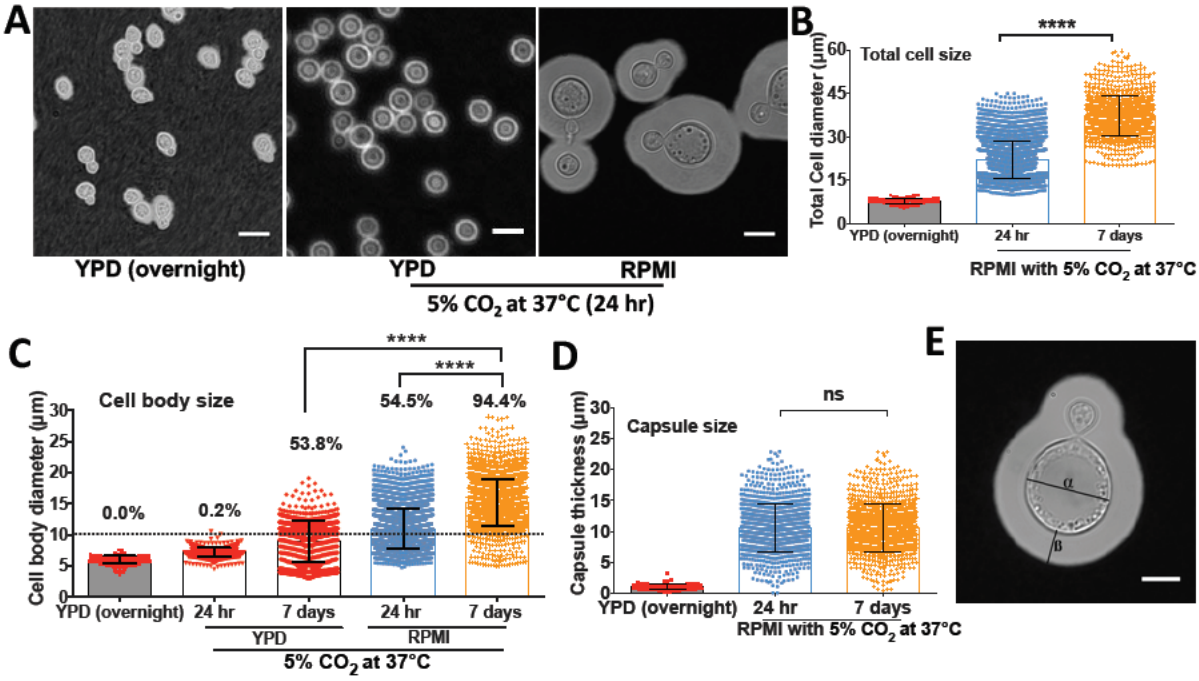

Figure 6.1: *C. gattii* (R265) exhibits cell body and capsule enlargement in response to growth in RPMI. A) Micrographs of R265 cells grown in YPD overnight at 25°C in atmospheric conditions (left panel), or at 37 °C in an atmosphere of 5% CO_2 either in YPD (middle panel) or RPMI (right panel). Scale bar=15µm. B) Total cell diameter (capsule included), C) cell body diameter (percentages represent percentage of cells more than 10µm in diameter) and D) capsule thickness of R265 cells all significantly increase after growth in RPMI at 37°C in 5% CO_2. The graphs represent at least 3 biological experimental repeats, and Kruskal-Wallis test was used to determine significance where **** = $p<0.0001$ and ns=$p>0.05$. E) Cellular morphology of R265 enlarged cells: cell body diameter (α) and capsule thickness (ß). Scale bar=15µm.

The cryptococcal yeast-titan transition occurs concomitantly with increasing capsule thickness [225]. Therefore, we characterized the capsule size (Fig. 6.1D and 1E [ß=capsule size]) of the *in vitro*-generated R265 enlarged cells. Relative to the YPD-grown capsule thickness, R265 enlarged cells demonstrated significantly thicker capsule [median capsule thickness: 10.28µm (0.34-22.9) vs 1.00µm (0.2-3.1), $p<0.0001$]. Although the cell body size progressively increased with induction time from 24 hr to 7 days (Fig. 6.1C), the capsule size of the enlarged cells reached a plateau at 24 hours and remained at a median size of 10.33µm (1.0-22.9) for the remaining six days of the assay (Fig. 6.1D). This suggests that the enlarged cells achieve their maximum capsule size much earlier than their maximum cell body size.

Titan cells exhibit altered cell wall composition [48, 51, 227]. Consequently, we characterized the cell wall of R265 *in vitro*-derived enlarged cells by staining for chitin with calcofluor white (CFW) [48]. In line with previous studies, we observed a significant increase ($P<0.0001$) in the chitin content of enlarged induced cells via flow cytometry (Fig 6.2B and 6.2C) that was also evident via fluorescence microscopy (CFW, Fig. 6.2A). In addition to displaying a titan-like capsule, cell body and cell wall, *C. gattii* (R265) enlarged cells bear a single large vacuole occupying almost the entire protoplasmic space (Fig. 6.2D), a characteristic previously described in both *in vivo* and *in vitro*-derived *C. neoformans* titan cells [49, 51].

In addition to morphological changes, the yeast-titan transition in *C. neoformans* involves a switch from a haploid to highly polyploid state [12, 48, 49, 51]. Thus, we evaluated the ploidy of RPMI *in vitro*-generated *C. gattii* enlarged cells. Whilst YPD grown yeast cells typically displayed a mix of cells with 1C or 2C DNA content (depending on which phase of the cell cycle they are in), RPMI-induced cells displayed DNA content ranging up to 16C after 7 days of induction (Fig. 6.2E). By DAPI staining the nucleus and visualizing by microscopy, we confirmed the enlarged cells were uninucleate (Fig. 6.2F). Thus, R265 titan-induced cells

exhibit all the key features of bona fide titan cells: cell enlargement, a large vacuole, altered cell wall composition and high ploidy. Interestingly, however, it was noted that in the case of R265, cell enlargement and increased DNA content do not necessarily occur at the same time. Indeed, R265 cells achieve significant cell body enlargement within 24hrs, but DNA content does not exceed 2C until much later (Fig. 6.2E). Taken together, the structural attributes exhibited by the *in vitro* RPMI-induced titan cells are typical of true titan cells.

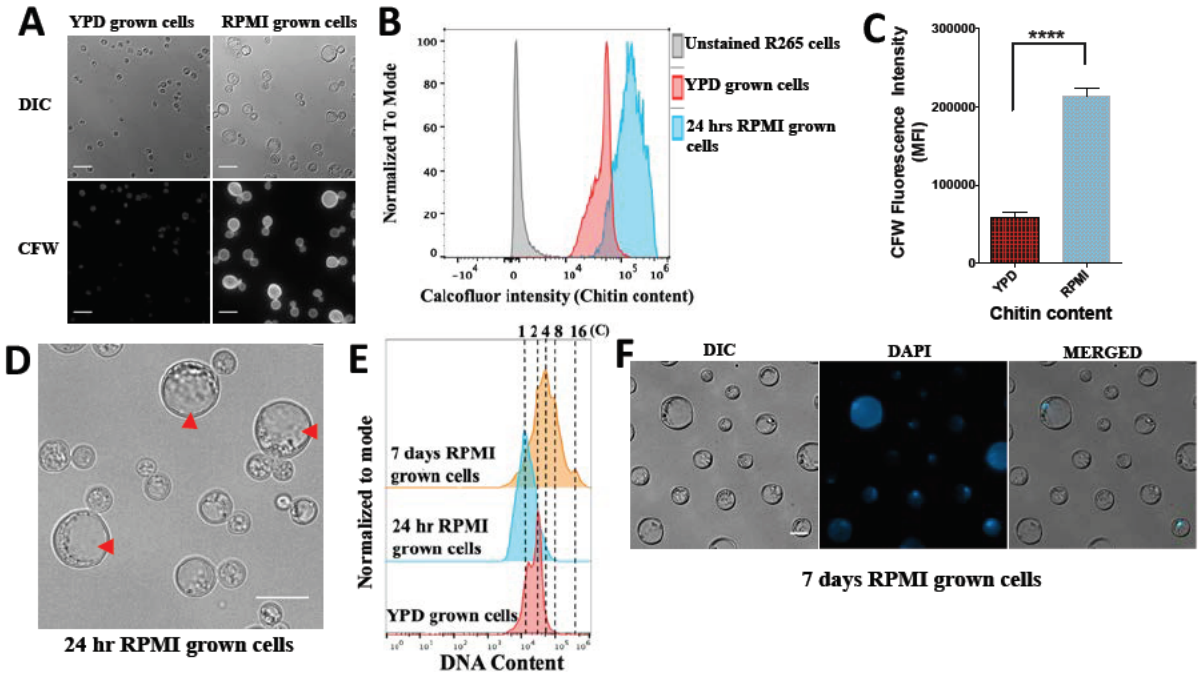

Figure 6.2: The cell wall chitin content and ploidy of enlarged cells are typical of titan cells. *In vitro* RPMI-generated enlarged cells displayed a significantly higher chitin level relative to YPD grown R265 cells, as indicated by the calcofluor white (CFW) fluorescence intensity shown using microscopy imaging in (A), via flow cytometry in (B) and graphically in (C, Median Fluorescence Intensity, MFI) ($p<0.00001$). Scale bar=15µm. Statistical significance was confirmed by Two-tailed *t*-test. D) Micrograph showing single large central vacuole of *in vitro*-generated enlarged cells. E) Ploidy measurement of RPMI-generated

enlarged cells based on flow cytometry analysis of DAPI staining. YPD grown cells (red) gated as 1C, 2C (haploid/diploid) were used as a control to determine ploidy (DNA content) of enlarged cells after 24 hr (blue) and 7days (orange) of induction. F) Micrographs showing the uninucleate nature of R265 titan cells upon staining with DAPI to visualize the nucleus. Scale bar=10μm.

6.2 In R265, cell enlargement is asynchronous with ploidy

To characterise the kinetics of cell size and ploidy changes more fully, we carried out a detailed time course analysis of R265 cells over a period of three weeks. By day 3 of induction, R265 cells showed significantly enlarged body diameter as compared with non-induced (YPD grown) cells [median size: 13.7μm (5.1-29.8) vs 6.5μm (4.9-8.89); ($p<0.0001$)] with 81.5% (5241/6431) of cells larger than 10μm (Fig. 6.3A). Despite this size increase, for the first three days all cells were 1C or 2C (reflecting a haploid cell cycle) (Fig 6.3B). The population reached the maximum cell size on day 5, and from day 5 to day 7, there was no change in the size of induced cells [median size being 14.9μm at day 5 and 14.7μm at day 7 ($p=0.7656$)]. However, the ploidy of these cells increased, with tetraploid (4C) cells apparent at day 5 and cells exhibiting DNA content of up to 16C present by day 7. In parallel, although the maximum size of induced cells no longer increased at this late stage of incubation, the proportion of the population with a large cell phenotype rose from 92.8% to 99.3% ($p<0.0001$) (Fig 6.3A). Thus, it appears that: a) size increase and ploidy increase are separable phenotypes during titanisation of R265, b) true titan cells (large and polyploid) appear only after around 5 days of induction and c) their maximum cell size is achieved rapidly during titanisation, but the proportion of cells adopting this fate rises steadily over a long time period.

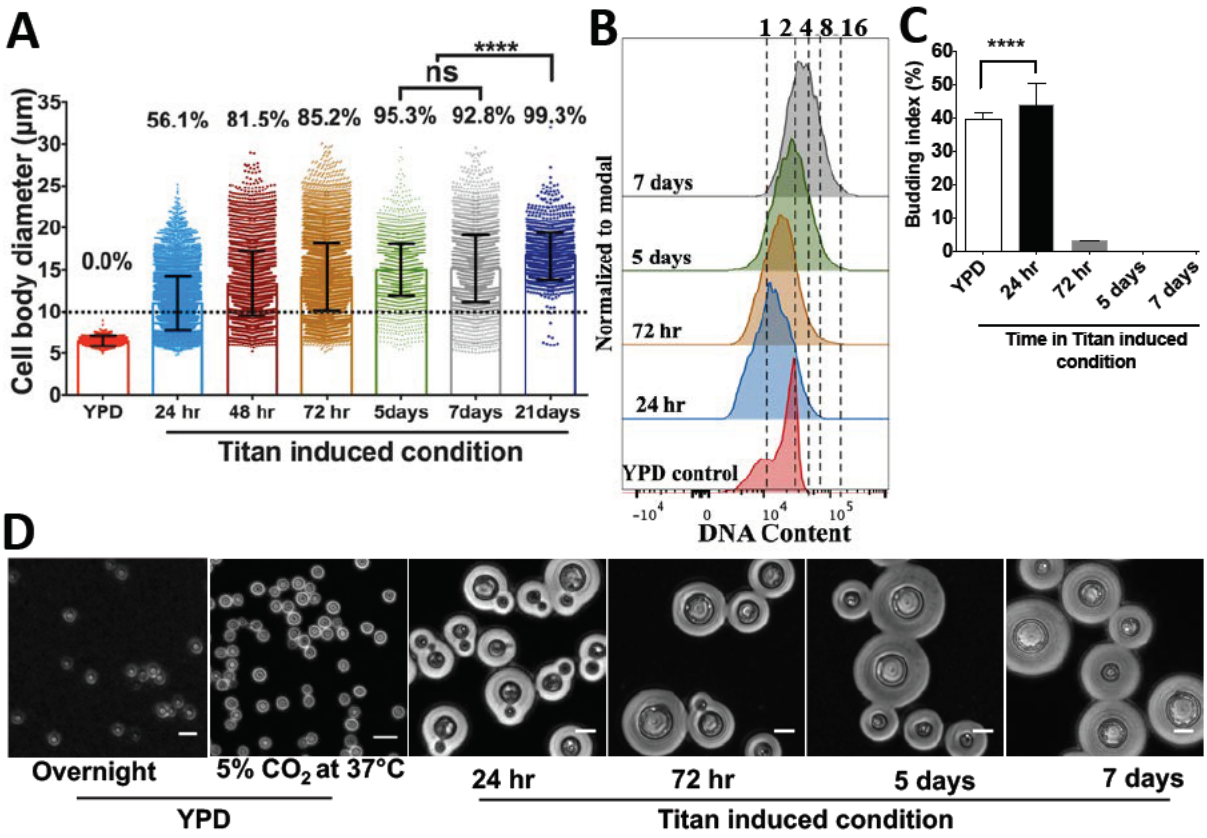

Figure 6.3 Cell enlargement, polyploidization and budding occur at different periods during titan induction in R265. A) Cell body diameter of R265 titan cells over prolonged induction (24 hr to 21 days) as compared to YPD grown cells. Enlarged cells were recovered at different time points, fixed and measured. The error bars represent median of 3 biological repeats, where ****=p<0.00001. B) Samples from all the induction time points were fixed, DAPI stained and analysed for ploidy by flow cytometry with reference to YPD grown cells, which were used to gate for 1C and 2C DNA content. C) Budding index of cells recovered from YPD and titan inducing condition. Budding index was expressed as percentage of budded cells per total number of cells. At least 3000 cells were analysed for each sample (the graph represents three biological repeats and significance was confirmed by one-way ANOVA where, ****=p<0.00001. D) Microscopy images showing the budding nature of cells obtained from YPD or at various timepoints after titan induction. Scale bar: 15µm.

6.3 The polyploid titan cells are unbudded

Within our *in vitro* model, after 3 days of induction, the R265 titan cells completely stop budding despite being polyploid (Fig. 6.3). This suggests that budding and DNA increase are decoupled, consistent with endoreduplication. During the first 3 days, budding index (the number of mother cells producing buds) fell from 44.4% (2552/5749 cells) at 24 hr to 2.8% (26/933) by day 3 and 0% (0/2971) by the fifth day of induction (Fig. 6.3C). Hence, we termed the period before 3 days of induction as the budded phase and the later period as the unbudded phase. During the budded phase, cells predominantly exhibited a 1C DNA content (Fig. 6.3B and Fig. 6.3D). However, during the unbudded phase (3 to 7 days) cells rapidly became polyploid, with DNA content rising from 2C to 4C to 16C (Fig. 6.3B and Fig. 6.3D). The 1C DNA content during the budded phase, coupled with cell enlargement, suggests that the cells spend longer in the G1 phase of their cell cycle during titan induction.

6.4 Unbudded titan cells are viable and metabolically active.

The unbudded state of *C. gattii* (R265) titan cells prompted us to investigate whether this cell cycle arrest occurs as a consequence of nutrient deprivation. By filtering 7 day old titan-induced cultures, we obtained the largest (>20μm) titan cells and re-cultured them on a rotary wheel at 20 rpm for i) 2 hr or ii) overnight at 25°C in YPD broth. These cells remained unbudded during the first 2 hrs (the generation period of *Cryptococcus* yeast) (Fig. 6.4A) but after overnight incubation produced daughter cells (Fig. 6.4B) resembling yeast cells in size and morphology (round-shaped with small capsule size) (Fig. 6.4C and Fig. 6.4D). Time-lapse observation revealed that titan cells starts budding after 2 hours (Video S1- [126]). The active proliferation in YPD (nutrient rich media) of the unbudded titan cells suggest that their exhibition of growth arrest is due to nutrient deprivation due to growth in RPMI.

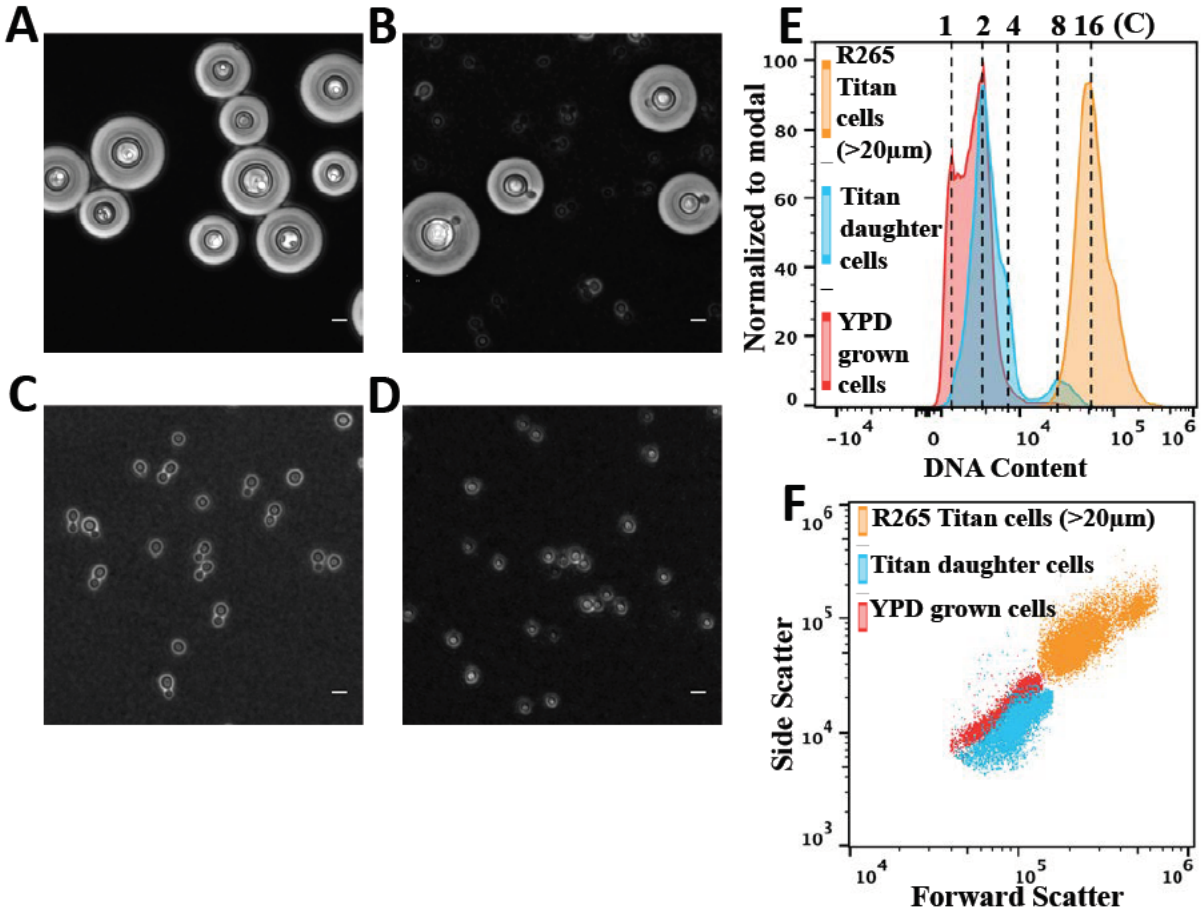
A
B
C
D
E
1 2 4 8 16 (C)
R265 Titan cells (>20µm)
Titan daughter cells
YPD grown cells
Normalized to modal
DNA Content
F
R265 Titan cells (>20µm)
Titan daughter cells
YPD grown cells
Side Scatter
Forward Scatter

G

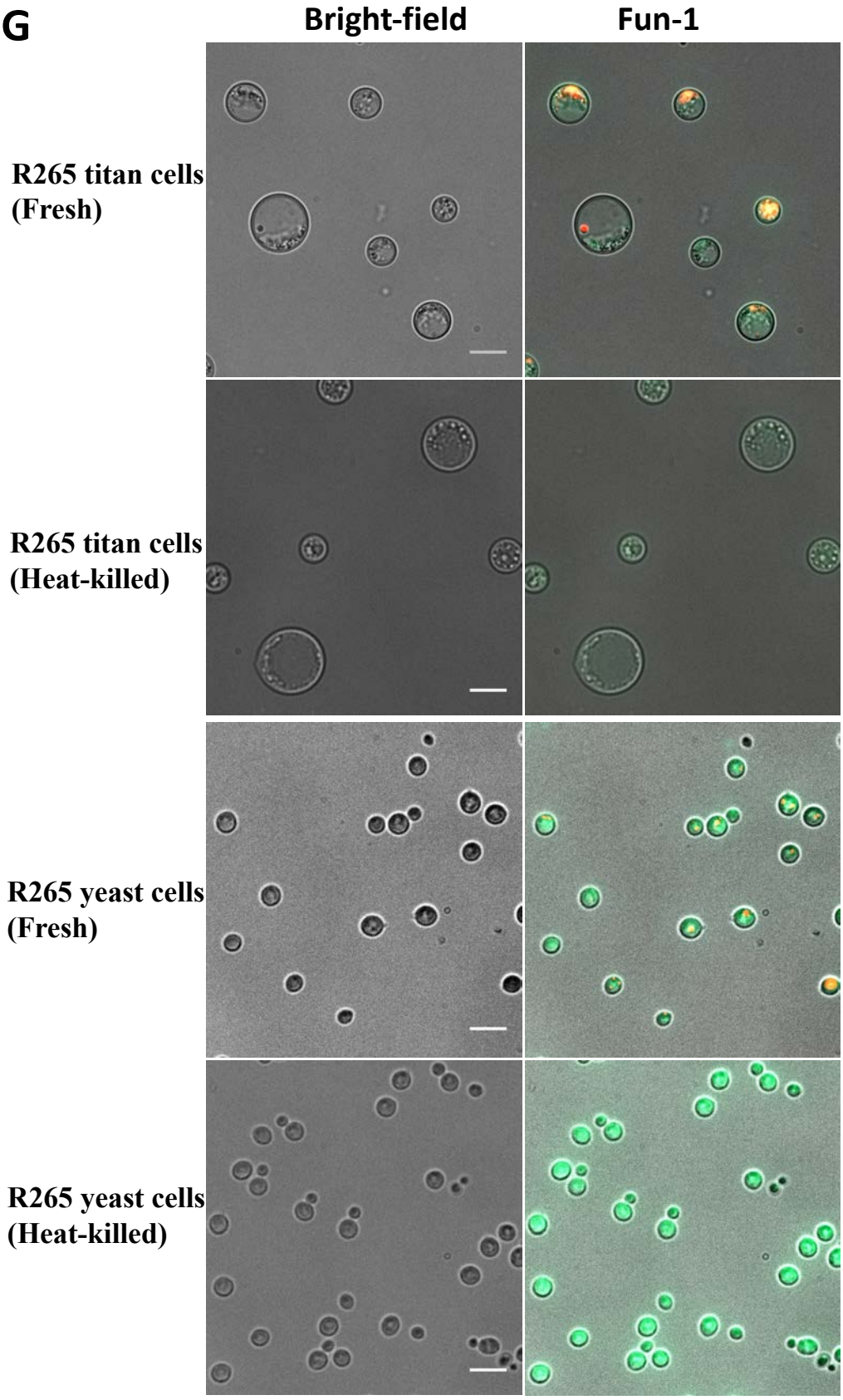
Bright-field
Fun-1
R265 titan cells (Fresh)
R265 titan cells (Heat-killed)
R265 yeast cells (Fresh)
R265 yeast cells (Heat-killed)

Figure 6.4 Characterization of daughter cells and metabolic state of R265 titan cells. 7 day old R265 titan cells were purified using a 20µm cell strainer (A) and then B) re-cultured overnight in YPD to induce budding. C) After 24hrs, daughter cells of R265 titan cells were isolated by filtration of the titan culture (through a >15µm cell strainer) and microscopically compared with D) YPD grown yeast R265 cells (control). E) DNA content of titan-derived daughter cells (Blue) cells as compared to YPD grown (red) and >20µm R265 titan cells (brown). F) Size distribution of daughter cells (blue), YPD grown (red) and >20µm R265 titan cells (orange). G) Microscopy images demonstrating the metabolic activity titan cells from 7 days old cultured (fresh vs heat-killed) and YPD grown yeast cells (fresh vs heat-killed). The cells were stained with the metabolic reporter dye Fun-1 which is converted from yellow-green to orange-red by metabolically active cells. Scale bar =10µm.

We tested whether unbudded R265 titan cells are quiescent, but metabolically active, by using the dye Fun-1, whose emission wavelength is converted from yellow-green to orange-red colour by metabolically active cells. Unbudded titan cells were able to convert the Fun-1 dye in a manner that was comparable to actively-growing yeast cells (Fig. 6.4 G). Thus, both timelapse imaging and metabolic profiling indicates that titan cells remain viable and metabolically active.

6.5 Titan cells produce polyploid, yeast-sized, daughter cells

To investigate if the cellular similarities observed between titan-derived daughter cells and yeast cells extend to their ploidy, we characterized the DNA content of daughter cells relative to their highly polyploid titan mother cells (>20µm) and haploid yeast cells. Despite having the cellular properties of yeast cells (Fig. 6.4C, 6.4D and 6.4F), titan-derived daughter cells exhibited a higher DNA content than normal yeast, with most cells displaying either diploid (2C) or polyploid (>4C) DNA content (Fig. 6.4E). Taken together, the delayed DNA

replication of R265 titan cells (Fig. 6.3B) coupled with the production of polyploid daughter cells (up to 8C) (Fig. 6.4E) is indicative of high ploidy elasticity in *C. gattii* titan cells.

By re-culturing titan-derived daughter cells in titan inducing condition, we assessed the ability of these 'second generation' cells to return to a titan state. Unlike the 'original' titan cells, these titan-derived daughters increased their DNA content within 24 hours, achieving genome sizes of 16C and 32C at 24hr and 7 days respectively (Fig. 6.5D). As with the original mother titan cells, titan-induced daughter cells underwent budding during the early induction period but formed unbudded titan cells by day 7 of induction (Fig. 6.5A and Fig. 6.5B).

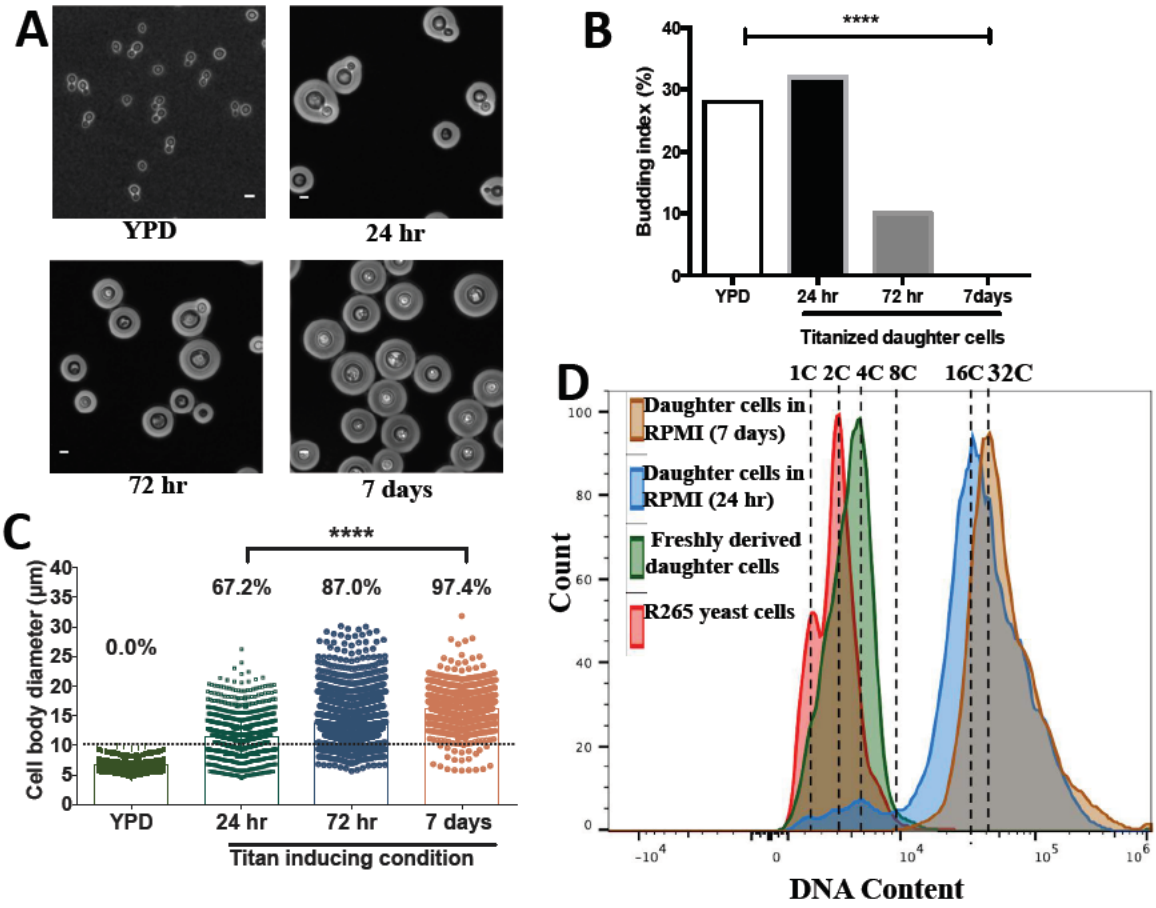

Figure 6.5 Characterization of budding nature and titanisation of R265 titan-derived daughter cells. A) Images showing the budding nature of daughter cells before and after titan induction for 24hr, 72 hr and 7 days. Scale bar= 5µm. B) Budding index of daughter cells

before and after titanisation. C) Cell body diameter was measured microscopically, and percentage of titan cells determined based on >10μm cell size. The data represents three independent biological repeats and significance was confirmed by Kruskal-Wallis test where, ****=p<0.00001. D) Daughter cells of R265 titan cells were isolated and returned to titan inducing condition and their ploidy was determined by DNA content measurement via flow cytometry before titan induction (green), after 24 hr (blue) and 7 days (brown) relative to R265 haploid yeast (red). E) Flow cytometry data showing the gating strategy employed to confirm cell ploidy of R265 titan daughter cells as compared to YPD grown yeast and (>20μm) filtered titan cells.

6.6 Strain specificity

There is considerable evolutionary divergence between clades within the *Cryptococcus* genus and indeed the nomenclature of this group is rapidly changing in recognition of potential cryptic species [228]. To begin to assess variation in titanisation capacity, I screened 42 different cryptococcal isolates comprising 32 *C. gattii* species complex strains (VGI – VGIV), 8 *C. neoformans* strains (VNI and VNII) and 2 *C. deneoformans* strains (VNIV) for their capacity to form titan cells in our *in vitro* protocol (3 days incubation in RPMI with 5% CO_2 at 37°C). Overall, the capacity to form titan cells in *C. gattii* strains was significantly higher than either *C. neoformans* or *C. deneoformans.* All 32 *C. gattii* strains produced titan cells, with an average of 60% titan cells at the end of the assay (Table 6). In contrast, only 4/8 of *C. neoformans* and 0/2 of *C. deneoformans* strains showed any level of titanisation (Table 6). Within the *C. gattii* species complex, VGII genotype strains (*C. deuterogattii*) displayed the highest titanisation capacity (averaging 80.0%) while VGIII (*C. gattii*) scored the lowest at 37.9% (Table 6).

Table 6. Capacity profile for titan cell formation among cryptococcal isolates. Percentage of titan cells was determined based on capacity to enlarge >10μm (Fig. 6.6) and having >2C ploidy (Fig. 6.7)

Species/strain	**Genotype**	**Median size [size range] (μm)**	**% Titan cells***
C. gattii			
WM265	VGI	10.9 [4.1-28.4]	62.7
WM179	VGI	11.3 [4.1-25.0]	67
CBS8755	VGI	11.0 [4.6-17.7]	62.8
C384	VGI	10.0 [4.2-27.9]	50.1
NIH312	VGI	8.0 [4.1-24.3]	29.3
B4546	VGI	8.9 [4.5-26.2]	35.3
EJB11	VGI	10.8 [5.3-25.6]	65.5
MMCO8-897	VGI	6.7 [4.4-16.3]	17.5
CBS1508	VGI	9.0 [4.7-17.4]	27.3
CBC1873	VGI	11.6 [5.8-22.7]	62.3
	Av. of VGI	**9.82**	**48.0**
R265	VGIIa	13.4 [5.1-29.6]	79.7
CDDR271	VGIIa	12.9 [4.4-26.5]	84.7
ENV152	VGIIa	10.6 [5.5-28.0]	54.8
CDCF2866	VGIIa	11.3 [4.6-19.9]	89.1
ICB180	VGII	12.7 [3.4-26.3]	82.6
CBS10089	VGII	13.3 [5.6-25.1]	89.1
CDCR272	VGIIb	13.5 [6.8-39.2]	90
B7735	VGIIb	12.9 [5.5-26.3]	86.4
EJB18	VGIIc	11.3 [4.7-19.5]	75.6
EJB52	VGIIc	11.1 [4.8-19.5]	68.3

	Av. of VGII	**12.3**	**80.0**
CBS6955	VGIII	8.24 [4.34-17.9]	66.3
CBS6993	VGIII	9.9 [4.8-22.6]	45.7
CBS1622	VGIII	5.4 [3.3-10.9]	4.4
WM1243	VGIII	10.1 [4.6-22.4]	50.7
B13C	VGIII	10.0 [4.4-23.5]	50
CA2350	VGIII	8.8 [4.7-21.7]	32.7
CA1227	VGIII	7.1 [4.4-15.2]	15.4
	Av. of VGIII	**9.1**	**37.9**
WM779	VGIV	11.8 [4.2-25.5]	66.5
CBS1010	VGIV	12.6 [4.3-22.2]	80
B5742	VGIV	8.9 [4.6-21.8]	37.3
B5748	VGIV	10.7 [4.8-22.9]	61.9
CBS10101	VGIV	10.9 [4.4-19.6]	62.7
	Av. of VGIV	**12.2**	**61.7**
All *C. gattii* (Average)		**10.75**	**60**
C. neoformans			
H99	VNI	7.7 [3.4-20.1]	21.3
Zc1	VNI	7.6 [4.46-15.9]	5.8
Zc8	VNI	12.4 [5.4-20.7]	76.1
Zc12	VNI	4.1 [2.1-7.0]	0
CBS8336	VNI	9.6 [4.6-24.8]	39.9
125.91	VNI	7.2 [4.6-16.3]	7.9
	Av. of VNI	**8.1**	**23.8**
Tu_406_1	VNII	10.0 [4.9-18.5]	0
HamdanC3'1	VNII	9.3 [4.5-22.1]	0

	Av. of VNII	**9.6**	**0**
All *C. neoformans* (Average)		**9.7**	**18.8**
(average)			
B3501	VNIV	7.2 [4.5-17.43]	0
CBS6995	VNIV	4.5 [3.4-11.1]	0
	Av. of VNIV	**5.85**	**0**
All *C. deneoformans* (Average)		**5.85**	**14.2**

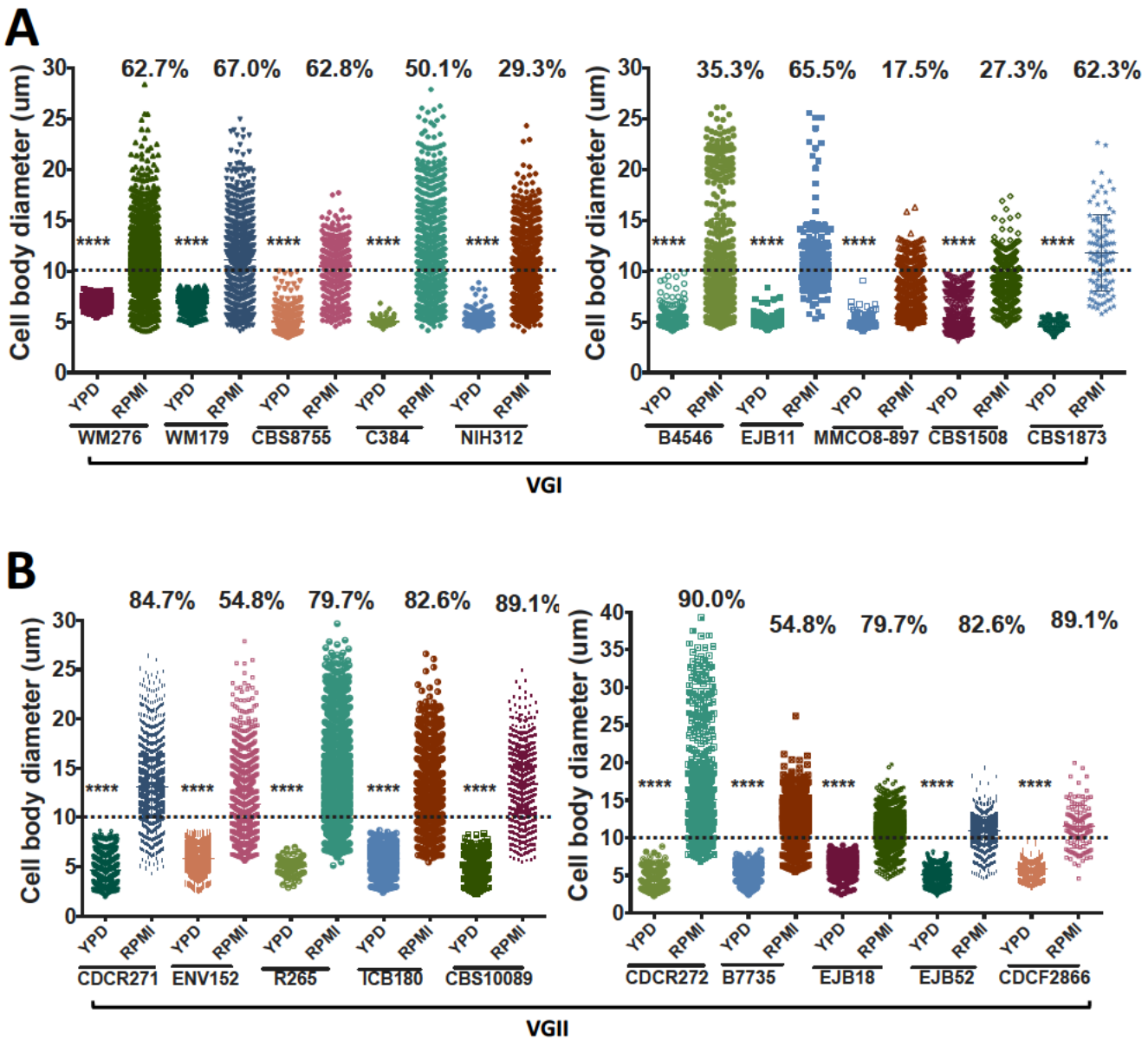
A
Cell body diameter (um)
62.7%
67.0%
62.8%
50.1%
29.3%
35.3%
65.5%
17.5%
27.3%
62.3%
****
YPD
RPMI
WM276
WM179
CBS8755
C384
NIH312
B4546
EJB11
MMCO8-897
CBS1508
CBS1873
VGI
B
84.7%
54.8%
79.7%
82.6%
89.1%
90.0%
CDCR271
ENV152
R265
ICB180
CBS10089
CDCR272
B7735
EJB18
EJB52
CDCF2866
VGII

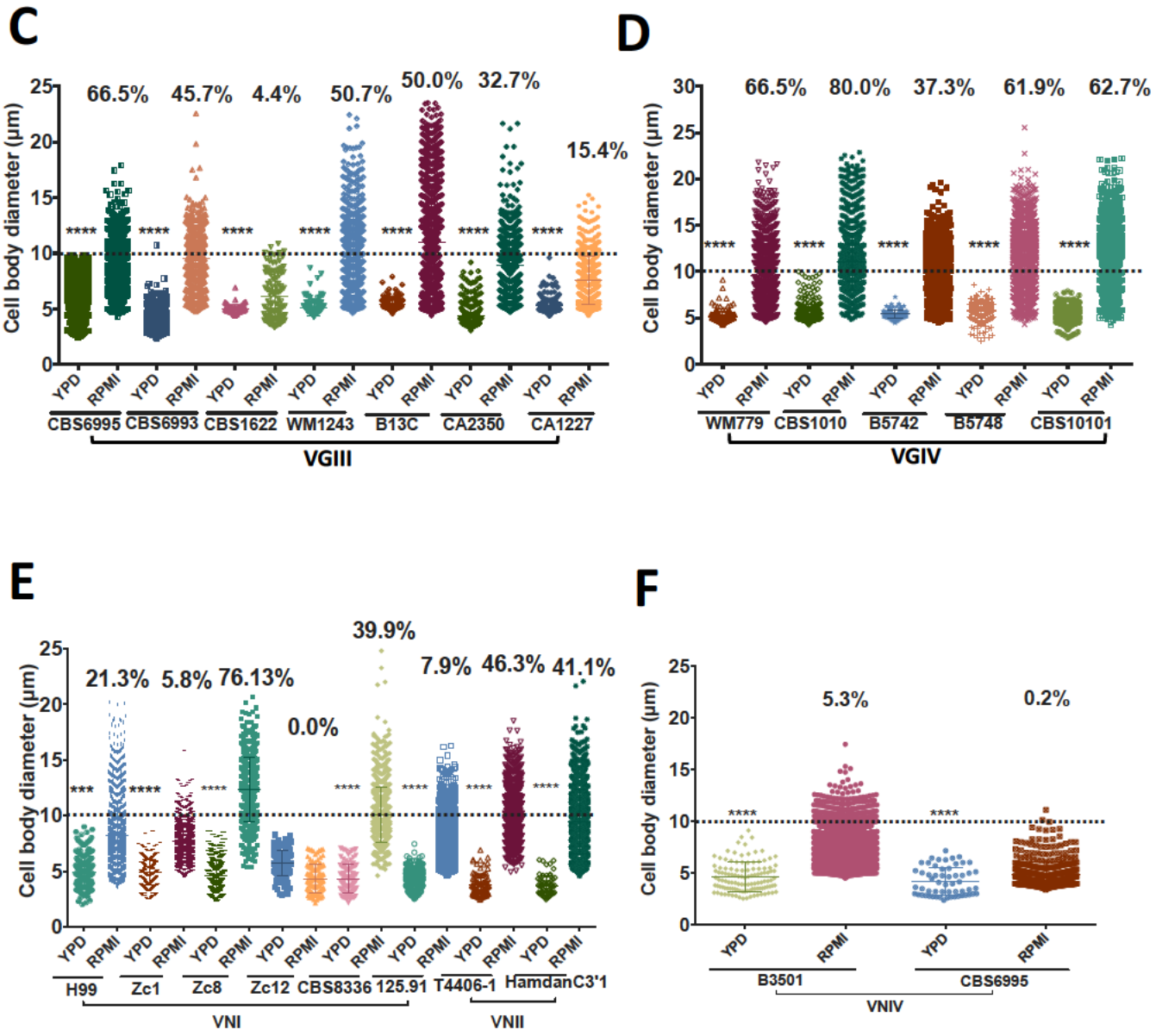

Figure 6.6 Cell body diameter of 42 YPD grown and titan-induced cryptococcal isolates representing the different genotypes within the *C. neoformans/gattii* complex species. All strains were induced for titan cell formation according to the *in vitro* protocol (Section 3.2.5.1). The cell body diameter was determined after 72hrs. A), B), C) and D) Cell body size distribution of isolates from *C. gattii* complex (VGI-VGIV) before induction (YPD) and after 72 hr of induction (RPMI). E), F) Cell body size distribution of isolates from *C. neoformans*

(VNI-VNII) and *C. deneoformans* (VNIV) before (YPD) and after 72 hr induction (RPMI) respectively.

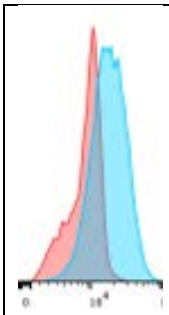	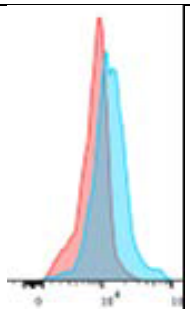	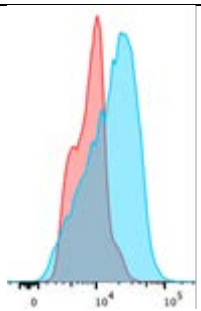	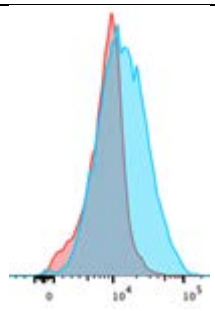
WM276/VGI	**WM179/VGI**	**CBS8755/VGI**	**C384/VGI**
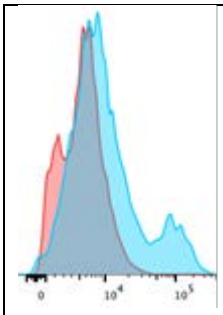	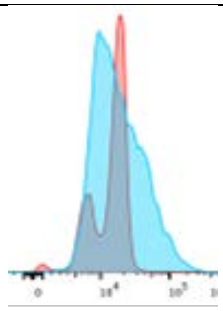	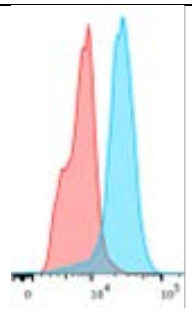	
B4546/VGI	**NIH312/VGI**	**EJB11/VGI**	**MMCO8-897/VGI**
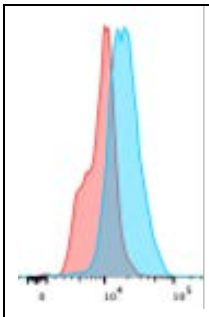	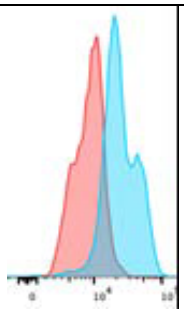	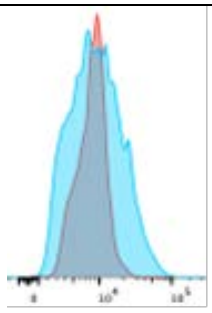	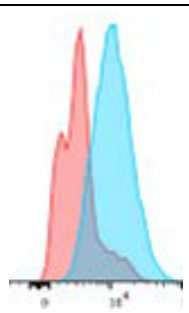
CBS1508/VGI	**CBC1873/VGI**	**MMCO8-897/VGI**	**CDC271/VGIIa**

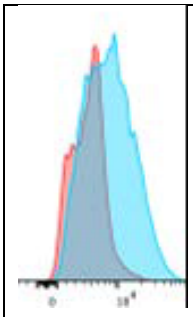	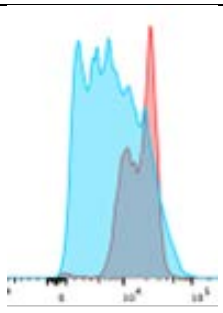	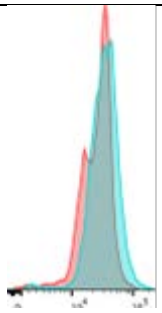	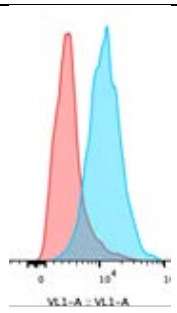
ENV152/VGIIa	**CDCF2866/VGIIa**	**R265/VGIIa**	**ICB180/VGII**
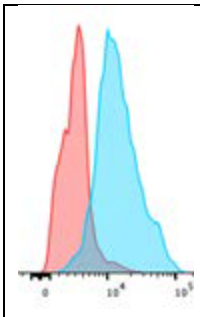	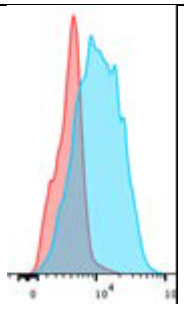	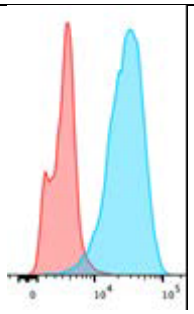	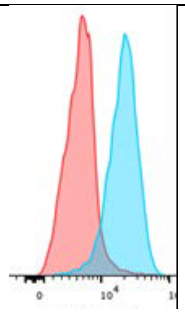
CBS10089/VGII	**CDCR272/VGIIb**	**B7735/VGIIb**	**EJB18/VGIIc**
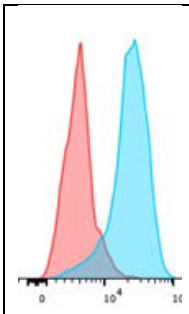	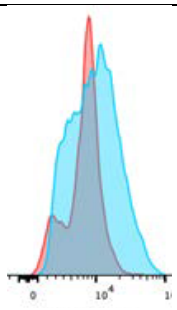		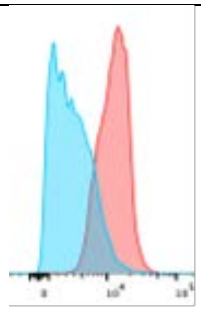
EJB52/VGIIc	**CBS6955/VGIII**	**CBS6993/VGIII**	**CBS1622/VGIII**
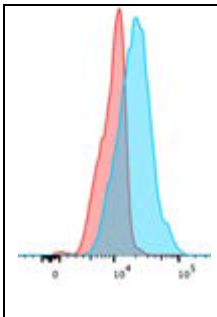	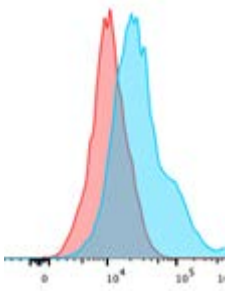	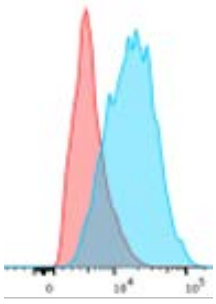	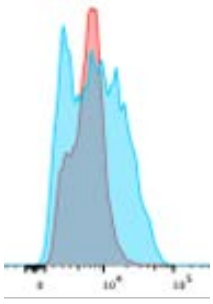
WM1243/VGIII	**B13C/VGIII**	**CA2350/VGIII**	**CA1227/VGIII**

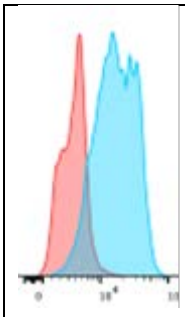	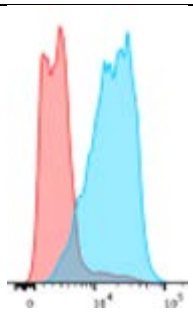	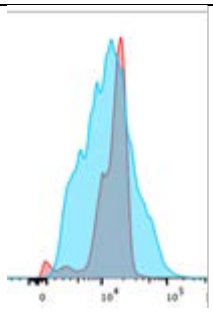	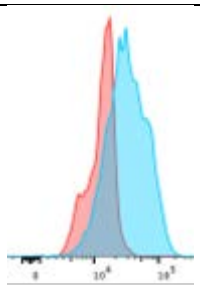
WM779/VGIV	**CBS1010/VGIV**	**B5742/VGIV**	**B5748/VGIV**

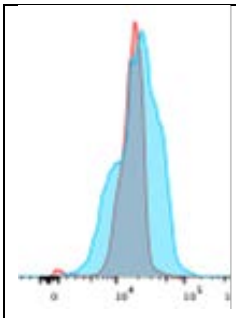	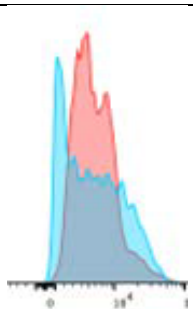	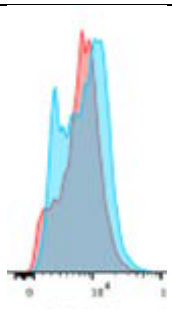	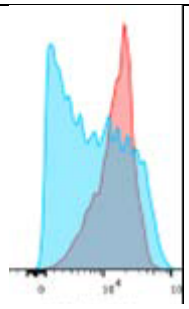
CBS10101/VGIV	**H99/VNI**	**ZC1/VNI**	**ZC8/VNI**

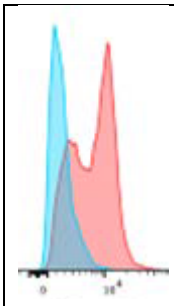	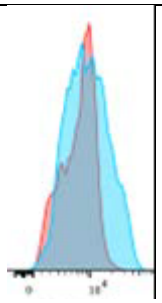	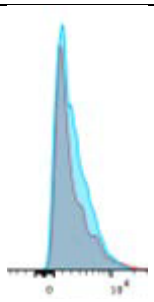	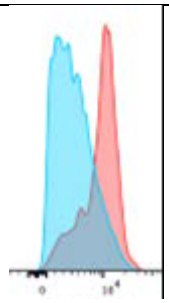
ZC12/VNI	**CBS8336/VNI**	**125.91/VNI**	**T4406-1/ VNII**

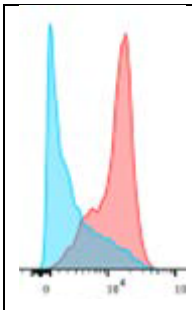	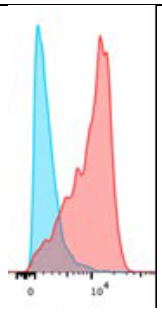	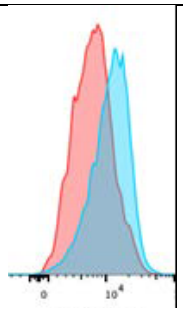
HamdanC3'1/VNII	**B3501/VNIV**	**CBS6995/VNIV**

Figure 6.7 DNA content of 42 YPD grown (red) and titan-induced (blue) cryptococcal isolates representing the different genotypes within the *C. neoformans/gattii* complex. All isolates were induced for titanisation according the *in vitro* induction model (as described in the "methods" section-3.2.5.1) after DNA content was confirmed by DAPI staining and flow cytometry analysis.

6.7 Titanisation in *C. gattii* is a polygenic trait

Several genetic regulators have been implicated in the control of titanisation in *C. neoformans* [12, 48, 49, 51, 226]. The interaction between these (nuclear genome-encoded) genetic regulators and mitochondrial activity has been proposed [173]. Consequently, we exploited a collection of parent/progeny crosses that we generated as part of an earlier study, and for which mitochondrial genotype is known, [229] to begin to investigate the genetic control of titanisation in *C. gattii*. Mitochondrial genotype and inheritance were confirmed by the expression of *ATP6* gene (encoded by the mitochondrial genome) [229].

Firstly, a cross between *C. gattii* R265 (MATα) and *C. gattii* LA584 (*MAT*a), where the progeny inherited their mitochondrial genotype from LA584, was investigated. LA584 is a strain that belongs to the same VGII group as R265 but shows a significantly lower capacity to titanise in the *in vitro* conditions (Fig 6.8A). The progeny from this cross showed considerable variation in titanisation capacity, with some scoring high titanisation capacity like R265 (high titan generating parent) and others scoring low titan cells proportion like LA584 (low titan generating parent). Ploidy measurement of parents/progeny based on flow cytometry analysis of DAPI staining for DNA content is shown in Fig. 6.9A**.** Notably, there was no correlation between titanisation capacity of individual progeny and the mitochondrial genotype (R265 or

LA584) that they had inherited, suggesting that mitochondrial genotype is not a major driver of this phenotype.

Next, a cross between R265 and a more distantly related strain, B4564 (VGIII), which shows relatively low levels of titanisation was assayed. In this outgroup cross, a 100% inheritance of the mitochondrial genome from B4564 (*MAT*a) was confirmed in 18 progeny [229]. Despite this uniparental mitochondrial inheritance, all the progeny exhibited a significantly higher capacity for titanization than B4564 (Fig. 6.8B). Ploidy measurement of parents/progeny based on flow cytometry analysis of DAPI staining for DNA content is shown in Fig. 6.9B. Furthermore, 12/18 progeny showed a higher capacity for titanisation than either parent ($p<0.0001$) with 5 progeny (P1, P5, P7, P8, P9 and P18) showing a remarkable >95% titan cell population by the end of the assay. Together, these data suggest that the nuclear genome, and not the mitochondrial genome, is the major source of variation in the capacity of different isolates to form titan cells.

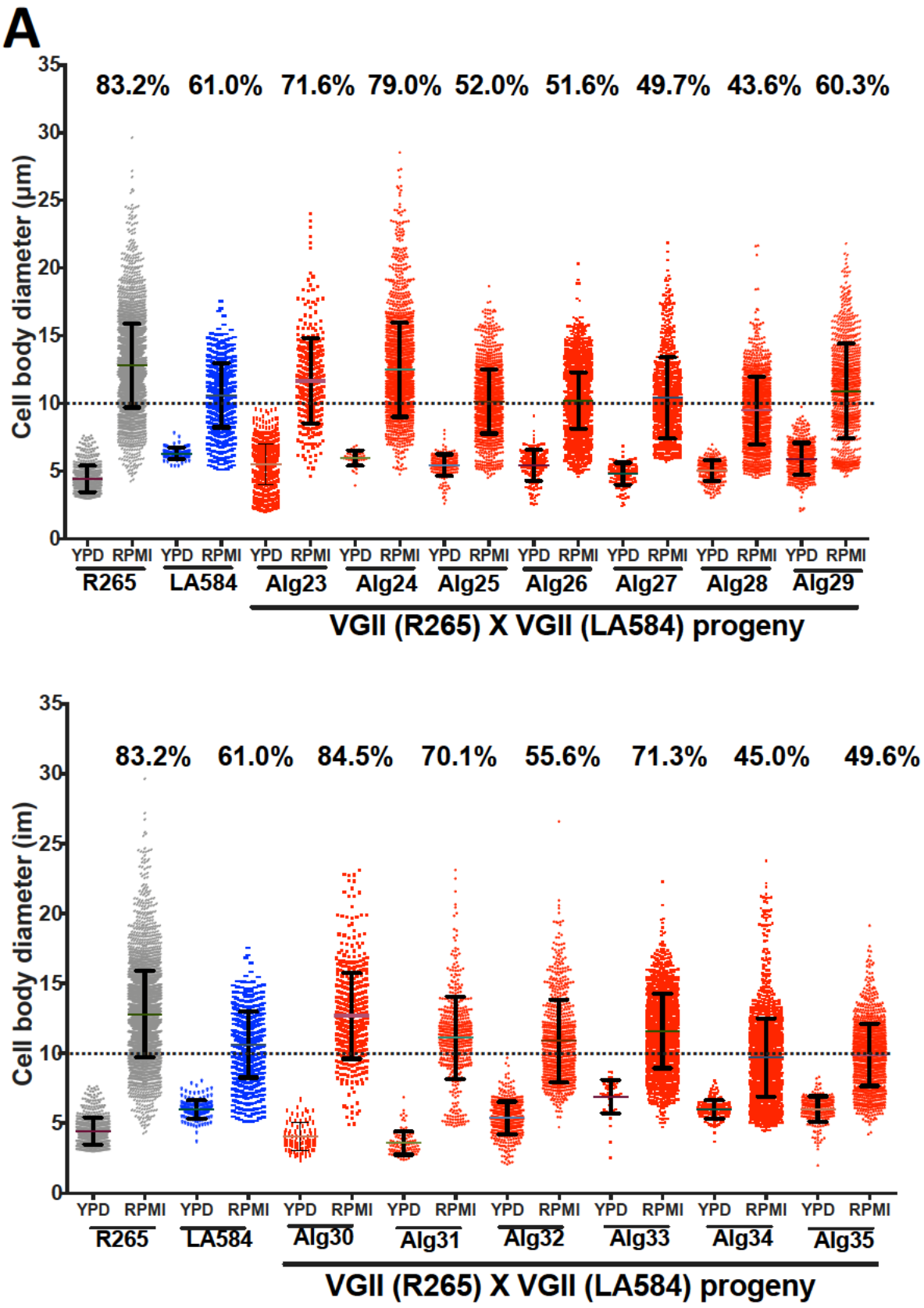
A
83.2% 61.0% 71.6% 79.0% 52.0% 51.6% 49.7% 43.6% 60.3%
Cell body diameter (µm)
0
5
10
15
20
25
30
35
YPD RPMI YPD RPMI YPD RPMI YPD RPMI YPD RPMI YPD RPMI YPD RPMI YPD RPMI YPD RPMI
R265 LA584 Alg23 Alg24 Alg25 Alg26 Alg27 Alg28 Alg29
VGII (R265) X VGII (LA584) progeny
83.2% 61.0% 84.5% 70.1% 55.6% 71.3% 45.0% 49.6%
Cell body diameter (im)
YPD RPMI YPD RPMI YPD RPMI YPD RPMI YPD RPMI YPD RPMI YPD RPMI YPD RPMI
R265 LA584 Alg30 Alg31 Alg32 Alg33 Alg34 Alg35
VGII (R265) X VGII (LA584) progeny

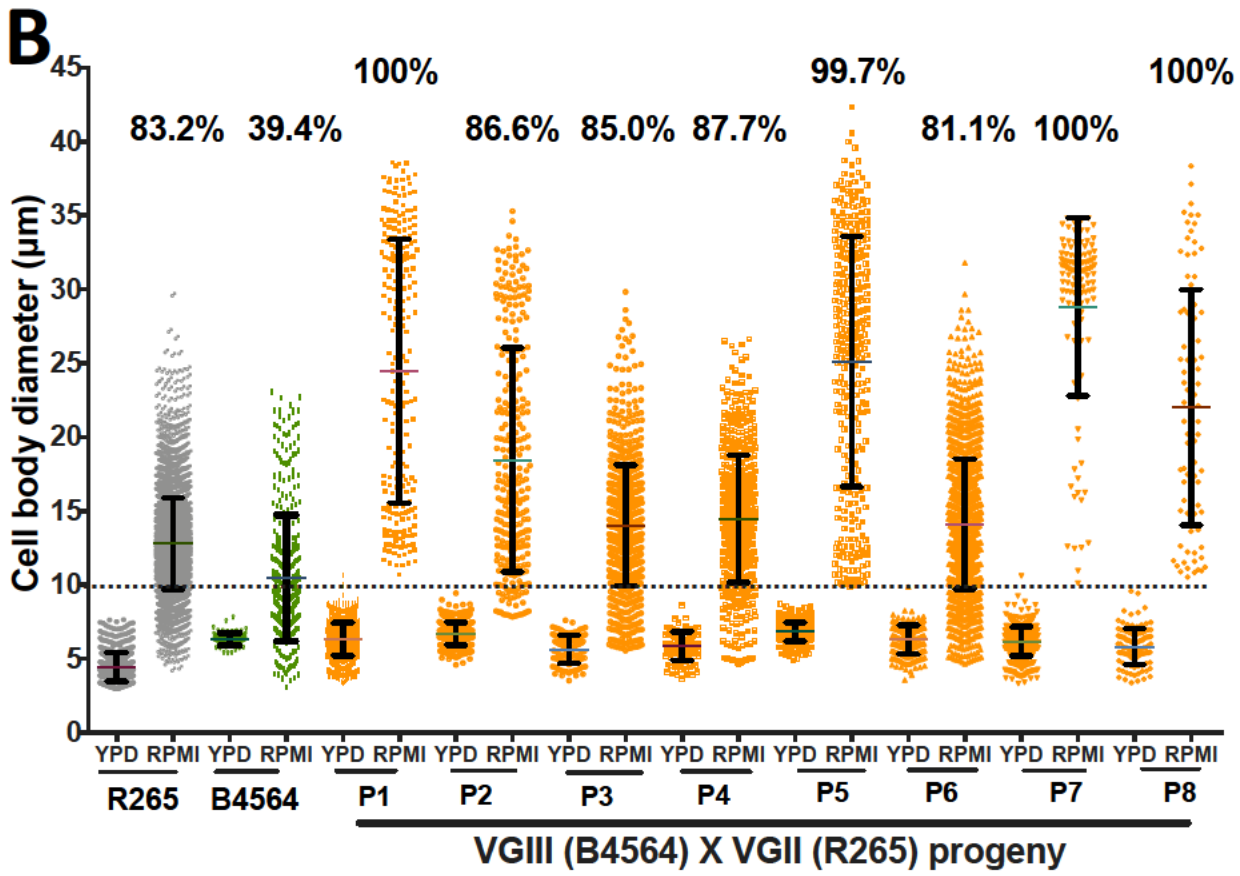
B
Cell body diameter (µm)
0
5
10
15
20
25
30
35
40
45
83.2%
39.4%
100%
86.6%
85.0%
87.7%
99.7%
81.1%
100%
100%
YPD RPMI YPD RPMI YPD RPMI YPD RPMI YPD RPMI YPD RPMI YPD RPMI YPD RPMI YPD RPMI YPD RPMI
R265
B4564
P1
P2
P3
P4
P5
P6
P7
P8
VGIII (B4564) X VGII (R265) progeny

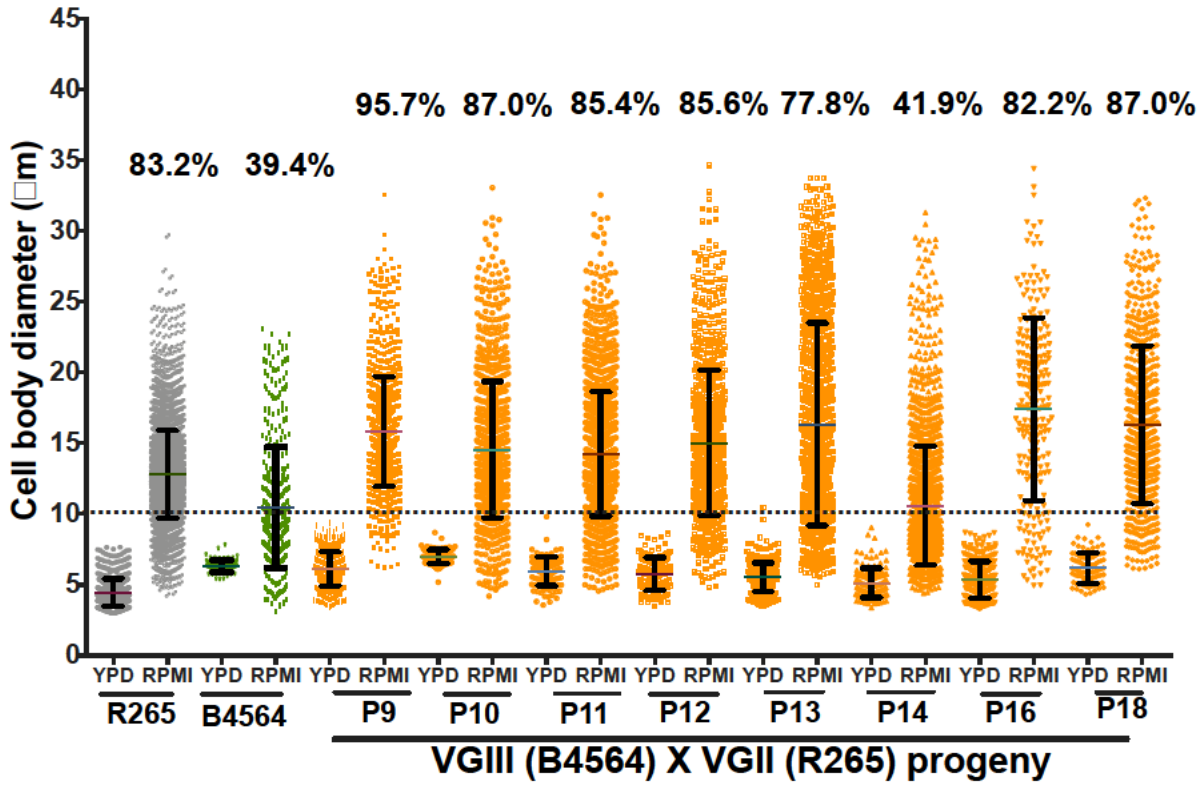

Figure 6.8 Titan cell formation capacity of *C. gattii* progeny arising from two crosses. (A) Titanisation pattern following three days of induction for R265 (VGII) x LA584 (VGII) and 13 progeny (Alg23-Alg35) arising from this cross [229]. (B) Titanisation pattern following three days of induction of R265 (VGII) x B4564 (VGIII) and 18 of the progeny (P1-P18) arising from this cross. All strains (parent and progeny) were induced for titan cell formation and DNA content was determined after 72hrs as described in the "methods" section-3.2.5.1.

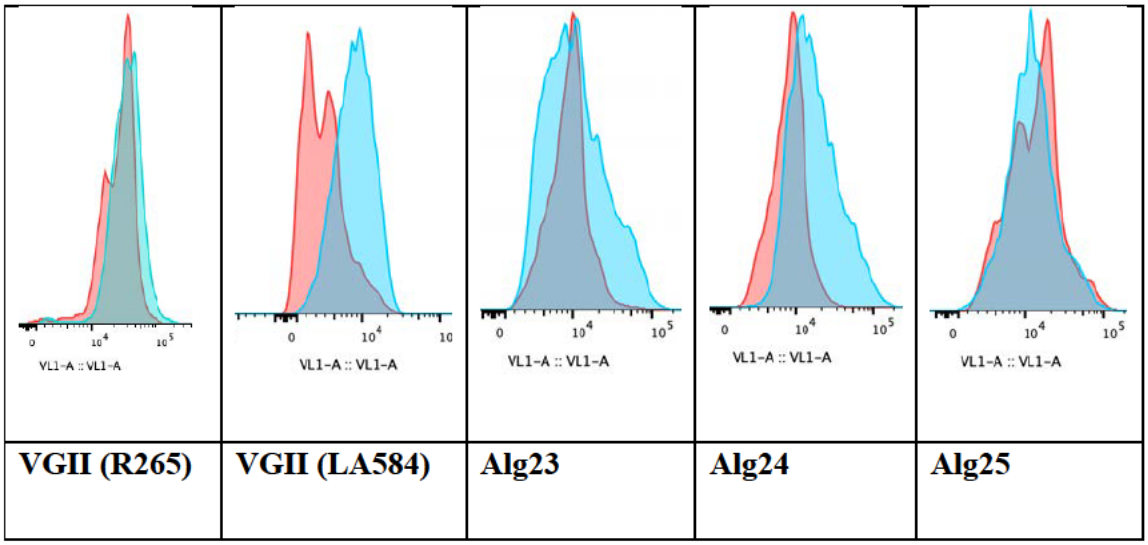

VGII (R265)	VGII (LA584)	Alg23	Alg24	Alg25

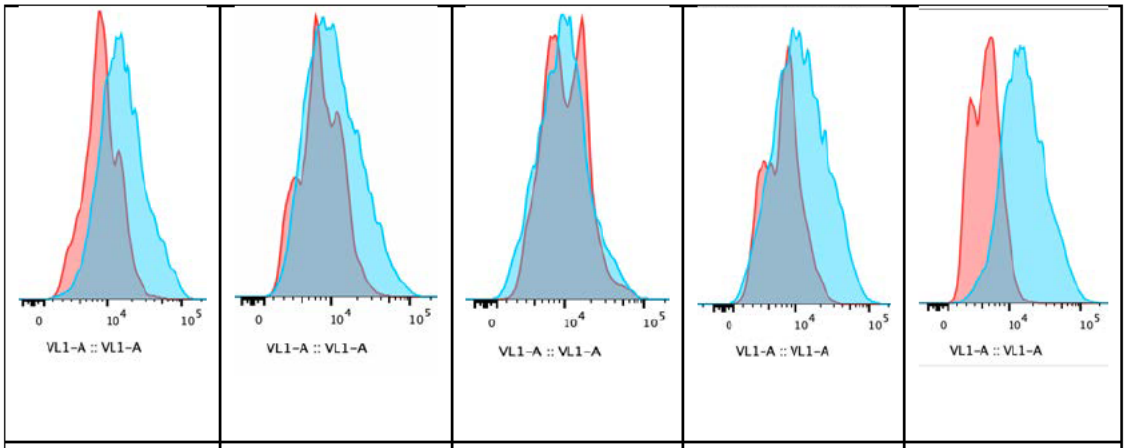

Alg26	ALg27	ALg28	ALg29	Alg30

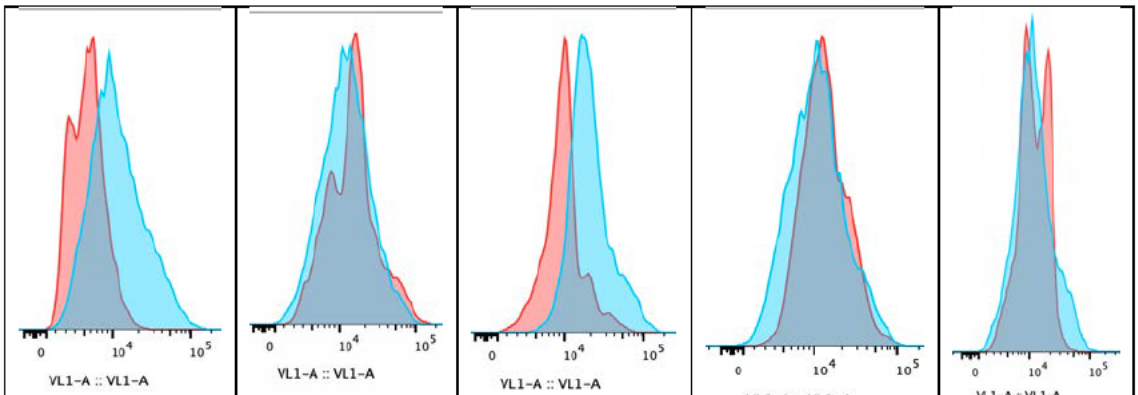

Alg31	Alg32	Alg33	Alg34	Alg35

A

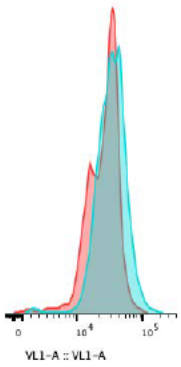	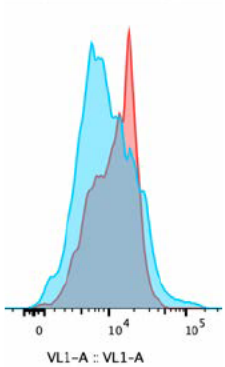	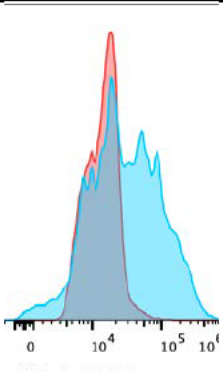	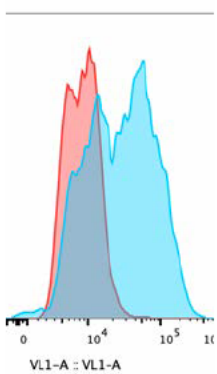	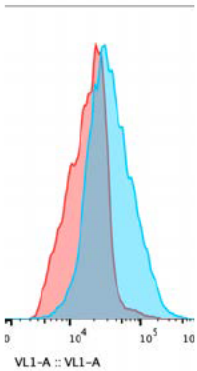
VGII (R265)	**VGIII (B4546)**	**P1**	**P2**	**P3**

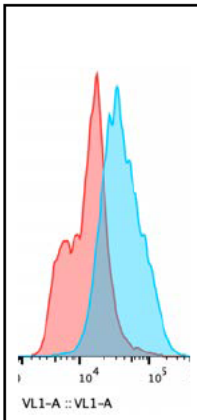	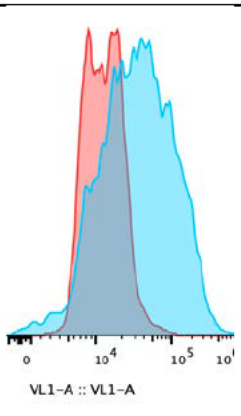	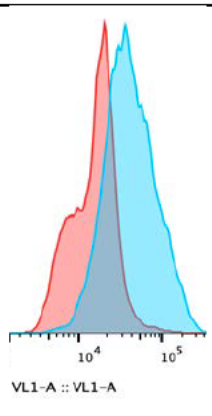	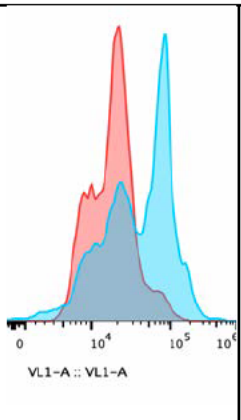	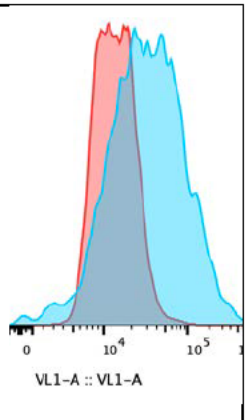
P4	**P5**	**P6**	**P7**	**P8**

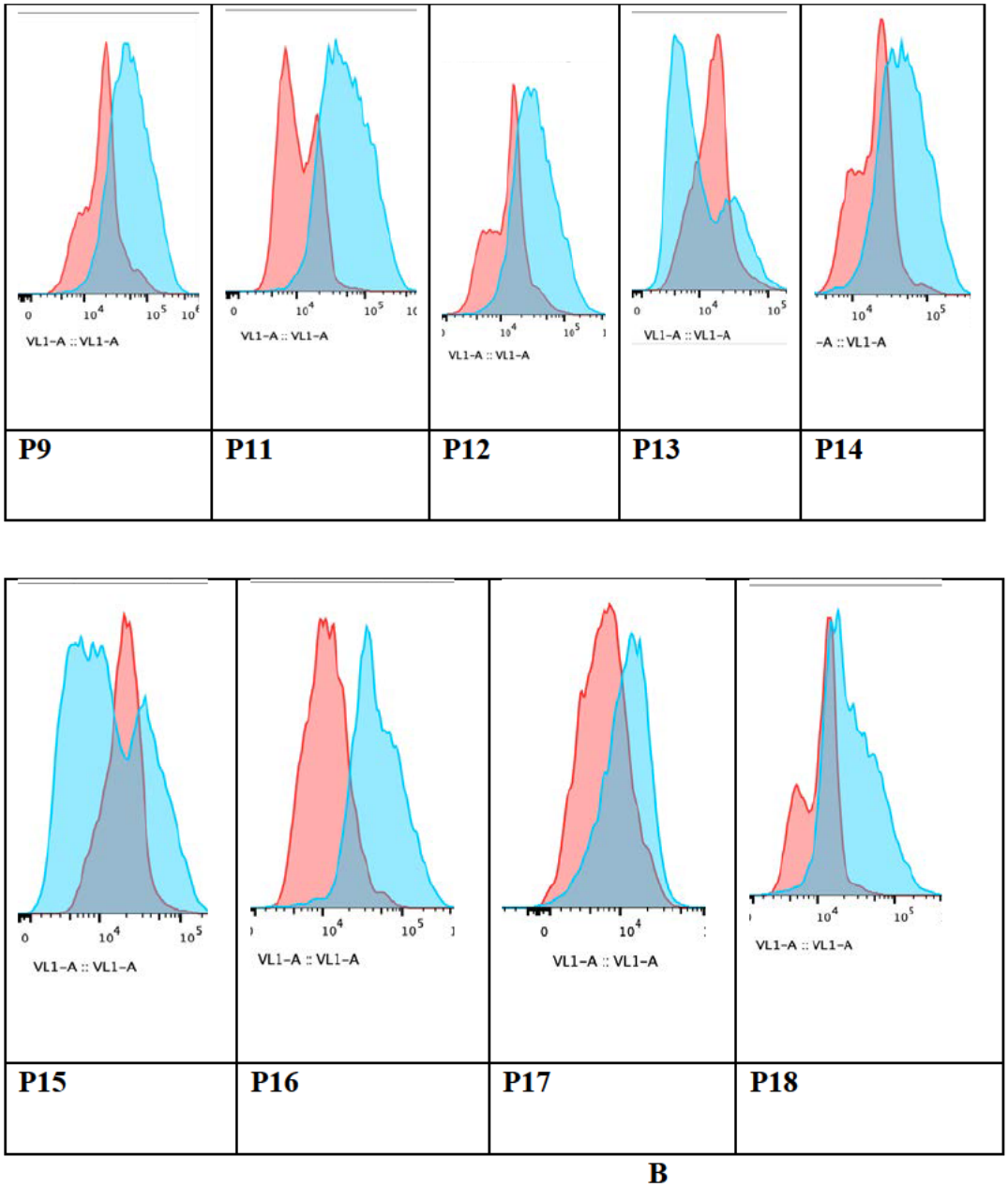

Figure 6.9 DNA content of 25 YPD grown (red) and titan-induced (blue) of *C. gattii* progeny arising from two crosses. A) DNA content of YPD grown (red) and titan-induced (blue) of ingroup crossing [VGII(R265) x VGII (LA584)] strains and their 13 progeny (Alg23-Alg35) after 3 days. B) DNA content of YPD grown (red) and titan-induced (blue) of outgroup crossing [VGII(R265) x VGIII (B4564) strains and their 18 progeny (P1-P18) after 3 days. All strains (parent and progeny) were induced for titan cell formation and DNA content was determined after 72hrs as described in the "methods" section-3.2.5.4.

6.8 Discussion

Cryptococcus adaptation to the host environment is accompanied by phenotypic, metabolic and genetic alterations that are essential for pathogenicity [2, 51, 230-235]. Typically measuring 5-7 μm, the cryptococcal yeast cell can undergo a morphological switch in the lungs to form enlarged polyploid titan cells, which have been studied *in vivo* [12, 49] and recently induced *in vitro* [48, 51, 217].

This chapter reports a new *in vitro* model for induction of *bone fide* titan cells. The protocol is a one-step incubation of cryptococcal cells in serum-free RPMI media with 5% CO_2 at 37ºC and is therefore highly amenable to high-throughput screens.

Using the *in vitro* protocol, a detailed analysis of titanisation in the *C. gattii* strain R265 (VGIIa) was conducted. As demonstrated by the results, R265 titan cells induced *in vitro* possess enlarged cell body size, a large central vacuole, thick capsule and cell wall, and were polyploid after 5 days. Consequently, they exhibit all the hallmarks of true titans produced during mammalian infection. Unlike other cryptococcal strains, however, R265 shows a separation between size and ploidy increase. This suggests that the asynchronous progression of these two events may be due to R265 undergoing cell size increase without passage through the cell cycle and then subsequently switching to DNA replication once the critical volume has been attained.

The lack of synchronisation between cell enlargement and DNA replication is a major difference between R265 titan cells and other well-studied *Cryptococcus* titan cells [12, 49-51, 127, 173, 217]. It suggests that the asynchronous progression of these two events is due to the prolonged time the titan cells spend in the G1 phase and/or cell cycle arrest at the G1/S checkpoint. This is supported by the ploidy of the 24 hr induction samples, where the vast majority of cells show a 1C DNA content. In yeast, a late G1 cell cycle arrest, known as

"Start", is part of the core cellular response to stress [236, 237].-In R265 it is observed that cell enlargement occurs before polyploidization during the early period of induction, so that the enlarged cells remain as 1C haploid yeast cells for the first two days of induction. By day 3 of induction, the enlarged cells begin to duplicate their DNA content to at least 2C but almost completely stop budding at the same time [budding index: 2.8% (26/933)] (Fig 6.3C). This leads to a major distinction between the species, in that *C. neoformans* titan cells can produce daughter cells within the *in vitro* titan induction model whilst C. *gattii* R265 titans do not (Fig. 6.10). It could be noted that this observation (unbudded phenotype) may be of value in studying cell cycle dynamics in *Cryptococcus* species (particularly *C. gattii*), since producing synchronised cryptococcal populations for such investigations has previously been methodologically challenging.

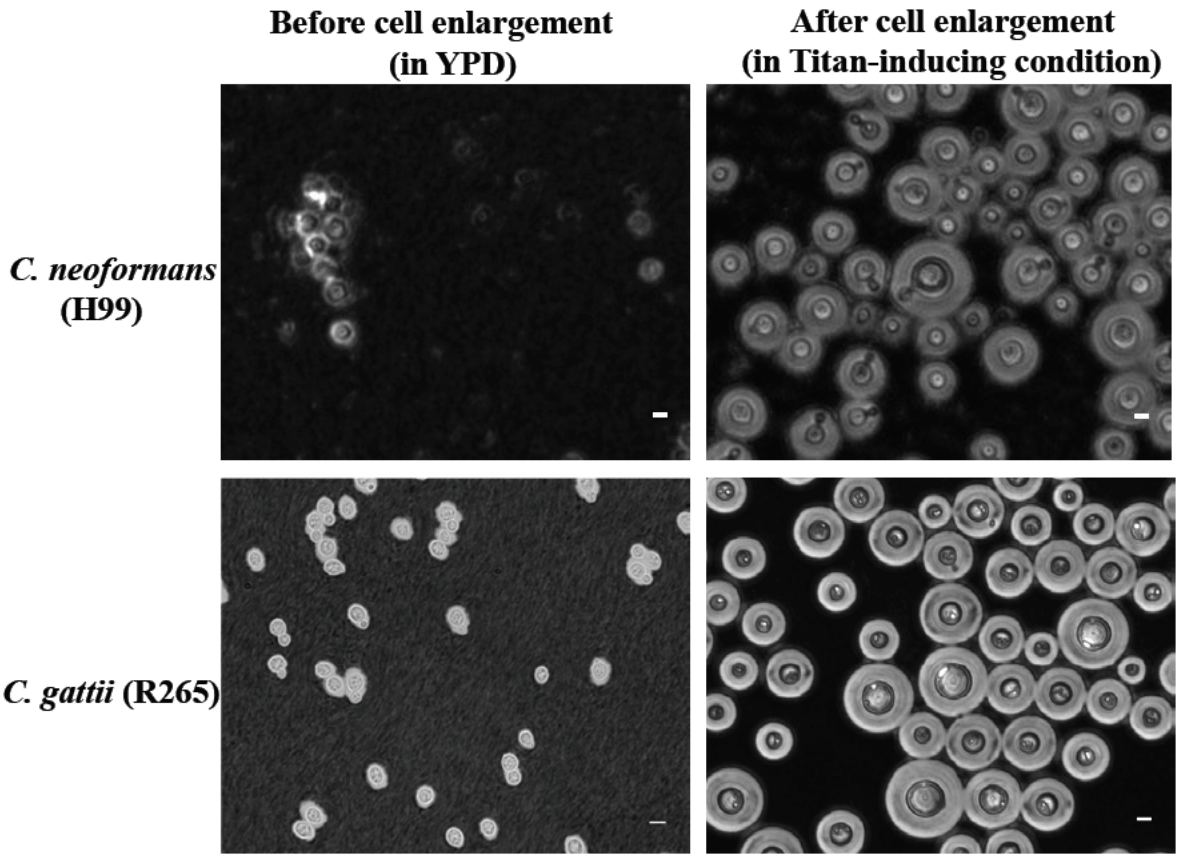

Figure 6.10 Morphological differences between *C. neoformans* and *C. gattii* before and after growth in *in vitro* titan inducing condition. Titan induction was performed by first growing cells in YPD overnight, followed by growth in RPMI at low density for 72 hours at 37 °C in an atmosphere of 5% CO_2. Scale bar=5µm.

To explain the unbudded phase of the induced cells, correlation was made between this phenotype with cell cycle progression with reference to *C. neoformans*. In *C. neoformans*, large unbudded G2 cells have been shown to emerge during stationary growth phase [33]. Recently, while scrutinizing the cell cycle regulation of titan cells in *C. neoformans*, Altamirano *et al* [176] described a two-step process of titanisation: a) typically-sized cells duplicate DNA to 2C and arrest in G2 as unbudded cells; and b) then the cells are released (by the combined influence of the cell cycle gene Cyclin Cln1 and "stress signals") to form polyploid titan cells. Contrary to this phenomenon, R265 cells exhibit an actively budding phase in the early period

of induction where the majority of the cells display 1C DNA content consistent with G1 and then undergo DNA replication to form G2 arrested unbudded polyploid titan cells at the later time point (day 5 onwards) where the 1C DNA content is totally lost (Fig. 6.3B).

The results also demonstrate that R265 titan cells produce daughter cells with a polyploid DNA content similar to their mother cells. In contrast, *C. neoformans* titan cells produce both haploid and aneuploid progeny [127], with sizes ranging between 5-7μm and 2-4μm respectively [51]. Given that population heterogeneity in *C. neoformans* is associated with preferential dissemination to the CNS [216, 238], it is possible that this lack of heterogeneity in *C. gattii* may contribute to the differences in disease etiology in this species. In particular, murine models have shown that *C. neoformans* isolates that produce high percentage of titan cells fail to disseminate to the brain and instead remain in the lung, consistent with pneumonia or chronic infection [71, 239].

Finally, using the *in vitro* protocol, the capacity for titan cell formation between and within cryptococcal species, was evaluated. Titanisation was observed particularly abundant within *C. gattii* /VGII (*C. deuterogattii*). Interestingly, Fernandes and colleagues reported a similar cell enlargement phenotype while screening for clinically relevant attributes in *C. gattii* [13]. To start to dissect the genetic regulation of this process, the titanisation profile of a collection of parent/progeny crosses that we generated in a previous study [229], was tested and analysed. It was striking to note the variation in this phenotype within recombinant progeny and, in particular, the very high rates of titanisation found in the offspring of 'outgroup' hybrids. Most of the progeny from this cross showed titanisation rates equal to or greater than that of R265 (the high titan cells generating parent). It is possible that this reflects a 'hybrid vigour' effect, resulting from the outcross. In the future, more detailed genomic investigation of these and

other crosses may potentially facilitate a more comprehensive understanding of titan cell formation in this genus.

Overall, the titan induction protocol is an efficient and high throughput approach for producing titan cells at scale. By employing this *in vitro* protocol, novel aspects of titanisation in *C. gattii* was discovered and the separation of DNA replication and cell size increase was revealed. Together, it is hoped that this approach will provide a platform for the future mechanistic investigation of titanisation in this important group of pathogens.

CHAPTER 7

GROWTH CONDITIONS AND CELL CYCLE REGULATORS OF *IN VITRO* TITAN CELL FORMATION IN *C. GATTII*

This chapter is part of an article that has been accepted for publication:

L. Saidykhan, Correia J, Romanyuk A, Desanti G. E, Taylor-Smith L, Makarova M, E.R Ballou, R. C. May. 2022. An in vitro method for inducing titan cells reveals novel features of yeast-to-titan switching in the human fungal pathogen *Cryptococcus gattii*. **PLOS Pathogens** (Proof of publication: appendix II).

The *in vitro* titan induction model described in Chapter 6 not only reveals unique features of *C. gattii* (R265) titan cells (unusual pattern of DNA replication and budding, suggesting an altered cell cycle) but also implies underlying triggers and regulators of these features. With the invention of in *vitro* induction models, key regulators of titan cell formation have been identified [173]. Exogenous factors including host-specific environmental conditions [such as physiological temperature (37°C) and CO_2 level (5%) coupled with hypoxia, nutrient limitation etc.] and other cues have been identified as essential signals, while low-density growth (via quorum sensing) serves as a regulator of titan cell formation [48, 71, 217]. Although many molecular details remain unclear, endogenous genetic regulators and transcription factors associated with titan cell formation in *C. neoformans* include several members of the cAMP/PKA pathway (including GPA1, CAC1, Ric8, PKA1 Rim101 and UsV101) [48, 71, 197]. Titan cell formation is also dependent on altered cell cycle progression, as cells undergo endoreduplication (replication of nuclear genome in the absence of mitosis) to form dramatically enlarged, polyploid cells [173]. During titanisation, *C. neoformans* yeast cells initially exhibit a stationary-phase growth during which DNA duplication occurs to form unbudded 2C/G2 arrested cells [176]. Thereafter, the cell cycle regulator Cln1 is suppressed, allowing DNA re-replication, creating polyploid titan cells. After titan cells have been formed, Cln1 is then upregulated in order to release cells from G2 arrest and enable them to re-enter the cell cycle and produce daughter cells. In this chapter I investigated the exogenous factors and cell cycle regulators of the novel titan features exhibited by *C. gattii*.

7.1 Titan cell formation is inversely correlated to cell density

Previous work in *C. neoformans* has shown that titan cells are preferentially produced at low cell density [48-50, 217]. We tested whether the same was true of R265 by growing yeast cells in RPMI at five decreasing inoculum concentrations (10^6, $5x10^5$, $5x10^4$, $5x10^3$ and 10^3

cells/mL) and incubating for 24hr at 37°C in 5% CO_2. The formation of titan cells was maximal [87.9% titan cells (>10µm)] at an initial inoculum of $5x10^3$ cells/mL, producing cells with a median cell body size of 14.8µm (4.2-26.28) (Fig. 7.1). The percentage of titan cells decreased with increasing cell densities, indicating that in *C. gattii*, as in *C. neoformans*, titan induction occurs primarily in low density cultures.

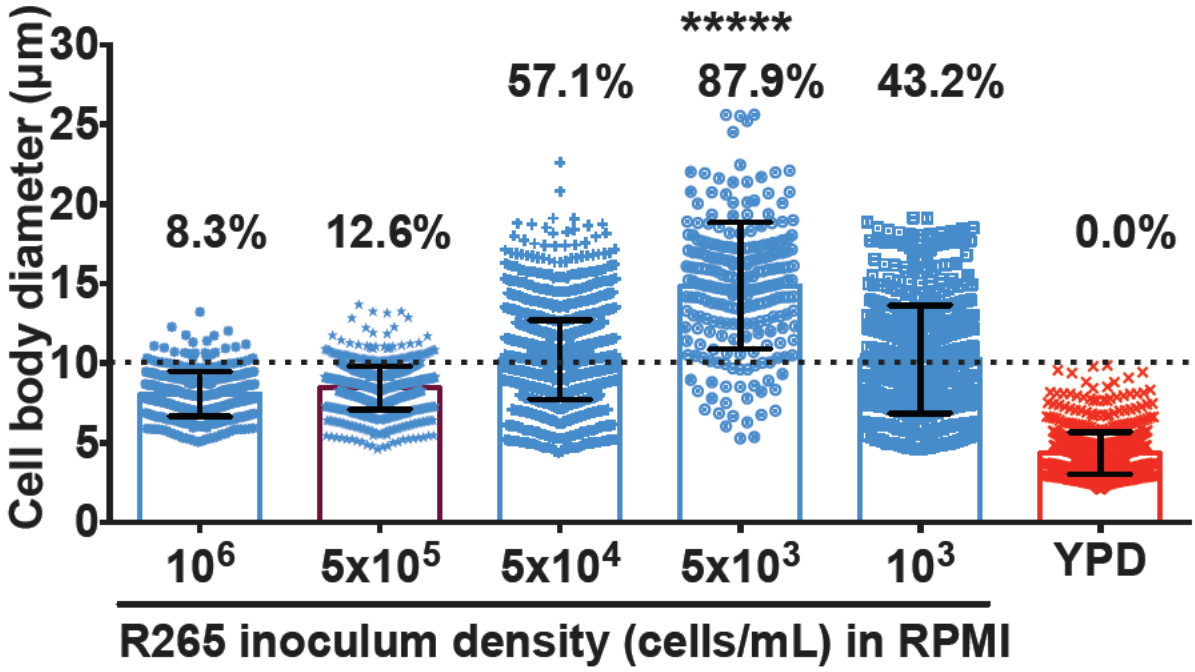

Figure 7.1 Effect of cell density on R265 cell enlargement. Cells were grown in RPMI for 72 hr at high and low inoculum concentration (10^6 - 10^3 cells/mL) and the inoculum concentration producing the maximum proportion of enlarged cells (>10 µm) was taken as the optimum concentration. The graph is a representation of three independent experimental results and statistical analysis was performed using a one-way ANOVA where ****=p<0.0001.

7.2 Quorum sensing effect

The density-dependence of titanisation is suggestive of a quorum sensing effect. Consequently, we tested the impact of the putative cryptococcal quorum sensing molecule Qsp1, a short

peptide previously reported to inhibit titanization in *C.neoformans* cells *in vitro* [48, 217]. By adding the Qsp1 peptide (NFGAPGGAYPW) at 20µM to RPMI, both the median cell body size of the R265 cells and the proportion of titan cells were significantly reduced [median cell size: 13.35µm vs 11.74µm ($p<0.0001$); percentage titan cells: 88.3% vs 75.8%]. In contrast, a 'sequence-scrambled' Qsp1 peptide (AYAPWFGNPG) had no effect (Fig. 7.2). Interestingly, the active peptide also impacted capsule growth by reducing capsule size of the titan induced cells significantly (see micrograph images of Fig. 7.2). Taken together, this indicates that titan cell formation in *C. gattii* is modulated by quorum sensing via the Qsp1 pathway, as previously described in *C. neoformans* [48, 217].

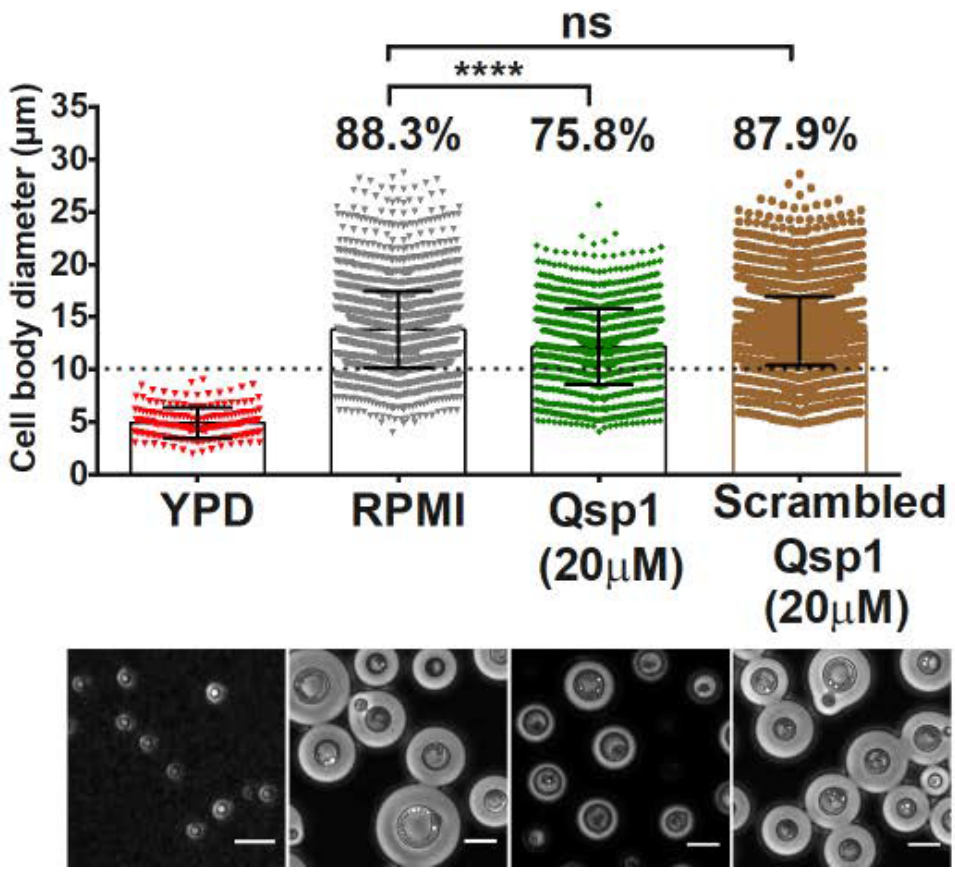

Figure 7.2 The impact of quorum sensing on R265 cell enlargement. B) The role of the quorum sensing peptide, Qsp1 (on titan cell formation) was determined by growing R265 yeast cells in RPMI supplemented with the intact and scrambled peptide (control) at 37°C with 5%

CO_2 and measuring the cell body size after 72 hr incubation. Microscopy images illustrating the morphological differences in titan cells production between these three conditions (RPMI, intact Qsp1 and scrambled Qsp1) are also shown. The cell body size distribution graph represents 3 biological experimental repeats, and Kruskal-Wallis test was used to determine significance where **** = $p<0.0001$.

7.3 High density growth in RPMI produces large, haploid, non-titan cells

The impact of culture density led to the question: what happens to R265 in non-titanising (high density) conditions? To answer this, R265 cells were inoculated in RPMI at 10^6 cells/mL and cell body size and ploidy were measured after 7 days. At high density, there was a statistically significant increase in cell body size from 24 hr to 7days (median size: 9.0µm vs 10.5µm, $p<0.0001$) (Fig 7.3A), but they did not become the very large titan cells that appear in low density cultures (Fig. 6.1C). At both time points in these high-density conditions, cell enlargement reached a maximum threshold of 15µm with 0.1% (4/4302) and 1.3% (46/3489) of cells scoring >15µm at 24 hr and 7 days respectively (Fig. 7.3A). The 7-day cultures were fully growth-arrested, as evidenced by their very low budding index of 2.1% (67/3122) (Fig. 7.3B and Fig 7.3C). Interestingly, however, these 7-day, non-titan cells displayed a dramatic capsule size increase as compared to YPD grown cells (Fig 7.3C), perhaps due to the effect of RPMI media and CO_2, which have been employed for capsule induction in *Cryptococcus* [86, 87, 215, 225]. Interestingly, unlike cells grown in low-density titan-inducing conditions, cells grown at high density remained haploid over the entire 7 day period (Fig 7.3D). The conclusion is that high-density long-term culture in RPMI induces a degree of cell enlargement in R265, but these large cells are distinct from the true titans that appear in low density culture.

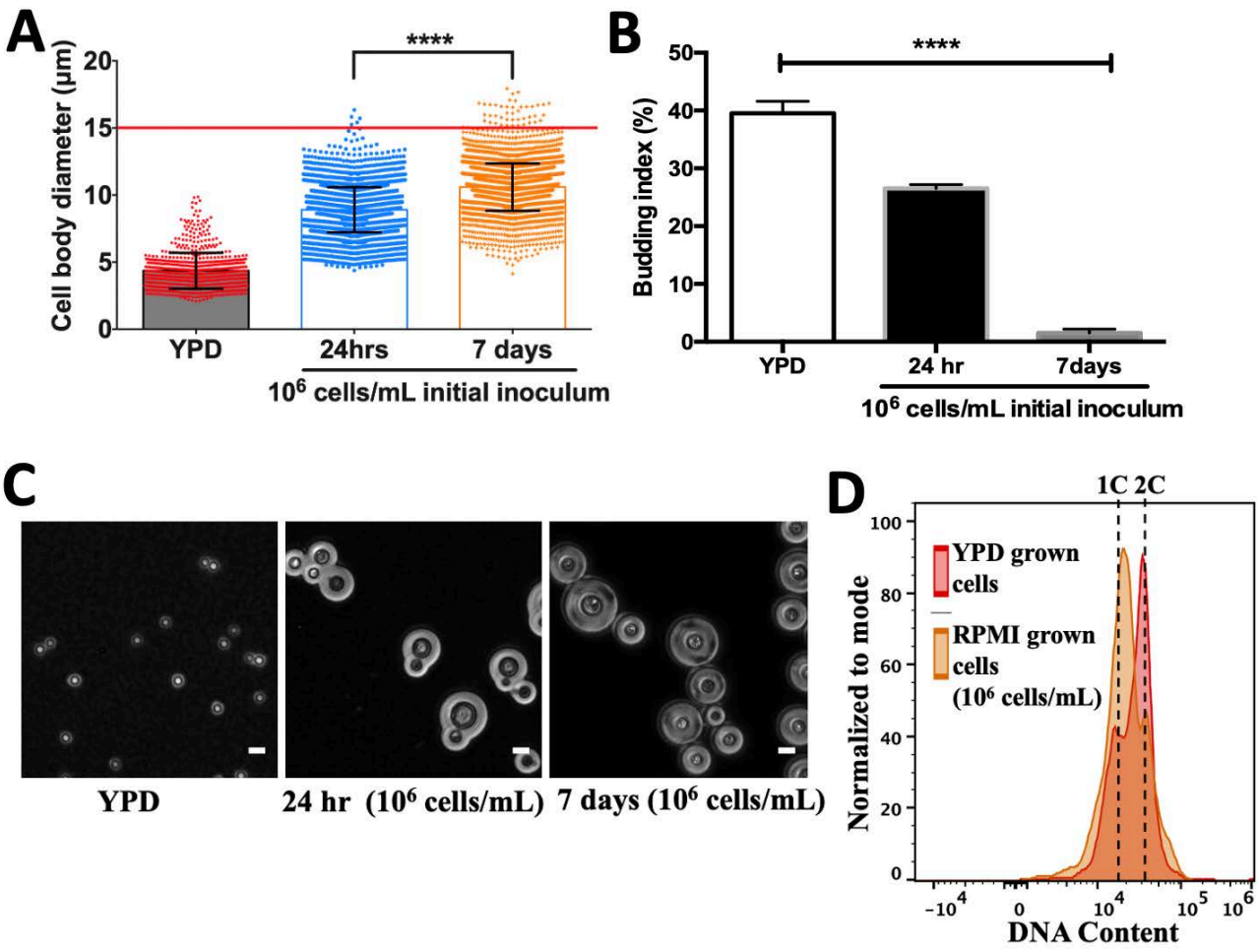

Figure 7.3 The R265 yeast cells can enlarge up to 15µm and still remain haploid. Maximum cell enlargement capacity (A), budding index (B) and micrographs (C) of R265 cells in RPMI at 10^6 cells/mL (high density growth) at 37°C with 5% CO_2 for 24 hr and 7 days. The cell body size distribution graph represents 3 biological experimental repeats, and Kruskal-Wallis test was used to determine significance where **** = $p<0.0001$. Budding index was expressed as percentage of budded cells per total number of cells. At least >3000 cells were analysed for each sample from two independent repeats and significance was determined by one-way ANOVA (****=$p<0.0001$). Scale bar: 10µm. D) Ploidy of YPD grown (red) and R265 cells grown in RPMI at 10^6 cells/mL (high density growth) at 37°C with 5% CO_2 and 7 days (orange).

7.4 Impact of temperature and CO_2 on Titan cell formation

Cryptococcus responds to human physiological temperature (37°C) by exhibiting a variety of morphological changes including capsule elaboration, cell body enlargement and cell shape alteration [16, 51, 78]. Hence, we investigated the role of temperature on R265 yeast-titan cell transformation by comparing cells grown in the presence of 5% CO_2 at either 37°C or 30°C. At 30°C incubation, no titan cells were generated and the median cell body size [5.03µm (1.04-12.85)] was significantly lower than at 37°C [11.17µm (4.04-28.6)]. A similar trend was observed for the proportion of titan cells (13.8% vs 2.2%) (Fig 7.4A). Thus, elevated temperature was essential to produce titan cells in the *in vitro* protocol (described in chapter 6).

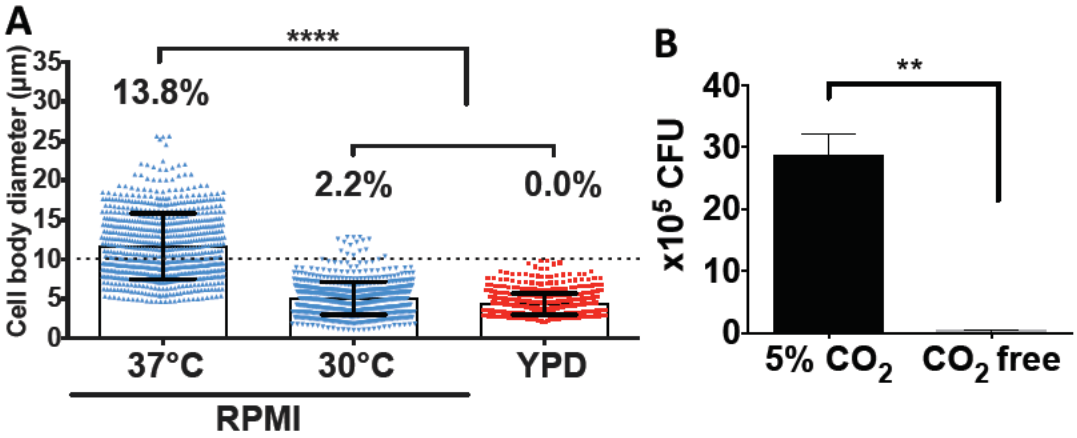

Figure 7.4 Impact of temperature and 5% CO_2 growth on cell enlargement. A) Cell body diameter of R265 cells after 24hrs of growth in RPMI with 5% CO_2 at 37°C or 30°C. The cell body size distribution graph represents 3 biological experimental repeats, and Kruskal-Wallis test was used to determine significance where **** = $p<0.0001$. B) The CFU of cells from 5% CO_2 and atmospheric growth were counted to evaluate viability. Statistical significance was confirmed by a Two-tailed t-test where ****=$p<0.001$

The most dramatic biological response of *Cryptococcus* to CO_2 is capsule biosynthesis which occurs concurrently with cell body enlargement [86, 87, 225]. Consequently, we compared cells grown at 37°C in 5% CO_2 with those grown under normal atmospheric conditions at 37°C. Relative to growth in 5% CO_2, the proliferation of R265 was significantly inhibited in ambient atmosphere [Mean CFU: CO_2=28.5 x10^5 cells/mL vs CO_2- free=0.29 x10^5 cells/mL; ($p<0.001$)] and no titan cells were observed in this condition (Fig. 7.4B). Thus, both elevated temperature and high CO_2 are required for *in vitro* titan cell formation.

Notably, the pH of YPD and RPMI remained close to neutral throughout the assay, ruling out a secondary impact on titan cell formation as a result of pH stress (Table 7).

Table 7. pH level of YPD and RPMI before and during titan induction (24 hr and 7 days). Titan cell induction was performed with the R265 (*C. gattii*) and pH level were measured using a pH meter.

Condition	**YPD (pH level)**	**RPMI (pH level)**
Before induction	**6.8**	**8.01**
At 24 hr induction	**6.2**	**7.31**
At 7 days induction	**7.38**	**7.38**

7.5 P-aminobenzoic acid is a major trigger of titanisation in RPMI

While comparing the titan induction capacity of RPMI (RPMI Medium 1640 (1X)) against Dulbecco's modified eagle medium (DMEM), it was noticed that the full titan cell phenotype emerged in RPMI but not DMEM after 24 hrs of induction. Notably, cells enlarged in both media, but cells grown in DMEM never achieved the same size as those in RPMI and did not become polyploid. Since RPMI and DMEM media have a close chemical composition, we

took advantage of this similarity and sequentially supplemented DMEM with RPMI-specific compounds with the aim of identifying an RPMI-specific factor that triggers titanisation in R265 cells. To more clearly distinguish between conditions, we used a higher threshold for titan cells in this assay (15 µm rather than 10 µm). After 24hrs of induction, 13.8% of cells in RPMI had a cell body size above 15 µm, whilst no cells of this size appeared in DMEM [median cell body size: 12.3µm (4.1-28.8) vs 9.9µm (4.5-14.9)] (Fig. 7.5). By 3 days of incubation, larger cells had appeared within the DMEM condition, but at a rate approximately three-fold lower than for RPMI (Fig. 7.7).

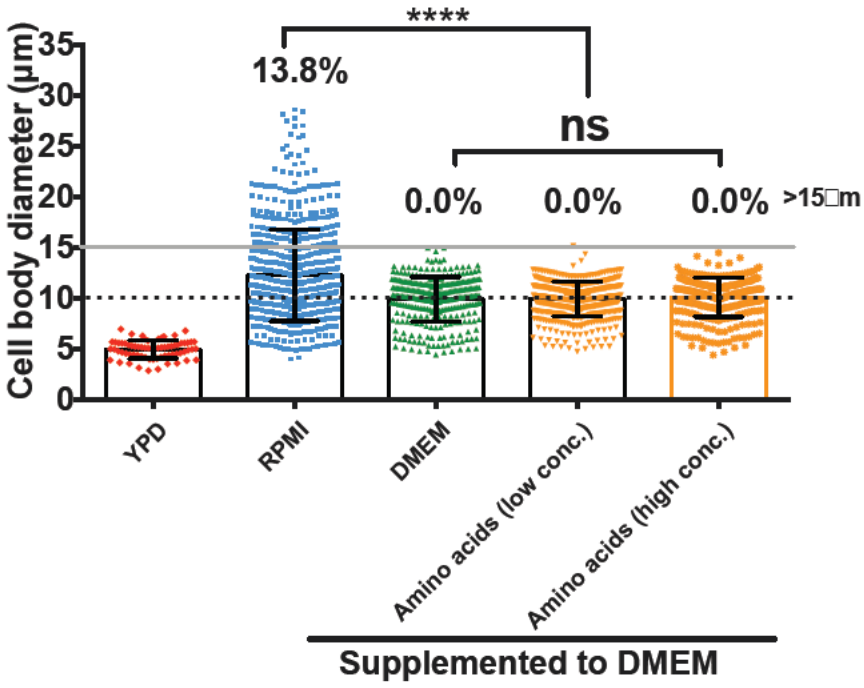

Figure 7.5 The effect of RPMI-specific amino acids on R265 titan cell formation. RPMI-specific amino acids (L-Glutamic acid, L-Aspartic acid, L-Arginine, L-Glutathione, L-Asparagine and L-Proline) were added to DMEM either at the concentration used in RPMI ('low conc.') or two-fold higher ('high conc.') and tested for their capacity to trigger titan cell formation after 24 hr induction at 37ºC in 5% CO_2. The graph represents 3 biological

experimental repeats, and Kruskal-Wallis test was used to determine significance where **** = p<0.0001.

RPMI differs from DMEM in its amino acid composition and so we first supplemented DMEM with 'RPMI-specific' amino acids (L-Glutamic acid, L-Aspartic acid, L-Arginine, L-Glutathione, L-Asparagine and L-Proline) either singly (data not shown) or as a mixture. However, none of these conditions were sufficient to confer titan-inducting capacity to DMEM, even when supplemented at twice their normal concentration (Fig. 7.5). We also increased the glucose concentration of DMEM from 1000mg/L to 2000 mg/L (RPMI concentration), but saw no significant impact on titan production (Fig. 7.6). Based on these results, it could be concluded that amino acid availability and glucose concentration are not the trigger for R265 titanisation.

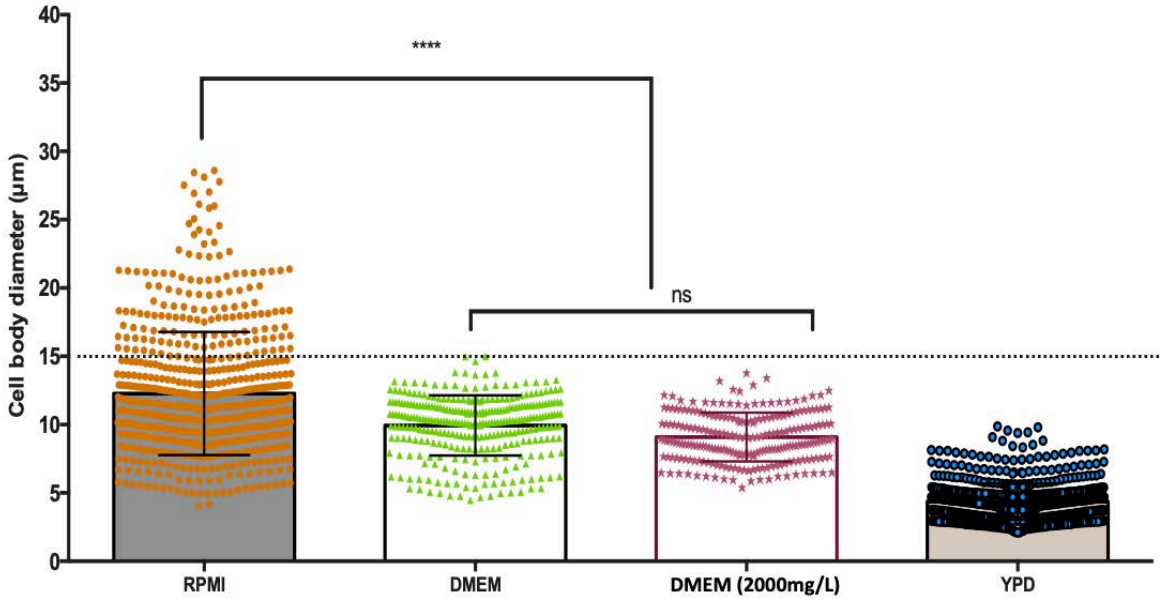

Figure 7.6. Effect of glucose on titan cell formation. DMEM media was supplemented with additional 1000mg/L (reaching 2000mg/L-the concentration in RPMI) and tested for capacity to induce cell enlargement (>15µm) as compared to RPMI. Titan induction was performed by

growing R265 yeast cells in the difference media conditions by 24 hrs incubation at 37°C in 5% CO_2. The graph represents 3 biological experimental repeats, and Kruskal-Wallis test was used to determine significance where **** = p<0.0001.

I continued by testing three additional compounds that are present in RPMI but absent from DMEM: Vitamin B12, Biotin, and para-aminobenzoic acid (pABA). Whilst vitamin B12 or biotin supplementation into DMEM had relatively little effect, addition of pABA significantly increased the production of titan cells from 13.7% to 29.0% (median cell diameter =11.94µm vs 12.82 µm, p <0.0001) (Fig. 7.7). Consequently, pABA appears to be a major trigger for titan cell formation in RPMI.

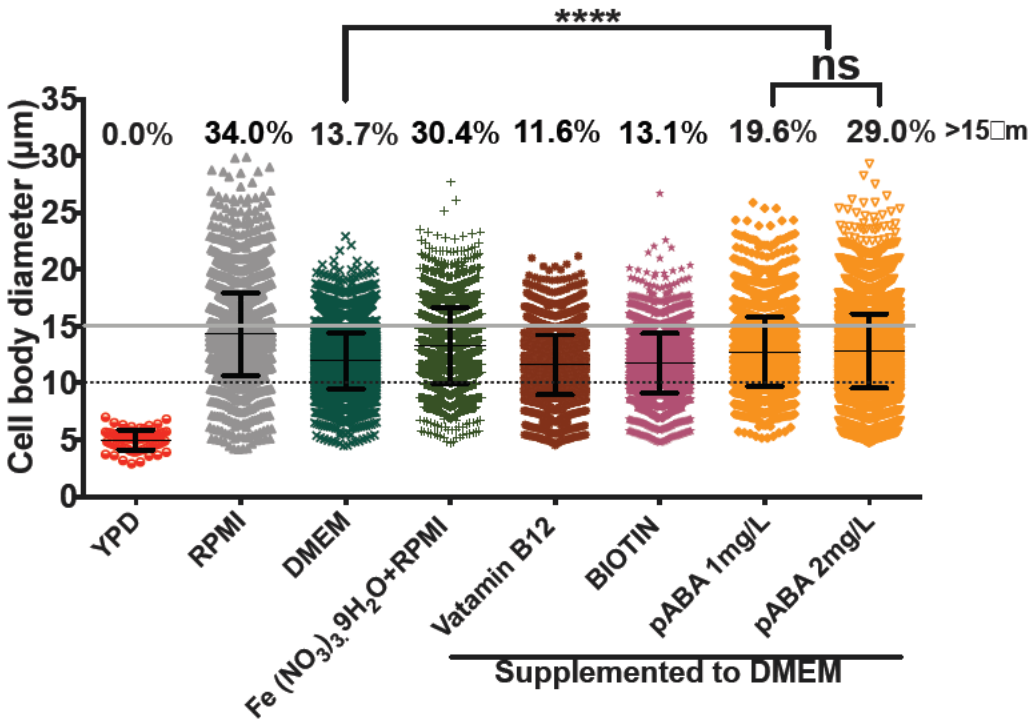

Figure 7.7 The effect of RPMI-specific compounds on R265 titan cell formation. RPMI-specific compounds [Vitamin B12, Biotin, and para aminobenzoic acid (pABA)] were supplemented to DMEM at the levels present in RPMI and then evaluated for their capacity to induce titan cell formation after 3 days incubation at 37ºC in 5% CO_2. The graph is

representative of 3 biological repeats and statistical significance was determined by one-way ANOVA, where ****=p<0.0001.

Finally, it was noted that supplementary iron (in the form of Iron (III) nitrate nonahydrate-Fe $(NO_3)_3.9H_2O$) is present in DMEM but absent from RPMI. We therefore tested whether iron availability may actively inhibit titanisation. Indeed, adding iron to RPMI (Fe $(NO_3)_3.9H_2O$+RPMI) slightly reduced the induction capacity of RPMI by ~4%. This was unsurprising as iron limitation induces titan cell formation in *C. neoformans* [217]. In summary, therefore, the efficient induction of titan cells in RPMI likely results from the combined presence of pABA and the absence of supplementary iron.

7.6 The titan cell cycle phenotypes are correlated with the expression of genes involved in cell cycle progression

The manner in which R265 progressively exhibits cell-cycle-associated phenotypes (cell enlargement, budding, DNA replication and finally growth arrest) to form unbudded polyploid titan cells led us to question the underlying cell cycle regulatory mechanism. We extracted RNA from R265 titan induced cells for 24 hr, 3 days, 5 days and 7 days of our *in* vitro protocol and then investigated the expression of a panel of cell cycle markers via quantitative RT-PCR (Section 3.2.6.3).

In line with the phenotypic changes that we observe during titan cell formation, the cell cycle markers we examined showed a clear shift from budding and mitosis to DNA replication and eventually cell-cycle arrest (Fig. 7.8). Thus, the *CDC11* gene, encoding a septin protein involved in bud formation, was highly expressed in YPD grown cells and for the first 24hrs of induction, but downregulated in the "unbudded phase" timepoints (Fig. 7.8A). The expression of the G1 cyclin *CLN1* similarly was reduced at day 3 compared to 24 hrs, while expression

was somewhat restored by day 5 (Fig. 7.8B). In contrast, *MCM6* and *BUB2,* associated with DNA replication and G2 arrest respectively, both peaked at 7 days where the titan cells exhibit maximum polyploidy and remain unbudded (Fig. 7.8C and Fig. 7.8D).

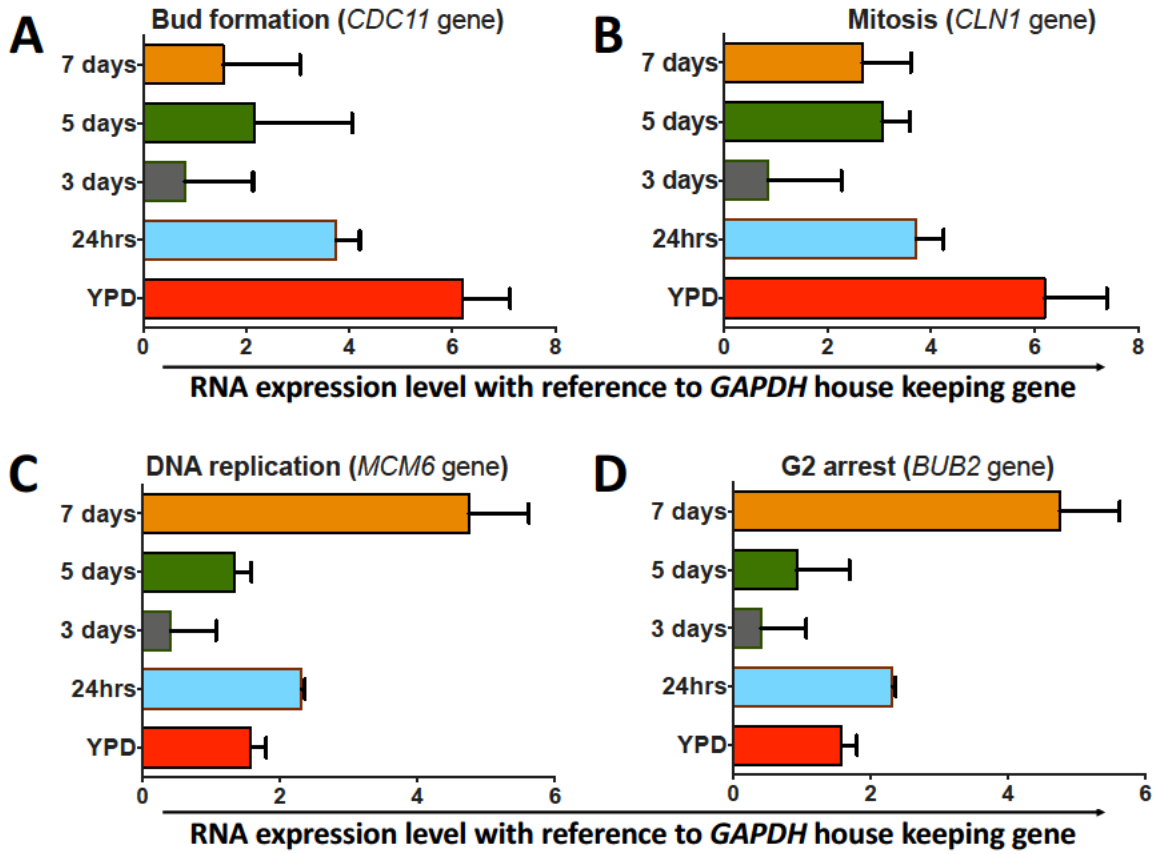

Figure 7.8 Transcription profile of R265 cell-cycle-regulating genes during titanisation. Quantitative expression analysis of four different cell cycle associated genes in R265 grown in either YPD (control) or titanising conditions for the indicated time points. Expression is shown relative to the housekeeping gene GAPDH. Genes quantified were A) *CDC11* (*CNBG_5339)*, involved in bud formation; B) *CLN1 (CNBG_4803)*, associated with balancing cell division and DNA replication [176]; C) *MCM6 (CNBG_5506*), involved in DNA replication; and D) *BUB2 (CNBG_4446)*, involved in G2 arrest. The graphs represent 3 biological repeats (3 technical replicates each), with error bars depicting the standard deviation of *delta-delta* C_T values.

7.7 Discussion

The *in vitro* formation of cryptococcal titan cells is finely modulated by the combined effect of exogenous factors and genetic regulators [48, 63]. As with *C. neoformans* [48-50, 217], *C. gattii* (R265) cells responded to the density within our *in vitro* model such that generation of titan cells was optimal at the low inoculating density of 5x 10^3 cells/mL (producing 87.9% titan cells) and significantly reduced at higher density (8.3% at 10^6 cells). This density effect is reminiscent of a quorum sensing (QS) regulating mechanism; a cell density-dependent communication strategy employed by microorganisms to synchronously respond to environmental signals [240, 241]. This behaviour is driven by exogenous signalling molecules (autoinducers) that are secreted at adequate concentration to trigger collective biological changes in a population of microbial cells. Similar to *C. neoformans* titan cells [48, 217], the *in vitro*-generation of *C. gattii* titan cells was negatively regulated by the putative cryptococcal quorum-sensing peptide, Qsp1 [220, 242].

The observation that elevated temperature (37°C) and CO_2 (5%) are obligatory environmental determinant for *in vitro* titan cells formation in *C. gattii* is consistent with the implication of these factors in *C. neoformans* titan cell formation [71, 217]. The *in vivo* model is considered as the gold standard for inducing titan cells and the *in vivo* lung physiological condition is characterized with elevated temperature and hypoxia (due to high CO_2 level) [63, 173]. Therefore, it is not surprising that the impact of these two conditions (temperature and CO_2) on *C. gattii* titanisation recapitulates the *in vivo* scenario. Taken together, *C. gattii in vitro* titan cell formation, similar to *C. neoformans,* is regulated by multiple environmental signals which are host-relevant factors.

The fact that RPMI, but not the very similar cell culture medium DMEM, induced R265 titan cells enabled us to identify p-Aminobenzoic acid (pABA) as a major driver of titanisation.

Interestingly, the titan induction effect of pABA was recapitulated when the *C. neoformans* strain, H99 was tested, although the very low titan formation capacity of this strain means that the effect was very weak (Fig. 7.9). The mechanism by which pABA triggers titanisation remains unclear at present. However, it is noted that pABA is an antifungal metabolite that has efficacy against several fungal plant pathogens such as *Fusarium graminearum*, *Magnaporthe oryzae*, *Rhizoctonia solani, Sclerotinia sclerotiorum* and *Valsa ambiens var. pyri*. [243]. Since titanisation is linked to the fungal stress response, it may be that low dose p-ABA induces a mild stress that triggers titanisation. In this context, modulation of the cell cycle and morphogenesis of *Colletotrichum fructicola* (a plant fungal pathogen) by pABA has been documented [244]. PABA interfers with the cell cycle progression by inhibiting the formation of actomysin and blocking septation of *C. fructicola.* The mode of action of pABA has been akinned [244] to the antifungal mechanism of bleomycin which triggers the formation of large unbudded (via inhibition of cell wall septation and cytokinesis) fungal cells of *Aspergillus fumigatus*, *Cryptococcus neoformans*, and *S. cerevisiae* [245]. Alternatively, pABA's well documented role in oxidative damage tolerance [246] and the role of reactive oxygen species in cryptococcal morphogenesis [247] may suggest a role for reactive oxygen balance in this phenomenon.

PABA is synthesized as an intermediary compound during the production of folate by bacterial [248]. Naturally found in the human body, pABA is generated by human gut microbiome such as E. Coli. We hypothesis that pABA is a host-relevant trigger for titan cell formation in the lungs (where titan cells are formed), since Bronchial Alveolar Lavage (BAL) which contains lung-resident bacteria has been shown to trigger titan cell formation in *C. neoformans* [71]. In fact, the specific BAL extract responsible for the inducing titan cells was associated the presence of bacterial cells.

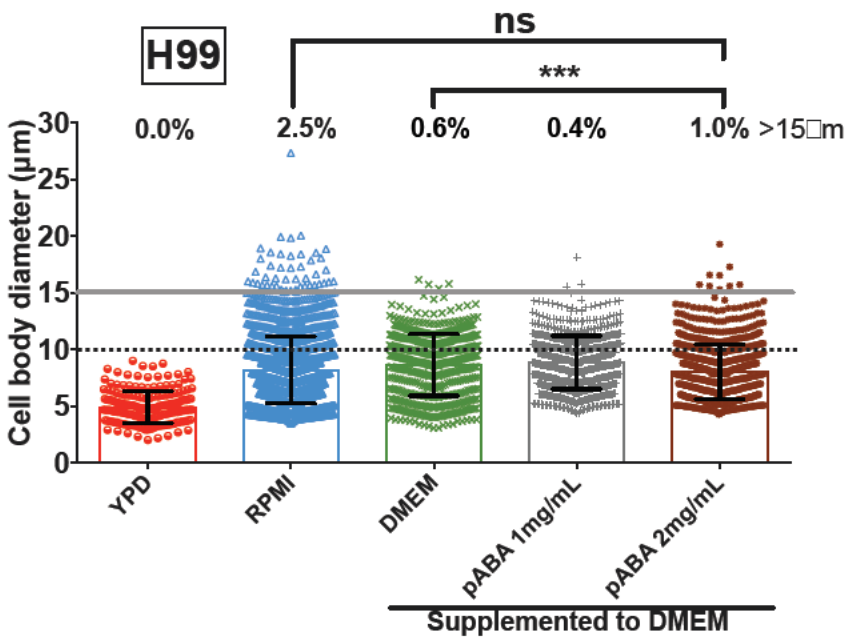

Figure 7.9. The influence of pABA on the titan induction in H99 (*C. neoformans*). Cell body size was measured after H99 yeast cells were grown in the difference induction media at 37°C in 5% CO_2 for 72 hr.

Contrary to *C. neoformans* (as described in Chapter 4), R265 titan cells exhibited an actively budding phase in the early period of induction where the majority of the cells display 1C DNA content consistent with G1 and then undergo DNA replication to form G2 arrested unbudded polyploid titan cells at the later time point (day 5 onwards) where the 1C DNA content is totally lost (Fig. 6.3B). In spite of these differences, the transcriptional profile of R265 cells undergoing titanisation mirrors their cell-cycle phenotype (Fig. 7.8). Consequently, the budding and mitosis genes, *CDC11* and *CLN1,* were expressed early and peaked at 24hrs (a point at which budding is prevalent and most cells have a 1C DNA content), suggesting that the cells were predominantly in either G1 or M phase. *CLN1* is required for releasing *C. neoformans* titan cells from G2 arrest (during cell cycle progression) [176] and therefore it is not surprising that *CLN1* is downregulated at day 3 (Fig. 7.8B) when the budding index drops significantly. However, it is intriguing that *CLN1* is partially upregulated at day 5 and 7. In *C. neoformans, CLN1* forms a critical balance between DNA replication and cell division [176].

Therefore, this data suggests that *CLN1* is involved in the regulation of cell division during the first 24 hr of induction and in DNA replication during the unbudded phases at 5 and 7 days. In conclusion, *C. gattii* titan cell formation is modulated by the combined effect of growth conditions signals (including initial inocula density, elevated temperature, CO_2 etc.), media factor, and cell cycle gene regulators.

CHAPTER 8

CONCLUSION AND RECOMMENDATIONS FOR FUTURE RESEARCH

8.1 Conclusion

This study reveals key cellular phenotypes that are potential adaptive features of *Cryptococcus* to its host. Interestingly, but not surprisingly, these phenotypes are not only predictors of *Cryptococcus* pathogenicity but also correlate with the increasingly recognized genotypic diversity among the *Cryptococcus* species complex. Whilst *C. neoformans* displayed a propensity for rapid replication, *C. gattii* instead showed a high capacity and novel mechanism to form titan cells. Triggered by host-relevant *in vitro* conditions, the expression of these phenotypes demonstrates the capacity of *in vitro* models to induce *Cryptococcus* features resembling those exhibited during *Cryptococcus*-host interactions.

The study unveils the possibility of cell cycle related phenotypes (cell enlargement, DNA replication and budding) to be asynchronously expressed during titan cell formation with novel triggers (such as p-Aminobenzoic acid) and endogenous regulators (including cell cycle associated genes). These phenotypes and associated genes could be potential therapeutic targets for intervention against cryptococcosis.

8.2 Recommendations for Future Research

Cryptococcus adaptive responses highlighted in this study reflect the behaviour of this human fungal pathogen during *in vivo* host interactions. Since these adaptive responses correlate with important virulence mechanisms, it will be worthwhile to further elucidate their occurrence in future *in vitro* and *in vivo* studies. In the future, it will be interesting to pursue these studies further in several distinct areas:

- To establish if the phenotypes induced by the conditioned media of host-derived mammalian cells': increased proliferation in *C. neoformans* and formation of enlarged polyploid titan cells in *C. gattii,* are recapitulative of *Cryptococcus* response to the host extracellular niche. To achieve this, I recommend employing an *in vitro* set up where

Cryptococcus is co-cultured with host immune cells (being in close interaction) or an *in vivo* mouse infection model and studying the phenotypic changes displayed by extracellular cryptococcal cells. This will confirm if the phenotypes are independent from physical contact between the fungus and host cells.

- To further characterize the physiochemical properties of the titan-inducing compounds in naïve and conditioned media of mammalian cells. Advanced analytical techniques such as fractionation and high-performance liquid chromatography (HPLC) can be applied to identify and describe the inducing factors. Also, the underlying metabolic mechanism for these triggers can be investigated using proteomics. As a stress-response phenotype, titan cell formation is thought to be associated with adaptive metabolic transition. Microbial organisms use alternative metabolism mechanisms when exposed to stressful environments with different nutritional profiles [249]. The cell enlargement due the conditioned media from mammalian cells (particularly alveolar macrophages and lung epithelial cells) may be caused by host-relevant compounds that trigger metabolic adaptation [2].
- To find effective inhibitors against quorum sensing (QS) detection and signaling pathways which have been implicated in regulating titan cell formation in *C. neoformans* [48, 217]. One of the most remarkable experimental observations in this study is the negative regulation of *C. gattii* titanisation by the putative cryptococcal QS molecule Qsp1. First discovered in bacteria, the role of QS in bacterial pathogenic life has been thoroughly defined and effective inhibitors against QS-driven virulence factors in both gram negative and gram positive bacteria have been found [250, 251]**.** Although QS mediates virulence mechanisms in *Cryptococcus* [242]**,** no inhibitors have yet been found. Qsp1 is a direct target of three transcription factors (Gat201, Gat204 and Liv3) required for virulence and qsp1*Δ* mutants exhibited attenuated

infection, slowed tissue accumulation and greater control by primary macrophages. Potentially, our *in vitro* titanisation assay offers a simple, high-throughput screen to identify such inhibitors in due course.

- To expound on the role of cell cycle regulation of *C. gattii* titan cells (described in this study). This can broaden our knowledge on how the unique progression of cell cycle phenotypes (cell enlargement, DNA replication and budding) and phases (G1, G2, S and M) are exhibited by *C. gattii* titan cells. On the other hand, the synchronized growth arrest (to form unbudded titan cells) and budding (after release) are desirable (since producing synchronised cryptococcal populations for such investigations has previously been methodologically challenging[252]) phenotypes that can be further studied to understand how cell cycle progression occurs during titanisation. Understanding cell-cycle regulation is essential for understanding cryptococcal virulence pathways/mechanisms since these two phenomena are linked [253, 254].
- To study the genetic mechanism underlying titan cell formation in *C. gattii.* A strong correlation between the cell cycle regulated phenotypes (cell enlargement, DNA replication, budding and growth arrest) and expression of their corresponding genes has been demonstrated in this study. However, whether and how these genes interact with other genes, especially those associated with cAMP/PKA signaling pathway (the most common pathway associated with virulence factors [255-258] including titanisation [12, 49, 173, 259] in *C. neoformans*) needs research attention. This will confirm if *C. gattii* titan cell formation is genetically regulated by the already-studied genes regulating titan cell formation in *C. neoformans,* or whether a unique set of genes and signaling pathways underlie titan cell formation in *C. gattii*. Through RNA-sequencing (the global transcriptional factors), genes and pathways underlying titan cell formation in *C. gattii* can be revealed, identifying potential antifungal drug targets. Also, I

recommend a chromosomal alignment and comparative genome hybridization between the outgroup crossing parents and progeny to decipher the genetic mechanisms controlling titan cell formation in *C. gattii.*

BIBLIOGRAPHY

1. May, R.C., et al., *Cryptococcus: from environmental saprophyte to global pathogen.* Nat Rev Microbiol, 2016. **14**(2): p. 106-17.
2. Kronstad, J., et al., *Adaptation of Cryptococcus neoformans to Mammalian Hosts: Integrated Regulation of Metabolism and Virulence.* Eukaryotic Cell, 2012. **11**(2): p. 109-118.
3. Rajasingham, R., et al., *Global burden of disease of HIV-associated cryptococcal meningitis: an updated analysis.* The Lancet. Infectious diseases, 2017. **17**(8): p. 873-881.
4. Park, B.J., et al., *Estimation of the current global burden of cryptococcal meningitis among persons living with HIV/AIDS.* AIDS, 2009. **23**(4): p. 525-30.
5. Chen, S.C., W. Meyer, and T.C. Sorrell, *Cryptococcus gattii infections.* Clin Microbiol Rev, 2014. **27**(4): p. 980-1024.
6. Bielska, E. and R.C. May, *What makes Cryptococcus gattii a pathogen?* FEMS Yeast Res, 2016. **16**(1): p. fov106.
7. Lakoh, S., et al., *Prevalence and mortality of cryptococcal disease in adults with advanced HIV in an urban tertiary hospital in Sierra Leone: a prospective study.* BMC Infect Dis, 2020. **20**(1): p. 141.
8. Casadevall, A., et al., *The 'Amoeboid Predator-Fungal Animal Virulence' Hypothesis.* Journal of fungi (Basel, Switzerland), 2019. **5**(1): p. 10.
9. Mitchell, T.G. and J.R. Perfect, *Cryptococcosis in the era of AIDS--100 years after the discovery of Cryptococcus neoformans.* Clin Microbiol Rev, 1995. **8**(4): p. 515-48.
10. Sorrell, T.C. and D.H. Ellis, *Ecology of Cryptococcus neoformans.* Rev Iberoam Micol, 1997. **14**(2): p. 42-3.
11. Kwon-Chung, K.J., *Filobasidiella Kwon-Chung (1975)*, in *The Yeasts*. 2011. p. 1443-1455.
12. Okagaki, L.H., et al., *Cryptococcal cell morphology affects host cell interactions and pathogenicity.* PLoS Pathog, 2010. **6**(6): p. e1000953.
13. Fernandes, K.E., et al., *Species in the Cryptococcus gattii complex differ in capsule and cell size following growth under capsule-inducing conditions.* Msphere, 2016. **1**(6): p. e00350-16.
14. Neilson, J.B., R.A. Fromtling, and G.S. Bulmer, *Pseudohyphal forms of Cryptococcus neoformans: decreased survival in vivo.* Mycopathologia, 1981. **73**(1): p. 57-9.
15. Feldmesser, M., Y. Kress, and A. Casadevall, *Dynamic changes in the morphology of Cryptococcus neoformans during murine pulmonary infection.* Microbiology, 2001. **147**(Pt 8): p. 2355-65.
16. Fries, B.C., et al., *Phenotypic switching in Cryptococcus neoformans results in changes in cellular morphology and glucuronoxylomannan structure.* Infect Immun, 1999. **67**(11): p. 6076-83.

17. Kwon-Chung, K.J., *A New Genus, Filobasidiella, the Perfect State of Cryptococcus neoformans.* Mycologia, 1975. **67**(6).
18. Kwon-Chung, K.J., et al., *(1557) Proposal to Conserve the Name Cryptococcus gattii against C. hondurianus and C. bacillisporus (Basidiomycota, Hymenomycetes, Tremellomycetidae).* Taxon, 2002. **51**(4): p. 804-806.
19. Kwon-Chung, K.J., *A new species of Filobasidiella, the sexual state of Cryptococcus neoformans B and C serotypes.* Mycologia, 1976. **68**(4): p. 943-6.
20. Kwon-Chung, K.J., et al., *Cryptococcus neoformans and Cryptococcus gattii, the etiologic agents of cryptococcosis.* Cold Spring Harb Perspect Med, 2014. **4**(7): p. a019760.
21. Hawksworth, D.L., et al., *The amsterdam declaration on fungal nomenclature.* IMA Fungus, 2011. **2**(1): p. 105-12.
22. Findley, K., et al., *Phylogeny and phenotypic characterization of pathogenic Cryptococcus species and closely related saprobic taxa in the Tremellales.* Eukaryot Cell, 2009. **8**(3): p. 353-61.
23. Fraser, J.A., et al., *Same-sex mating and the origin of the Vancouver Island Cryptococcus gattii outbreak.* Nature, 2005. **437**(7063): p. 1360-4.
24. Emerson, B.C. and N. Kolm, *Species diversity can drive speciation.* Nature, 2005. **434**(7036): p. 1015-7.
25. Montagna, M.T., et al., *Molecular characterization of Cryptococcus neoformans and Cryptococcus gattii from environmental sources and genetic comparison with clinical isolates in Apulia, Italy.* Environ Res, 2018. **160**: p. 347-352.
26. F. Dromer, E.G., O Ronin, Bo Dupont, *Serotyping of Cryptococcus neoformans by Using a Monoclonal Antibody Specific for Capsular Polysaccharide.* 1993.
27. Meyer, W., et al., *Consensus multi-locus sequence typing scheme for Cryptococcus neoformans and Cryptococcus gattii.* Medical Mycology, 2009. **47**(6): p. 561-570.
28. Maziarz, E.K. and J.R. Perfect, *Cryptococcosis.* Infect Dis Clin North Am, 2016. **30**(1): p. 179-206.
29. Litvintseva, A.P. and T.G. Mitchell, *Population genetic analyses reveal the African origin and strain variation of Cryptococcus neoformans var. grubii.* PLoS Pathog, 2012. **8**(2): p. e1002495.
30. Hagen, F., et al., *Recognition of seven species in the Cryptococcus gattii/Cryptococcus neoformans species complex.* Fungal Genet Biol, 2015. **78**: p. 16-48.
31. Farrer, R.A., et al., *A New Lineage of Cryptococcus gattii (VGV) Discovered in the Central Zambezian Miombo Woodlands.* mBio, 2019. **10**(6).
32. Hull, C.M. and J. Heitman, *Genetics of Cryptococcus neoformans.* Annu Rev Genet, 2002. **36**: p. 557-615.
33. Takeo, K., et al., *Unbudded G2 as well as G1 arrest in the stationary phase of the basidiomycetous yeast Cryptococcus neoformans.* FEMS Microbiol Lett, 1995. **129**(2-3): p. 231-5.
34. Heitman, J., *Sexual reproduction and the evolution of microbial pathogens.* Curr Biol, 2006. **16**(17): p. R711-25.
35. Denham, S.T. and J.C.S. Brown, *Mechanisms of Pulmonary Escape and Dissemination by Cryptococcus neoformans.* J Fungi (Basel), 2018. **4**(1).
36. Alanio, A., et al., *Cryptococcus neoformans host adaptation: toward biological evidence of dormancy.* mBio, 2015. **6**(2).
37. Hu, G., et al., *Metabolic adaptation in Cryptococcus neoformans during early murine pulmonary infection.* Molecular microbiology, 2008. **69**(6): p. 1456-1475.

38. Boyer-Chammard, T., et al., *Recent advances in managing HIV-associated cryptococcal meningitis.* F1000Res, 2019. **8**.
39. Denham, S.T. and J. Brown, *Mechanisms of pulmonary escape and dissemination by Cryptococcus neoformans.* Journal of Fungi, 2018. **4**(1): p. 25.
40. Sabiiti, W. and R.C. May, *Mechanisms of infection by the human fungal pathogen Cryptococcus neoformans.* Future Microbiol, 2012. **7**(11): p. 1297-313.
41. Osterholzer, J.J., et al., *Role of dendritic cells and alveolar macrophages in regulating early host defense against pulmonary infection with Cryptococcus neoformans.* Infect Immun, 2009. **77**(9): p. 3749-58.
42. Del Poeta, M., *Role of phagocytosis in the virulence of Cryptococcus neoformans.* Eukaryot Cell, 2004. **3**(5): p. 1067-75.
43. Smith, L.M., E.F. Dixon, and R.C. May, *The fungal pathogen Cryptococcus neoformans manipulates macrophage phagosome maturation.* Cell Microbiol, 2015. **17**(5): p. 702-13.
44. Gilbert, A.S., et al., *Vomocytosis of live pathogens from macrophages is regulated by the atypical MAP kinase ERK5.* Sci Adv, 2017. **3**(8): p. e1700898.
45. Galeas-Pena, M., N. McLaughlin, and D. Pociask, *The role of the innate immune system on pulmonary infections.* Biol Chem, 2019. **400**(4): p. 443-456.
46. Mukaremera, L. and K. Nielsen, *Adaptive Immunity to Cryptococcus neoformans Infections.* J Fungi (Basel), 2017. **3**(4).
47. Crabtree, J.N., et al., *Titan cell production enhances the virulence of Cryptococcus neoformans.* Infect Immun, 2012. **80**(11): p. 3776-85.
48. Hommel, B., et al., *Titan cells formation in Cryptococcus neoformans is finely tuned by environmental conditions and modulated by positive and negative genetic regulators.* PLoS Pathog, 2018. **14**(5): p. e1006982.
49. Zaragoza, O., et al., *Fungal cell gigantism during mammalian infection.* PLoS Pathog, 2010. **6**(6): p. e1000945.
50. Zaragoza, O. and K. Nielsen, *Titan cells in Cryptococcus neoformans: cells with a giant impact.* Curr Opin Microbiol, 2013. **16**(4): p. 409-13.
51. Dambuza, I.M., et al., *The Cryptococcus neoformans Titan cell is an inducible and regulated morphotype underlying pathogenesis.* PLoS Pathog, 2018. **14**(5): p. e1006978.
52. García-Barbazán, I., et al., *The formation of titan cells in Cryptococcus neoformans depends on the mouse strain and correlates with induction of Th2-type responses.* Cellular Microbiology, 2016. **18**(1): p. 111-124.
53. De Leon-Rodriguez, C.M., et al., *The Outcome of the Cryptococcus neoformans-Macrophage Interaction Depends on Phagolysosomal Membrane Integrity.* J Immunol, 2018. **201**(2): p. 583-603.
54. Chayakulkeeree, M., et al., *SEC14 is a specific requirement for secretion of phospholipase B1 and pathogenicity of Cryptococcus neoformans.* Molecular microbiology, 2011. **80**(4): p. 1088-1101.
55. Gilbert, A.S., R.T. Wheeler, and R.C. May, *Fungal Pathogens: Survival and Replication within Macrophages.* Cold Spring Harbor perspectives in medicine, 2014. **5**(7): p. a019661-a019661.
56. Lev, S., et al., *Fungal Inositol Pyrophosphate IP7 Is Crucial for Metabolic Adaptation to the Host Environment and Pathogenicity.* mBio, 2015. **6**(3): p. e00531-15.
57. De Leon-Rodriguez, C.M., et al., *The Capsule of Cryptococcus neoformans Modulates Phagosomal pH through Its Acid-Base Properties.* mSphere, 2018. **3**(5): p. e00437-18.

58. Angkasekwinai, P., et al., *Cryptococcus gattii infection dampens Th1 and Th17 responses by attenuating dendritic cell function and pulmonary chemokine expression in the immunocompetent hosts.* Infect Immun, 2014. **82**(9): p. 3880-90.
59. Angkasekwinai, P., et al., *Cryptococcus gattii infection dampens Th1 and Th17 responses by attenuating dendritic cell function and pulmonary chemokine expression in the immunocompetent hosts.* Infection and immunity, 2014. **82**(9): p. 3880-3890.
60. Casadevall, A., A.L. Rosas, and J.D. Nosanchuk, *Melanin and virulence in Cryptococcus neoformans.* Current opinion in microbiology, 2000. **3**(4): p. 354-358.
61. Cooney, N.M. and B.S. Klein, *Fungal adaptation to the mammalian host: it is a new world, after all.* Curr Opin Microbiol, 2008. **11**(6): p. 511-6.
62. Brown, A.J.P., et al., *Stress Adaptation.* Microbiology spectrum, 2017. **5**(4): p. 10.1128/microbiolspec.FUNK-0048-2016.
63. Ballou, E.R. and S.A. Johnston, *The cause and effect of Cryptococcus interactions with the host.* Curr Opin Microbiol, 2017. **40**: p. 88-94.
64. Jain, N., et al., *Phenotypic switching in a Cryptococcus neoformans variety gattii strain is associated with changes in virulence and promotes dissemination to the central nervous system.* Infect Immun, 2006. **74**(2): p. 896-903.
65. Zhu, X. and P.R. Williamson, *Role of laccase in the biology and virulence of Cryptococcus neoformans.* FEMS Yeast Res, 2004. **5**(1): p. 1-10.
66. Feder, V., et al., *Cryptococcus gattii urease as a virulence factor and the relevance of enzymatic activity in cryptococcosis pathogenesis.* Febs j, 2015. **282**(8): p. 1406-18.
67. Bahn, Y.S. and K.W. Jung, *Stress signaling pathways for the pathogenicity of Cryptococcus.* Eukaryot Cell, 2013. **12**(12): p. 1564-77.
68. Jung, K.W., et al., *Systematic functional profiling of transcription factor networks in Cryptococcus neoformans.* Nat Commun, 2015. **6**: p. 6757.
69. Geunes-Boyer, S., et al., *Surfactant protein D facilitates Cryptococcus neoformans infection.* Infection and immunity, 2012. **80**(7): p. 2444-2453.
70. Carreto-Binaghi, L.E., M. Aliouat el, and M.L. Taylor, *Surfactant proteins, SP-A and SP-D, in respiratory fungal infections: their role in the inflammatory response.* Respir Res, 2016. **17**(1): p. 66.
71. Dambuza, I.M., et al., *The Cryptococcus neoformans Titan cell is an inducible and regulated morphotype underlying pathogenesis.* PLoS pathogens, 2018. **14**(5): p. e1006978-e1006978.
72. Kronstad, J.W., G. Hu, and J. Choi, *The cAMP/Protein Kinase A Pathway and Virulence in Cryptococcus neoformans.* Mycobiology, 2011. **39**(3): p. 143-50.
73. Lodge, J.K., et al., *Targeted gene replacement demonstrates that myristoyl-CoA: protein N-myristoyltransferase is essential for viability of Cryptococcus neoformans.* Proc Natl Acad Sci U S A, 1994. **91**(25): p. 12008-12.
74. Fuchs, B.B., R.J. Tang, and E. Mylonakis, *The temperature-sensitive role of Cryptococcus neoformans ROM2 in cell morphogenesis.* PLoS One, 2007. **2**(4): p. e368.
75. Perfect, J.R., *Cryptococcus neoformans: the yeast that likes it hot.* FEMS Yeast Res, 2006. **6**(4): p. 463-8.
76. Odom, A., et al., *Calcineurin is required for virulence of Cryptococcus neoformans.* The EMBO journal, 1997. **16**(10): p. 2576-2589.
77. Chow, E.W., et al., *Elucidation of the calcineurin-Crz1 stress response transcriptional network in the human fungal pathogen Cryptococcus neoformans.* PLoS Genet, 2017. **13**(4): p. e1006667.

78. Fuchs, B.B., R.J. Tang, and E. Mylonakis, *The temperature-sensitive role of Cryptococcus neoformans ROM2 in cell morphogenesis.* PloS one, 2007. **2**(4): p. e368-e368.
79. Alspaugh, J.A., et al., *RAS1 regulates filamentation, mating and growth at high temperature of Cryptococcus neoformans.* Mol Microbiol, 2000. **36**(2): p. 352-65.
80. Nichols, C.B., Z.H. Perfect, and J.A. Alspaugh, *A Ras1-Cdc24 signal transduction pathway mediates thermotolerance in the fungal pathogen Cryptococcus neoformans.* Mol Microbiol, 2007. **63**(4): p. 1118-30.
81. Ballou, E.R., et al., *Ras1 acts through duplicated Cdc42 and Rac proteins to regulate morphogenesis and pathogenesis in the human fungal pathogen Cryptococcus neoformans.* PLoS Genet, 2013. **9**(8): p. e1003687.
82. Walton, F.J., J. Heitman, and A. Idnurm, *Conserved elements of the RAM signaling pathway establish cell polarity in the basidiomycete Cryptococcus neoformans in a divergent fashion from other fungi.* Molecular biology of the cell, 2006. **17**(9): p. 3768-3780.
83. Odom, A., et al., *Calcineurin is required for virulence of Cryptococcus neoformans.* Embo Journal, 1997. **16**(10): p. 2576-2589.
84. You, M. and J. Xu, *The effects of environmental and genetic factors on the germination of basidiospores in the Cryptococcus gattii species complex.* Sci Rep, 2018. **8**(1): p. 15260.
85. Kraus, P.R., et al., *Identification of Cryptococcus neoformans temperature-regulated genes with a genomic-DNA microarray.* Eukaryot Cell, 2004. **3**(5): p. 1249-60.
86. Mogensen, E.G., et al., *Cryptococcus neoformans senses CO2 through the carbonic anhydrase Can2 and the adenylyl cyclase Cac1.* Eukaryotic cell, 2006. **5**(1): p. 103-111.
87. Bahn, Y.S., et al., *Carbonic anhydrase and CO2 sensing during Cryptococcus neoformans growth, differentiation, and virulence.* Curr Biol, 2005. **15**(22): p. 2013-20.
88. Ren, P., V. Chaturvedi, and S. Chaturvedi, *Carbon dioxide is a powerful inducer of monokaryotic hyphae and spore development in Cryptococcus gattii and carbonic anhydrase activity is dispensable in this dimorphic transition.* PLoS One, 2014. **9**(12): p. e113147.
89. Effros, R.M. and F.P. Chinard, *The in vivo pH of the extravascular space of the lung.* The Journal of clinical investigation, 1969. **48**(11): p. 1983-1996.
90. Ost, K.S., et al., *The Cryptococcus neoformans alkaline response pathway: identification of a novel rim pathway activator.* PLoS Genet, 2015. **11**(4): p. e1005159.
91. Heung, L.J., *Innate Immune Responses to Cryptococcus.* Journal of fungi (Basel, Switzerland), 2017. **3**(3): p. 35.
92. O'Meara, T.R., et al., *Cryptococcus neoformans Rim101 is associated with cell wall remodeling and evasion of the host immune responses.* mBio, 2013. **4**(1).
93. Ng, A.W., A. Bidani, and T.A. Heming, *Innate host defense of the lung: effects of lung-lining fluid pH.* Lung, 2004. **182**(5): p. 297-317.
94. Chun, C.D. and H.D. Madhani, *Applying Genetics and Molecular Biology to the Study of the Human Pathogen Cryptococcus neoformans*, in *Guide to Yeast Genetics: Functional Genomics, Proteomics, and Other Systems Analysis*. 2010. p. 797-831.
95. Kipnis, E., et al., *Proteomic analysis of undiluted lung epithelial lining fluid.* Chest, 2008. **134**(2): p. 338-345.
96. Griese, M., *Pulmonary surfactant in health and human lung diseases: state of the art.* Eur Respir J, 1999. **13**(6): p. 1455-76.

97. Nicod, L.P., *Lung defences: an overview.* European Respiratory Review, 2005. **14**(95): p. 45-50.
98. Bals, R. and P.S. Hiemstra, *Innate immunity in the lung: how epithelial cells fight against respiratory pathogens.* European Respiratory Journal, 2004. **23**(2): p. 327-333.
99. Taylor-Smith, L.M., *Cryptococcus-Epithelial Interactions.* J Fungi (Basel), 2017. **3**(4).
100. Arcos, J., et al., *Human lung hydrolases delineate Mycobacterium tuberculosis-macrophage interactions and the capacity to control infection.* J Immunol, 2011. **187**(1): p. 372-81.
101. Moliva, J.I., et al., *The Lung Mucosa Environment in the Elderly Increases Host Susceptibility to Mycobacterium tuberculosis Infection.* J Infect Dis, 2019. **220**(3): p. 514-523.
102. Gatti, F. and R. Eeckels, *An atypical strain of Cryptococcus neoformans (San Felice) Vuillemin 1894. I. Description of the disease and of the strain.* Ann Soc Belges Med Trop Parasitol Mycol, 1970. **50**(6): p. 689-93.
103. Perfect, J.R., *Cryptococcosis: a model for the understanding of infectious diseases.* J Clin Invest, 2014. **124**(5): p. 1893-5.
104. Rajasingham, R., et al., *Global burden of disease of HIV-associated cryptococcal meningitis: an updated analysis.* Lancet Infect Dis, 2017. **17**(8): p. 873-881.
105. Granados, D.P. and E. Castaneda, *Isolation and characterization of Cryptococcus neoformans varieties recovered from natural sources in Bogota, Colombia, and study of ecological conditions in the area.* Microb Ecol, 2005. **49**(2): p. 282-90.
106. Brandt, M.E., et al., *Molecular subtype distribution of Cryptococcus neoformans in four areas of the United States. Cryptococcal Disease Active Surveillance Group.* J Clin Microbiol, 1996. **34**(4): p. 912-7.
107. Byrnes, E.J., 3rd, et al., *Emergence and pathogenicity of highly virulent Cryptococcus gattii genotypes in the northwest United States.* PLoS Pathog, 2010. **6**(4): p. e1000850.
108. Bartlett, K.H., S.E. Kidd, and J.W. Kronstad, *The emergence of Cryptococcus gattii in British Columbia and the Pacific Northwest.* Current infectious disease reports, 2008. **10**(1): p. 58-65.
109. Xu, J., R. Vilgalys, and T.G. Mitchell, *Multiple gene genealogies reveal recent dispersion and hybridization in the human pathogenic fungus Cryptococcus neoformans.* Molecular Ecology, 2000. **9**(10): p. 1471-1481.
110. Ngamskulrungroj, P., et al., *Genetic diversity of the Cryptococcus species complex suggests that Cryptococcus gattii deserves to have varieties.* PloS one, 2009. **4**(6): p. e5862.
111. Firacative, C., L. Trilles, and W. Meyer, *MALDI-TOF MS enables the rapid identification of the major molecular types within the Cryptococcus neoformans/C. gattii species complex.* PLoS One, 2012. **7**(5): p. e37566.
112. Bovers, M., et al., *Six monophyletic lineages identified within Cryptococcus neoformans and Cryptococcus gattii by multi-locus sequence typing.* Fungal Genetics and Biology, 2008. **45**(4): p. 400-421.
113. D'Souza, C.A., et al., *Genome variation in Cryptococcus gattii, an emerging pathogen of immunocompetent hosts.* mBio, 2011. **2**(1): p. e00342-10.
114. Chen, S.C.A., W. Meyer, and T.C. Sorrell, *Cryptococcus gattii infections.* Clinical microbiology reviews, 2014. **27**(4): p. 980-1024.
115. Byrnes III, E.J., et al., *Cryptococcus gattii: an emerging fungal pathogen infecting humans and animals.* Microbes and infection, 2011. **13**(11): p. 895-907.

116. Kidd, S.E., et al., *A rare genotype of Cryptococcus gattii caused the cryptococcosis outbreak on Vancouver Island (British Columbia, Canada).* Proc Natl Acad Sci U S A, 2004. **101**(49): p. 17258-63.
117. Kidd, S.E., et al., *A rare genotype of Cryptococcus gattii caused the cryptococcosis outbreak on Vancouver Island (British Columbia, Canada).* Proceedings of the national academy of sciences, 2004. **101**(49): p. 17258-17263.
118. Billmyre, R.B., et al., *Highly recombinant VGII Cryptococcus gattii population develops clonal outbreak clusters through both sexual macroevolution and asexual microevolution.* MBio, 2014. **5**(4): p. e01494-14.
119. Farrer, R.A., et al., *Genome evolution and innovation across the four major lineages of Cryptococcus gattii.* MBio, 2015. **6**(5): p. e00868-15.
120. Lin, X., C.M. Hull, and J. Heitman, *Sexual reproduction between partners of the same mating type in Cryptococcus neoformans.* Nature, 2005. **434**(7036): p. 1017-1021.
121. Firacative, C., S. Duan, and W. Meyer, *Galleria mellonella model identifies highly virulent strains among all major molecular types of Cryptococcus gattii.* PloS one, 2014. **9**(8): p. e105076-e105076.
122. Franzot, S.P., I.F. Salkin, and A. Casadevall, *Cryptococcus neoformans var. grubii: separate varietal status for Cryptococcus neoformans serotype A isolates.* J Clin Microbiol, 1999. **37**(3): p. 838-40.
123. Xie, S., et al., *Difference in Cryptococcus neoformans cellular and capsule size in sequential pulmonary and meningeal infection: a postmortem study.* Diagn Microbiol Infect Dis, 2012. **73**(1): p. 49-52.
124. Fernandes, K.E., et al., *Phenotypic variability correlates with clinical outcome in Cryptococcus isolates obtained from Botswanan HIV/AIDS patients.* MBio, 2018. **9**(5): p. e02016-18.
125. Thompson III, G.R., et al., *Phenotypic differences of Cryptococcus molecular types and their implications for virulence in a Drosophila model of infection.* Infection and immunity, 2014. **82**(7): p. 3058-3065.
126. Saidykhan, L., et al., *An in vitro method for inducing titan cells reveals novel features of yeast-to-titan switching in the human fungal pathogen Cryptococcus gattii.* PLoS Pathog, 2022. **18**(8): p. e1010321.
127. Gerstein, A.C., et al., *Polyploid titan cells produce haploid and aneuploid progeny to promote stress adaptation.* mBio, 2015. **6**(5): p. e01340-15.
128. Malliaris, S.D., J.N. Steenbergen, and A. Casadevall, *Cryptococcus neoformans var. gattii can exploit Acanthamoeba castellanii for growth.* Medical mycology, 2004. **42**(2): p. 149-158.
129. Zaragoza, O., et al., *The capsule of the fungal pathogen Cryptococcus neoformans.* Advances in applied microbiology, 2009. **68**: p. 133-216.
130. O'Meara, T.R. and J.A. Alspaugh, *The Cryptococcus neoformans capsule: a sword and a shield.* Clinical microbiology reviews, 2012. **25**(3): p. 387-408.
131. Nosanchuk, J.D., et al., *Melanization of Cryptococcus neoformans in murine infection.* Molecular and cellular biology, 1999. **19**(1): p. 745-750.
132. de Sousa, H.R., et al., *Faster Cryptococcus melanization increases virulence in experimental and human cryptococcosis.* bioRxiv, 2020.
133. Garcia-Rivera, J. and A. Casadevall, *Melanization of Cryptococcus neoformans reduces its susceptibility to the antimicrobial effects of silver nitrate.* Sabouraudia, 2001. **39**(4): p. 353-357.
134. Ma, H. and R.C. May, *Virulence in Cryptococcus species.* Advances in applied microbiology, 2009. **67**: p. 131-190.

135. Oliveira, L.S.d.S., et al., *Comparison of Cryptococcus gattii/neoformans species complex to related genera (Papiliotrema and Naganishia) reveal variances in virulence associated factors and antifungal susceptibility.* Frontiers in cellular and infection microbiology, 2021. **11**: p. 573.
136. Gilbert, A.S., R.T. Wheeler, and R.C. May, *Fungal pathogens: survival and replication within macrophages.* Cold Spring Harbor perspectives in medicine, 2015. **5**(7): p. a019661.
137. Byrnes, E.J., 3rd and K.A. Marr, *The Outbreak of Cryptococcus gattii in Western North America: Epidemiology and Clinical Issues.* Current infectious disease reports, 2011. **13**(3): p. 256-261.
138. Galanis, E., et al., *Epidemiology of Cryptococcus gattii, British Columbia, Canada, 1999-2007.* Emerging infectious diseases, 2010. **16**(2): p. 251-257.
139. Chen, S.C.-A., et al., *Clinical Manifestations of Cryptococcus gattii Infection: Determinants of Neurological Sequelae and Death.* Clinical Infectious Diseases, 2012. **55**(6): p. 789-798.
140. Gerstein, A.C. and K. Nielsen, *It's not all about us: evolution and maintenance of Cryptococcus virulence requires selection outside the human host.* Yeast, 2017. **34**(4): p. 143-154.
141. Lalloo, D., et al., *Cryptococcal meningitis (C. neoformans var. gattii) leading to blindness in previously healthy Melanesian adults in Papua New Guinea.* Q J Med, 1994. **87**(6): p. 343-9.
142. Harris, J.R., et al., *Cryptococcus gattii in the United States: clinical aspects of infection with an emerging pathogen.* Clin Infect Dis, 2011. **53**(12): p. 1188-95.
143. Martins, L.M.S., et al., *Genotypes of Cryptococcus neoformans and Cryptococcus gattii as agents of endemic cryptococcosis in Teresina, Piauí (northeastern Brazil).* Memorias do Instituto Oswaldo Cruz, 2011. **106**: p. 725-730.
144. Freeman, S.A. and S. Grinstein, *Phagocytosis: receptors, signal integration, and the cytoskeleton.* Immunol Rev, 2014. **262**(1): p. 193-215.
145. Huang, H.-R., et al., *Dectin-3 Recognizes Glucuronoxylomannan of Cryptococcus neoformans Serotype AD and Cryptococcus gattii Serotype B to Initiate Host Defense Against Cryptococcosis.* Frontiers in immunology, 2018. **9**: p. 1781-1781.
146. Fonseca, F.L., et al., *Immunomodulatory effects of serotype B glucuronoxylomannan from Cryptococcus gattii correlate with polysaccharide diameter.* Infection and immunity, 2010. **78**(9): p. 3861-3870.
147. Illnait-Zaragozi, M.-T., et al., *Cryptococcus gattii induces a cytokine pattern that is distinct from other cryptococcal species.* PloS one, 2013. **8**(1): p. e55579.
148. Campuzano, A. and F.L. Wormley, *Innate Immunity against Cryptococcus, from Recognition to Elimination.* Journal of fungi (Basel, Switzerland), 2018. **4**(1): p. 33.
149. Rohatgi, S. and L.-A. Pirofski, *Host immunity to Cryptococcus neoformans.* Future microbiology, 2015. **10**(4): p. 565-581.
150. Kaiko, G.E., et al., *Immunological decision-making: how does the immune system decide to mount a helper T-cell response?* Immunology, 2008. **123**(3): p. 326-338.
151. Jolink, H., et al., *Pulmonary immune responses against Aspergillus fumigatus are characterized by high frequencies of IL-17 producing T-cells.* Journal of Infection, 2017. **74**(1): p. 81-88.
152. Zhang, Y., et al., *Robust Th1 and Th17 immunity supports pulmonary clearance but cannot prevent systemic dissemination of highly virulent Cryptococcus neoformans H99.* The American journal of pathology, 2009. **175**(6): p. 2489-2500.

153. Conti, H.R. and S.L. Gaffen, *IL-17-Mediated Immunity to the Opportunistic Fungal Pathogen Candida albicans.* J Immunol, 2015. **195**(3): p. 780-8.
154. Müller, U., et al., *IL-13 induces disease-promoting type 2 cytokines, alternatively activated macrophages and allergic inflammation during pulmonary infection of mice with Cryptococcus neoformans.* J Immunol, 2007. **179**(8): p. 5367-77.
155. Huston, S.M., et al., *Cryptococcus gattii is killed by dendritic cells, but evades adaptive immunity by failing to induce dendritic cell maturation.* The Journal of Immunology, 2013. **191**(1): p. 249-261.
156. Chaturvedi, V. and S. Chaturvedi, *Cryptococcus gattii: a resurgent fungal pathogen.* Trends Microbiol, 2011. **19**(11): p. 564-71.
157. Marr, K.A., *Cryptococcus gattii as an important fungal pathogen of western North America.* Expert review of anti-infective therapy, 2012. **10**(6): p. 637-643.
158. Ma, H., et al., *The fatal fungal outbreak on Vancouver Island is characterized by enhanced intracellular parasitism driven by mitochondrial regulation.* Proceedings of the National Academy of Sciences, 2009. **106**(31): p. 12980.
159. Voelz, K., et al., *'Division of labour'in response to host oxidative burst drives a fatal Cryptococcus gattii outbreak.* Nature communications, 2014. **5**(1): p. 1-12.
160. Byrnes III, E.J., et al., *Molecular evidence that the range of the Vancouver Island outbreak of Cryptococcus gattii infection has expanded into the Pacific Northwest in the United States.* The Journal of infectious diseases, 2009. **199**(7): p. 1081-1086.
161. Bielska, E., et al., *Pathogen-derived extracellular vesicles mediate virulence in the fatal human pathogen Cryptococcus gattii.* Nature communications, 2018. **9**(1): p. 1-9.
162. Zhang, S., et al., *The Hsp70 member, Ssa1, acts as a DNA-binding transcriptional co-activator of laccase in Cryptococcus neoformans.* Molecular microbiology, 2006. **62**(4): p. 1090-1101.
163. Janbon, G., et al., *Characterizing the role of RNA silencing components in Cryptococcus neoformans.* Fungal Genetics and Biology, 2010. **47**(12): p. 1070-1080.
164. Cheng, P.Y., A. Sham, and J.W. Kronstad, *Cryptococcus gattii isolates from the British Columbia cryptococcosis outbreak induce less protective inflammation in a murine model of infection than Cryptococcus neoformans.* Infect Immun, 2009. **77**(10): p. 4284-94.
165. Decote-Ricardo, D., et al., *Immunomodulatory Role of Capsular Polysaccharides Constituents of Cryptococcus neoformans.* Frontiers in medicine, 2019. **6**: p. 129-129.
166. Okagaki, L.H. and K. Nielsen, *Titan cells confer protection from phagocytosis in Cryptococcus neoformans infections.* Eukaryot Cell, 2012. **11**(6): p. 820-6.
167. Botts, M.R., et al., *Isolation and characterization of Cryptococcus neoformans spores reveal a critical role for capsule biosynthesis genes in spore biogenesis.* Eukaryot Cell, 2009. **8**(4): p. 595-605.
168. Maxson, M.E., et al., *The volume and hydration of the Cryptococcus neoformans polysaccharide capsule.* Fungal Genet Biol, 2007. **44**(3): p. 180-6.
169. McFadden, D.C., et al., *Capsule structural heterogeneity and antigenic variation in Cryptococcus neoformans.* Eukaryot Cell, 2007. **6**(8): p. 1464-73.
170. Zaragoza, O., et al., *The capsule of the fungal pathogen Cryptococcus neoformans.* Adv Appl Microbiol, 2009. **68**: p. 133-216.
171. Frases, S., et al., *Cryptococcus neoformans capsular polysaccharide and exopolysaccharide fractions manifest physical, chemical, and antigenic differences.* Eukaryot Cell, 2008. **7**(2): p. 319-27.

172. Freitas, G.J. and D.A. Santos, *Cryptococcus gattii polysaccharide capsule: An insight on fungal-host interactions and vaccine studies.* European Journal of Immunology, 2021. **51**(9): p. 2206-2209.
173. Zhou, X. and E.R. Ballou, *The Cryptococcus neoformans titan cell: from in vivo phenomenon to in vitro model.* Current Clinical Microbiology Reports, 2018. **5**(4): p. 252-260.
174. Lin, X., *Cryptococcus neoformans: morphogenesis, infection, and evolution.* Infect Genet Evol, 2009. **9**(4): p. 401-16.
175. Alspaugh, J.A., R.C. Davidson, and J. Heitman, *Morphogenesis of Cryptococcus neoformans.* Contributions to microbiology, 2000. **5**: p. 217-238.
176. Altamirano, S., et al., *The Cyclin Cln1 Controls Polyploid Titan Cell Formation following a Stress-Induced G2 Arrest in Cryptococcus.* mBio, 2021. **12**(5): p. e0250921.
177. da Silva-Junior, E.B., et al., *The role of Toll-like receptor 9 in a murine model of Cryptococcus gattii infection.* Scientific Reports, 2021. **11**(1): p. 1-11.
178. Probert, M., et al., *A Glucuronoxylomannan Epitope Exhibits Serotype-Specific Accessibility and Redistributes towards the Capsule Surface during Titanization of the Fungal Pathogen Cryptococcus neoformans.* Infect Immun, 2019. **87**(4).
179. Dos Santos, M.H., et al., *Titan Cells and Yeast Forms of Cryptococcus neoformans and Cryptococcus gattii Are Recognized by GXMR-CAR.* Microorganisms, 2021. **9**(9).
180. Liebana-Jordan, M., et al., *Extracellular vesicles in the fungi kingdom.* International Journal of Molecular Sciences, 2021. **22**(13): p. 7221.
181. Gill, S., R. Catchpole, and P. Forterre, *Extracellular membrane vesicles in the three domains of life and beyond.* FEMS microbiology reviews, 2019. **43**(3): p. 273-303.
182. de Oliveira, H.C., et al., *Pathogenic Delivery: The Biological Roles of Cryptococcal Extracellular Vesicles.* Pathogens, 2020. **9**(9).
183. Oliveira, D.L., et al., *Extracellular vesicles from Cryptococcus neoformans modulate macrophage functions.* Infection and immunity, 2010. **78**(4): p. 1601-1609.
184. Rodrigues, M.L., et al., *Extracellular vesicles produced by Cryptococcus neoformans contain protein components associated with virulence.* Eukaryotic cell, 2008. **7**(1): p. 58-67.
185. Rizzo, J., et al., *Cryptococcus extracellular vesicles properties and their use as vaccine platforms.* Journal of extracellular vesicles, 2021. **10**(10): p. e12129.
186. Rizzo, J., A. Taheraly, and G. Janbon, *Structure, composition and biological properties of fungal extracellular vesicles.* microLife, 2021. **2**.
187. Wolf, J.M., et al., *Interaction of Cryptococcus neoformans extracellular vesicles with the cell wall.* Eukaryotic cell, 2014. **13**(12): p. 1484-1493.
188. Hu, G., et al., *The endosomal sorting complex required for transport machinery influences haem uptake and capsule elaboration in C ryptococcus neoformans.* Molecular microbiology, 2015. **96**(5): p. 973-992.
189. Chang, Y.C. and K. Kwon-Chung, *Complementation of a capsule-deficient mutation of Cryptococcus neoformans restores its virulence.* Molecular and cellular biology, 1994. **14**(7): p. 4912-4919.
190. García-Rivera, J., et al., *Cryptococcus neoformans CAP59 (or Cap59p) is involved in the extracellular trafficking of capsular glucuronoxylomannan.* Eukaryotic cell, 2004. **3**(2): p. 385-392.
191. Grijpstra, J., et al., *The Cryptococcus neoformans cap10 and cap59 mutant strains, affected in glucuronoxylomannan synthesis, differentially activate human dendritic cells.* FEMS Immunol Med Microbiol, 2009. **57**(2): p. 142-50.

192. Chang, Y.C., L.A. Penoyer, and K.J. Kwon-Chung, *The second capsule gene of cryptococcus neoformans, CAP64, is essential for virulence.* Infect Immun, 1996. **64**(6): p. 1977-83.
193. Chang, Y. and K. Kwon-Chung, *Isolation of the third capsule-associated gene, CAP60, required for virulence in Cryptococcus neoformans.* Infection and Immunity, 1998. **66**(5): p. 2230-2236.
194. Moyrand, F., T. Fontaine, and G. Janbon, *Systematic capsule gene disruption reveals the central role of galactose metabolism on Cryptococcus neoformans virulence.* Mol Microbiol, 2007. **64**(3): p. 771-81.
195. García-Rodas, R., et al., *Capsule growth in Cryptococcus neoformans is coordinated with cell cycle progression.* mBio, 2014. **5**(3): p. e00945-14.
196. O'Meara, T.R., et al., *Interaction of Cryptococcus neoformans Rim101 and protein kinase A regulates capsule.* PLoS pathogens, 2010. **6**(2): p. e1000776.
197. Gong, J., et al., *A Ric8/synembryn homolog promotes Gpa1 and Gpa2 activation to respectively regulate cyclic AMP and pheromone signaling in Cryptococcus neoformans.* Eukaryotic cell, 2014. **13**(10): p. 1290-1299.
198. García-Rodas, R., et al., *Role of Cln1 during melanization of Cryptococcus neoformans.* Frontiers in microbiology, 2015. **6**: p. 798.
199. Chen, L.C., E.S. Blank, and A. Casadevall, *Extracellular proteinase activity of Cryptococcus neoformans.* Clin Diagn Lab Immunol, 1996. **3**(5): p. 570-4.
200. Ma, H. and R.C. May, *Virulence in Cryptococcus species.* Adv Appl Microbiol, 2009. **67**: p. 131-90.
201. Seoane, P.I. and R.C. May, *Vomocytosis: what we know so far.* Cellular microbiology, 2020. **22**(2): p. e13145.
202. Olszewski, M.A., et al., *Urease expression by Cryptococcus neoformans promotes microvascular sequestration, thereby enhancing central nervous system invasion.* The American journal of pathology, 2004. **164**(5): p. 1761-1771.
203. Merkel, G.J. and B.A. Scofield, *The in vitro interaction of Cryptococcus neoformans with human lung epithelial cells.* FEMS Immunol Med Microbiol, 1997. **19**(3): p. 203-13.
204. Matsunaga, K., et al., *Alveolar macrophage cell line MH-S is valuable as an in vitro model for Legionella pneumophila infection.* Am J Respir Cell Mol Biol, 2001. **24**(3): p. 326-31.
205. Bligh, E.G. and W.J. Dyer, *A rapid method of total lipid extraction and purification.* Can J Biochem Physiol, 1959. **37**(8): p. 911-7.
206. Olszewski, M.A., et al., *In Vitro Analysis of Metabolites Secreted during Infection of Lung Epithelial Cells by Cryptococcus neoformans.* Plos One, 2016. **11**(4).
207. Dragotakes, Q. and A. Casadevall, *Automated Measurement of Cryptococcal Species Polysaccharide Capsule and Cell Body.* J Vis Exp, 2018(131).
208. Martinez, L.R. and A. Casadevall, *Susceptibility of Cryptococcus neoformans biofilms to antifungal agents in vitro.* Antimicrob Agents Chemother, 2006. **50**(3): p. 1021-33.
209. Kronstad, J., et al., *Adaptation of Cryptococcus neoformans to mammalian hosts: integrated regulation of metabolism and virulence.* Eukaryot Cell, 2012. **11**(2): p. 109-18.
210. Nassar, F., E. Brummer, and D.A. Stevens, *Different components in human serum inhibit multiplication of Cryptococcus neoformans and enhance fluconazole activity.* Antimicrob Agents Chemother, 1995. **39**(11): p. 2490-3.
211. Steen, B.R., et al., *Temperature-regulated transcription in the pathogenic fungus Cryptococcus neoformans.* Genome Res, 2002. **12**(9): p. 1386-400.

212. Garcia-Barbazan, I., et al., *The formation of titan cells in Cryptococcus neoformans depends on the mouse strain and correlates with induction of Th2-type responses.* Cell Microbiol, 2016. **18**(1): p. 111-24.
213. Voelz, K., D.A. Lammas, and R.C. May, *Erratum for Voelz et al., Cytokine Signaling Regulates the Outcome of Intracellular Macrophage Parasitism by Cryptococcus neoformans.* Infect Immun, 2016. **84**(12): p. 3656.
214. Hu, G., et al., *Comparative hybridization reveals extensive genome variation in the AIDS-associated pathogen Cryptococcus neoformans.* Genome Biol, 2008. **9**(2): p. R41.
215. Zaragoza, O. and A. Casadevall, *Experimental modulation of capsule size in Cryptococcus neoformans.* Biol Proced Online, 2004. **6**: p. 10-15.
216. Fernandes, K.E., et al., *Phenotypic Variability Correlates with Clinical Outcome in Cryptococcus Isolates Obtained from Botswanan HIV/AIDS Patients.* MBio, 2018. **9**(5).
217. Trevijano-Contador, N., et al., *Cryptococcus neoformans can form titan-like cells in vitro in response to multiple signals.* PLoS Pathog, 2018. **14**(5): p. e1007007.
218. Gupta, G. and B.C. Fries, *Variability of phenotypic traits in Cryptococcus varieties and species and the resulting implications for pathogenesis.* Future Microbiol, 2010. **5**(5): p. 775-87.
219. Thompson, G.R., 3rd, et al., *Phenotypic differences of Cryptococcus molecular types and their implications for virulence in a Drosophila model of infection.* Infect Immun, 2014. **82**(7): p. 3058-65.
220. Albuquerque, P., et al., *Quorum sensing-mediated, cell density-dependent regulation of growth and virulence in Cryptococcus neoformans.* mBio, 2013. **5**(1): p. e00986-13.
221. Fernandes, K.E., et al., *Species in the Cryptococcus gattii Complex Differ in Capsule and Cell Size following Growth under Capsule-Inducing Conditions.* mSphere, 2016. **1**(6).
222. Nyazika, T.K., et al., *Cryptococcus tetragattii as a major cause of cryptococcal meningitis among HIV-infected individuals in Harare, Zimbabwe.* J Infect, 2016. **72**(6): p. 745-752.
223. Qu, J., et al., *Clinical analysis in immunocompetent and immunocompromised patients with pulmonary cryptococcosis in western China.* Sci Rep, 2020. **10**(1): p. 9387.
224. Speed, B. and D. Dunt, *Clinical and host differences between infections with the two varieties of Cryptococcus neoformans.* Clin Infect Dis, 1995. **21**(1): p. 28-34; discussion 35-6.
225. García-Rodas, R., et al., *Cryptococcus neoformans capsular enlargement and cellular gigantism during Galleria mellonella infection.* PLoS One, 2011. **6**(9): p. e24485.
226. Okagaki, L.H., et al., *Cryptococcal Titan Cell Formation Is Regulated by G-Protein Signaling in Response to Multiple Stimuli ▽.* Eukaryotic Cell, 2011. **10**(10): p. 1306-1316.
227. Mukaremera, L., et al., *Titan cell production in Cryptococcus neoformans reshapes the cell wall and capsule composition during infection.* The Cell Surface, 2018. **1**: p. 15-24.
228. Hagen, F., et al., *Recognition of seven species in the Cryptococcus gattii/Cryptococcus neoformans species complex.* Fungal Genetics and Biology, 2015. **78**: p. 16-48.
229. Voelz, K., et al., *Transmission of Hypervirulence traits via sexual reproduction within and between lineages of the human fungal pathogen cryptococcus gattii.* PLoS Genet, 2013. **9**(9): p. e1003771.

230. Feldmesser, M., Y. Kress, and A. Casadevall, *Dynamic changes in the morphology of Cryptococcus neoformans during murine pulmonary infection.* Microbiology (Reading), 2001. **147**(Pt 8): p. 2355-2365.
231. Fries, B.C., et al., *Phenotypic switching of Cryptococcus neoformans occurs in vivo and influences the outcome of infection.* The Journal of clinical investigation, 2001. **108**(11): p. 1639-1648.
232. Li, Z. and K. Nielsen, *Morphology Changes in Human Fungal Pathogens upon Interaction with the Host.* Journal of fungi (Basel, Switzerland), 2017. **3**(4): p. 66.
233. May, R.C., et al., *Cryptococcus: from environmental saprophyte to global pathogen.* Nature reviews. Microbiology, 2016. **14**(2): p. 106-117.
234. O'Meara, T.R. and J.A. Alspaugh, *The Cryptococcus neoformans capsule: a sword and a shield.* Clin Microbiol Rev, 2012. **25**(3): p. 387-408.
235. Chang, A.L. and T.L. Doering, *Maintenance of Mitochondrial Morphology in Cryptococcus neoformans Is Critical for Stress Resistance and Virulence.* mBio, 2018. **9**(6).
236. Hartwell, L.H. and M.W. Unger, *Unequal division in Saccharomyces cerevisiae and its implications for the control of cell division.* The Journal of cell biology, 1977. **75**(2 Pt 1): p. 422-435.
237. Hartwell, L.H., et al., *Genetic control of the cell division cycle in yeast.* Science, 1974. **183**(4120): p. 46-51.
238. Ngamskulrungroj, P., et al., *The primary target organ of Cryptococcus gattii is different from that of Cryptococcus neoformans in a murine model.* mBio, 2012. **3**(3): p. e00103-12.
239. Reuwsaat, J.C.V., et al., *The Transcription Factor Pdr802 Regulates Titan Cell Formation and Pathogenicity of Cryptococcus neoformans.* mBio, 2021. **12**(2): p. e03457-20.
240. Albuquerque, P., et al., *Quorum sensing-mediated, cell density-dependent regulation of growth and virulence in Cryptococcus neoformans.* mBio, 2013. **5**(1): p. e00986.
241. Bassler, B.L., *How bacteria talk to each other: regulation of gene expression by quorum sensing.* Curr Opin Microbiol, 1999. **2**(6): p. 582-7.
242. Homer, C.M., et al., *Intracellular Action of a Secreted Peptide Required for Fungal Virulence.* Cell Host Microbe, 2016. **19**(6): p. 849-64.
243. Laborda, P., et al., *Production of Antifungal p-Aminobenzoic Acid in Lysobacter antibioticus OH13.* J Agric Food Chem, 2018. **66**(3): p. 630-636.
244. Laborda, P., et al., *Antifungal Metabolite p-Aminobenzoic Acid (pABA): Mechanism of Action and Efficacy for the Biocontrol of Pear Bitter Rot Disease.* J Agric Food Chem, 2019. **67**(8): p. 2157-2165.
245. Moore, C.W., et al., *Fungal cell wall septation and cytokinesis are inhibited by bleomycins.* Antimicrob Agents Chemother, 2003. **47**(10): p. 3281-9.
246. Lu, Z., et al., *Para-aminobenzoic acid (PABA) synthase enhances thermotolerance of mushroom Agaricus bisporus.* PloS one, 2014. **9**(3): p. e91298-e91298.
247. Warris, A. and E.R. Ballou, *Oxidative responses and fungal infection biology.* Semin Cell Dev Biol, 2019. **89**: p. 34-46.
248. Wegkamp, A., et al., *Characterization of the role of para-aminobenzoic acid biosynthesis in folate production by Lactococcus lactis.* Appl Environ Microbiol, 2007. **73**(8): p. 2673-81.
249. Olin-Sandoval, V., et al., *Lysine harvesting is an antioxidant strategy and triggers underground polyamine metabolism.* Nature, 2019. **572**(7768): p. 249-253.

250. Rutherford, S.T. and B.L. Bassler, *Bacterial quorum sensing: its role in virulence and possibilities for its control.* Cold Spring Harb Perspect Med, 2012. **2**(11).
251. Park, J., et al., *Infection control by antibody disruption of bacterial quorum sensing signaling.* Chem Biol, 2007. **14**(10): p. 1119-27.
252. Kelliher, C.M., et al., *Investigating Conservation of the Cell-Cycle-Regulated Transcriptional Program in the Fungal Pathogen, Cryptococcus neoformans.* PLoS genetics, 2016. **12**(12): p. e1006453-e1006453.
253. Kelliher, C.M. and S.B. Haase, *Connecting virulence pathways to cell-cycle progression in the fungal pathogen Cryptococcus neoformans.* Curr Genet, 2017. **63**(5): p. 803-811.
254. Kelliher, C.M., et al., *Investigating Conservation of the Cell-Cycle-Regulated Transcriptional Program in the Fungal Pathogen, Cryptococcus neoformans.* PLoS Genet, 2016. **12**(12): p. e1006453.
255. Alspaugh, J.A., J.R. Perfect, and J. Heitman, *Cryptococcus neoformans mating and virulence are regulated by the G-protein alpha subunit GPA1 and cAMP.* Genes Dev, 1997. **11**(23): p. 3206-17.
256. D'Souza, C.A., et al., *Cyclic AMP-dependent protein kinase controls virulence of the fungal pathogen Cryptococcus neoformans.* Mol Cell Biol, 2001. **21**(9): p. 3179-91.
257. Pukkila-Worley, R., et al., *Transcriptional network of multiple capsule and melanin genes governed by the Cryptococcus neoformans cyclic AMP cascade.* Eukaryot Cell, 2005. **4**(1): p. 190-201.
258. Gish, S.R., et al., *Computational Analysis Reveals a Key Regulator of Cryptococcal Virulence and Determinant of Host Response.* mBio, 2016. **7**(2): p. e00313-16.
259. Okagaki, L.H., et al., *Cryptococcal titan cell formation is regulated by G-protein signaling in response to multiple stimuli.* Eukaryotic cell, 2011. **10**(10): p. 1306-1316.

APPENDIX I

PLOS NEGLECTED TROPICAL DISEASES

REVIEW

The *Cryptococcus gattii* species complex: Unique pathogenic yeasts with understudied virulence mechanisms

Lamin Saidykhan[1,2], Chinaemerem U. Onyishi[1], Robin C. May[1]*

1 Institute of Microbiology & Infection and School of Biosciences, University of Birmingham, Edgbaston, Birmingham, United Kingdom, 2 Division of Physical and Natural Science, University of The Gambia, Brikama Campus, West Coast Region, The Gambia

*

Abstract

Members of *Cryptococcus gattii/neoformans* species complex are the etiological agents of he potentially fatal human fungal infection cryptococcosis. *C. gattii* and its sister species cause disease in both immunocompetent and immunocompromised hosts, while the closely related species *C. neoformans and C. deneoformans* predominantly infect immunocompromised hosts. To date, most studies have focused on similarities in pathogenesis between hese two groups, but over recent years, important differences have become apparent. In his review paper, we highlight some of the major phenotypic differences between the *C. gattii* and *neoformans* species complexes and justify the need to study the virulence and pathogenicity of the *C. gattii* species complex as a distinct cryptococcal group.

Citation: Saidykhan L, Onyishi CU, May RC (2022) The *Cryptococcus gattii* species complex: Unique pathogenic yeasts with understudied virulence mechanisms. PLoS Negl Trop Dis 16(12): e0010916. https://doi.org/10.1371/journal.pntd.0010916

Editor: Joshua Nosanchuk, Albert Einstein College of Medicine, UNITED STATES

Published: December 15, 2022

Funding: CUO has been supported by a PhD scholarship from the Darwin Trust of Edinburgh. LS has been supported by a PhD scholarship from the Islamic Development Bank. The funders had no role in study design, data collection and analysis, decision to publish, or preparation of the manuscript.

Competing interests: The authors have declared that no competing interests exist.

Introduction

Cryptococcus gattii (*sensu stricto*) was first recognized and described as a distinct cryptococcal strain from *Cryptococcus neoformans* in 1970 [1]. Initially recognized as a variety of *Cryptococcus*, the *Cryptococcus neoformans* var. *gattii* lineage was subsequently elevated to species status as *C. gattii* [2]. Further genetic, biochemical, morphological, ecological, and serological characterization of *C. gattii* environmental and clinical isolates provided more evidence for the classification of *C. gattii* as a unique cryptococcal species [2–10].

The *C. gattii* divergence from *C. neoformans* is estimated to have occurred 37 to 49 million years ago [11,12]. Since then, *C. gattii* has maintained diversity by continuous recombination and evolution into novel lineages with significant genetic diversity that warranted their classification into monophyletic genotypes [12–14]. Recently, the five recognized *C. gattii* genotypes, VGI, VGII, VGIII, VGIV, and VGVI were elevated to five individual species: *C. gattii*, *C. deuterogattii*, *C. bacillisporus*, *C. tetragattii*, and *C. decagattii*, respectively, while the two main lineages of *C. neoformans* were raised to species level, becoming *C. neoformans* and *C. deneoformans* [15]. Different phylogenetic analysis based on concatenated genetic loci unanimously identified *C. deuterogattii*/VGII to be the basal lineage of the *C. gattii* species complex [11,12,14]. VGI, VGIV, and VGIII diverged from VGII approximately 12.4 million years ago [12,16]. Thereafter, *C. tetragattii*/VGIV diverged from *C. bacillisporus*/VGIII and *C. gattii*/VGI

APPENDIX II

PLOS PATHOGENS

RESEARCH ARTICLE

An *in vitro* method for inducing titan cells reveals novel features of yeast-to-titan switching in the human fungal pathogen *Cryptococcus gattii*

Lamin Saidykhan[1,2], Joao Correia[1], Andrey Romanyuk[1,3], Anna F. A. Peacock[3], Guillaume E. Desanti[1], Leanne Taylor-Smith[1], Maria Makarova[1], Elizabeth R. Ballou[1,4]*, Robin C. May[1]*

1 Institute of Microbiology & Infection and School of Biosciences, University of Birmingham, Edgbaston, United Kingdom, **2** Division of Physical and Natural Science, University of The Gambia, Brikama, The Gambia, **3** School of Chemistry, University of Birmingham, Edgbaston, United Kingdom, **4** MRC Centre for Medical Mycology, University of Exeter, Exeter, United Kingdom

[redacted] ERB) [redacted] (RCM)

OPEN ACCESS

Citation: Saidykhan L, Correia J, Romanyuk A, Peacock AFA, Desanti GE, Taylor-Smith L, et al. (2022) An *in vitro* method for inducing titan cells reveals novel features of yeast-to-titan switching in the human fungal pathogen *Cryptococcus gattii*. PLoS Pathog 18(8): e1010321. https://doi.org/10.1371/journal.ppat.1010321

Editor: Kirsten Nielsen, University of Minnesota, UNITED STATES

Received: February 1, 2022

Accepted: July 7, 2022

Published: August 15, 2022

Peer Review History: PLOS recognizes the benefits of transparency in the peer review process; therefore, we enable the publication of all of the content of peer review and author responses alongside final, published articles. The editorial history of this article is available here: https://doi.org/10.1371/journal.ppat.1010321

Data Availability Statement: All relevant data are within the manuscript and supporting files.

Abstract

Cryptococcosis is a potentially lethal fungal infection of humans caused by organisms within the *Cryptococcus neoformans/gattii* species complex. Whilst *C. neoformans* is a relatively common pathogen of immunocompromised individuals, *C. gattii* is capable of acting as a primary pathogen of immunocompetent individuals. Within the host, both species undergo morphogenesis to form titan cells: exceptionally large cells that are critical for disease establishment. To date, the induction, defining attributes, and underlying mechanism of titanisation have been mainly characterized in *C. neoformans*. Here, we report the serendipitous discovery of a simple and robust protocol for *in vitro* induction of titan cells in *C. gattii*. Using this *in vitro* approach, we reveal a remarkably high capacity for titanisation within *C. gattii*, especially in strains associated with the Pacific Northwest Outbreak, and characterise strain-specific differences within the clade. In particular, this approach demonstrates for the first time that cell size changes, DNA amplification, and budding are not always synchronous during titanisation. Interestingly, however, exhibition of these cell cycle phenotypes was correlated with genes associated with cell cycle progression including *CDC11*, *CLN1*, *BUB2*, and *MCM6*. Finally, our findings reveal exogenous p-Aminobenzoic acid to be a key inducer of titanisation in this organism. Consequently, this approach offers significant opportunities for future exploration of the underlying mechanism of titanisation in this genus.

Author summary

Cryptococcus gattii is a fungal pathogen that causes lethal infections in humans and other animals. Upon entry to the lung, some (but not all) cryptococcal cells are induced to become so-called 'titan cells'; huge cells with thickened cell walls, altered capsule and highly duplicated DNA. As a key virulence determinant, titan cells can manipulate the